

# **Pipeline Leak Detection Using Distributed Fibre Optic Temperature, Strain and Vibration Sensing: Final Report**

Report to the  
**WATER RESEARCH COMMISSION**

by

**SW JACOBSZ**  
University of Pretoria

**WRC Report No. 3165/1/24**

**ISBN 978-0-6392-0650-9**

**August 2024**



**Obtainable from**

Water Research Commission  
Bloukrans Building, Lynnwood Bridge Office Park  
4 Daventry Street  
Lynnwood Manor  
PRETORIA

[hendrickm@wrc.org.za](mailto:hendrickm@wrc.org.za) or download from [www.wrc.org.za](http://www.wrc.org.za)

This is the final report of WRC project no. C2019/2020-00113.

**DISCLAIMER**

This report has been reviewed by the Water Research Commission (WRC) and approved for publication. Approval does not signify that the contents necessarily reflect the views and policies of the WRC, nor does mention of trade names or commercial products constitute endorsement or recommendation for use.

# EXECUTIVE SUMMARY

## BACKGROUND

Millions of litres of water are lost on a daily basis due to leaking pipes that are buried underground. The research conducted as part of this study, as discussed in this report, was done with the aim of developing a leak detection system based on distributed fibre optic strain measurement in fibre optic cables caused by water leaks.

The study follows an earlier project for the Water Research Commission (Responsive pipe networks K5/2726/3) demonstrating discrete fibre optic ground strain measurement using Bragg gratings as a successful means of leak detection on pipelines installed in unsaturated ground. To be of practical value it is necessary to assess whether distributed fibre optic ground strain measurement would also be capable of detecting leakage-induced ground strain. The type of fibre optic cable to use plays a critical part in the performance of the proposed system and assessment of the optimal type of fibre optic cable form the subject of this report.

This is the final report of a WRC study to assess the use of fibre optic cables as a means of leak detection on underground pipelines. The report describes a laboratory- and two field studies that were conducted to determine the performance of fibre optic leak detection system relying on the detection of leak-induced strain and temperature changes by means of distributed fibre optic sensing. In the laboratory study three different types of fibre optic cables were tested in three soil types to assess the performance of the proposed leak detection system under ideal laboratory conditions. Following the laboratory study, a field study was carried out on the Hillcrest campus of the University of Pretoria in which 5 different types of fibre optic cables were tested in the field. Following the identification of the most suitable fibre optic cable, a single flexible, dual-core, tight-buffered (TB) fibre optic cable was installed along a newly constructed 200mm uPVC potable water pipeline in Tom Jenkins Drive and Kameel Street in Rietondale, Pretoria. The fibre optic cable was monitored for Brillouin Frequency Shift (BFS) at two-hourly intervals and an artificial leak test was carried out which was successfully detected, demonstrating the potential of the proposed leak detection system.

## RATIONALE

On average 25-50% of the purified water than is input into a water distribution network is lost. This portion of water is known as non-revenue-water (NRW) as it is water which is does not bring revenue into the water distribution service. The major contributing factor to NRW is leaking pipes.

If a pipe starts to leak visibly, remedial action can be taken to repair it. However, large portions of a water distribution network are comprised of pipes which are buried underground. If these pipes

become damaged and start leaking there is often no visible way to detect the location of the leak so that remedial action is deferred. If a passive system could be created to detect whether a buried pipe is leaking, it will benefit water conservation and prevent any further damage that the leaked water could impose on the surrounding environment.

When a water pipe leaks, the moisture content of the surrounding soil is changed. This change in moisture content causes the soil to undergo strain due to pore water suctions which may amount to many kilo-Pascal. Brillouin backscatter occurs when light is passed along an optical fibre. Strain, whether mechanical or thermal, causes a change in the frequency of the Brillouin back scatter, referred to as Brillouin Frequency Shift (BFS). By measuring Brillouin Frequency Shift in an optical fibre, changes relative the unstrained state can be detected and such changes can be indicative of a pipe leak.

The proposed leak detection system consists of a fibre optic cable buried next to an underground pipeline in the same pipe trench. If the pipe begins to leak, the change in soil moisture content would cause the soil to strain and the fibre optic cable buried next to the pipeline would strain with the soil. The strain and temperature change in the fibre optic cable will induce a change in the Brillouin Frequency Shift (BFS) in the cable, which will indicate that the associated pipe is leaking.

## **OBJECTIVES AND AIMS**

### **AIM 1**

Determine performance of distributed strain and temperature sensing to detect leaks in the laboratory – the subject of report no 1.

### **AIM 2**

Determine the performance of distributed strain and temperature measurement to detect leaks in the field – the subject of report no 2.

### **AIM 3**

Demonstrate performance of proposed leakage detection system on working pipeline – the subject of report no 3.

### **AIM 4**

Establish performance of fibre optic acoustic vibration detection to detect leaks. This work was excluded from the scope of the project as explained in Chapter 6.

## **METHODOLOGY**

### **Literature Study**

A literature study was conducted to outline the fundamental concepts upon which the leak detection system is founded. An explanation of how soils behave under changing moisture contents has been presented and its application to the leak detection system is explained. In addition, the fibre optic measuring technique that was used to conduct the experiments, the Brillouin Frequency Shift (BFS), has been reviewed.

### **Experimental setup**

#### **Laboratory work – University of Pretoria Hatfield campus**

The experimental setup consisted of three different types of fibre optic cables that were fed through a concrete beam mould that was filled with soil. The fibre optic cables were connected to a BFS interrogator. The performance of BFS as a means of leak detected was investigated in three different soil types namely a clean coarse silica sand, a clean fine silica sand and a clayey sand.

With the concrete mould filled with soil, the BFS in the optic fibres was measured over a 48 hours period to obtain baseline readings. The BFS is measured at 5cm intervals along the entire length of the optic fibre. Thereafter 1L (one litre) of water was poured into the soil to model an artificial leak. The BFS was then monitored for another 48 hours after wetting of the soil and was then compared against the baseline readings to assess whether a change in BFS resulted from the artificial leak.

Three different soils were used in the experiment, a coarse sand, a fine sand and a natural red clayey soil found on Hillcrest Campus of the University of Pretoria. The concrete mould was sequentially filled with each soil and the experimental procedure outlined above was carried out for each soil.

Three different fibre optic cables were used in the experiment. A low-cost, locally produced telecommunication grade cable, an imported fibre optic cable design for strain measurement and an imported fibre optic cable designed for temperature measurement. These cables were placed along the length of the concrete mould parallel to one another and BFS measurements were measure simultaneously in each cable through the course of the experiment. In the analysis the change in BFS measurements between the dry and wet soil detected by each cable were compared with each other.

#### **Field work – University of Pretoria Hillcrest campus**

The experimental setup consisted of a 150m long trench comprising of three sections, excavated to depths of 0.5m, 1.0m and 1.5m respectively, and five different types of fibre optic cable buried in the trench. A total of nine artificial leak points, three along each depth section, were installed. These leak points comprise of 25mm HDPE pipes extending to near the optical fibres and allowed for water to be introduced to wet up the soil around the cables to test their responses to a water leak. The

fibre optic cables were connected to a BFS interrogator and BFS was recorded at two-hourly intervals over the course of the study.

Having the BFS interrogator monitoring the fibre optic cable installation for two weeks allowed the collection of some baseline data which provided certain insight in the response of these cables. It is important to monitor baseline data over as long a period as possible as the strain-induced BFS measured on the cables are affected by ground strain and temperature changes which vary seasonally and due to significant rainfall events. A total of five different fibre optic cables were monitored as listed below. A reference code for referring to the respective cables are given in brackets.

- An Aerial Self Support (industrial strength) 72-fibre, 6-core cable (72F-6C-LC)
- A 6-fibre Tight-buffered Field Deployable Cable (6F-TB)
- A 4-fibre Dual Purpose Drop Cable (4F-DC)
- A 2-fibre Tight-buffered Field Deployable Cable (2F-TB)
- A BRUsens strain V9 cable (Strain Cable – TB)

The abovementioned cables resort in two classes, i.e. loose core (LC) and tight-buffered (TB) cables. A loose core cable is mechanically isolated from its sheath, usually by means of a lubricating gel so that it is relatively insensitive to strains acting on the cable. A tight-buffered cable, on the other hand, is firmly bonded to its sheath to be sensitive to strain changes acting on the cable. The performance of these two classes of cables were studied.

Two leak tests involving the discharge of respectively 40 and 50 litres of water were conducted on the fibre optic cable trench experimental setup. The results of the leaks tests showed that each type of fibre optic cable tested was able to detect the ingress of water into the surrounding soil, either by registering a temporary temperature response, or a combination of a temperature and a soil strain response. The different cable types did not all perform equally well as leak detection sensors. It has been conclusively shown that TB cables provide the best performance as leak detection sensors and that LC cables and even cables designed to specifically measure strain when cast into concrete give inferior performance to TB communication grade cables. Comparing different TB cables showed that the less stiff TB cables gave the best performance as leak detection sensors.

### **Leak detection on full-scale pipe installation**

This work was carried out in Tom Jenkins Drive and Kameel Street in Rietondale, Pretoria. The experimental setup consisted of a 180m long section of 200mm diameter uPVC pipeline along which a flexible, dual core, tight-buffered fibre optic cable was installed in the same pipe trench. An artificial leak point was installed comprising of a 25mm HDPE pipe extending to the bottom of the pipe trench which allowed for water to be introduced to wet up the soil around the pipe to test the leak detection system's responses to a water leak. The fibre optic cable was connected to a BFS interrogator and

BFS was recorded at two-hourly intervals over the course of one month from 24 August 2021 to 24 September 2021 to allow baseline measurements to be determined. This was followed by a 7-day leak test during which 40 litres of water per hour was introduced at the leak point. After the leak test terminated on 1 October the optical fibre was monitored for a further two months to gain an understanding of BFS change over time in the absence of a leak.

The cable used was a dual core tight-buffered field deployable cable. A tight-buffered cable is firmly bonded to its sheath to be sensitive to strain changes acting on the cable.

## **RESULTS**

### **AIM 1: Determine performance of distributed strain and temperature sensing to detect leaks in the laboratory – Presented previously in Deliverable 1.**

The BFS profiles along the optical fibres measured before and after a change in soil moisture content clearly showed changes where the fibres had been buried in the soil. It showed insignificant BFS changes where the cables were not exposed to a leak-induced external disturbance. It was found that the three different soils investigated imposed different changes in the measured BFS. The BFS depended on the soil's particle size distribution as this controls the magnitude of pore water suction associated with a leak, which, in turn, controls the leakage-induced ground strain.

It was found that the type of fibre optic cable used as leakage detection sensor plays a very important role in the performance of BFS as a means of leak detection. Depending on the type of fibre optic cable used, moisture content changes in BFS can be very prominent, or it can be virtually undetected. The locally produced telecom cable measured very similar changes in BFS in all three soils. This cable performed well to detect soil moisture content changes. However, the change in BFS was not found to vary significantly between soil type.

The strain-sensing fibre optic cable was found to detect BFS changes of different magnitude in the three soil types investigated, with the largest in the clay and the smallest in the coarse sand. The strain-sensing cable therefore appears sensitive to the soil type in which it is placed.

The temperature-detection cable was found to give very small changes in BFS readings as compared with the telecom cable and the Strain Cable, as it is largely insensitive to strain, sensitive instead to temperature changes.

### **AIM 2: Determine the performance of distributed strain and temperature measurement to detect leaks in the field**

During baseline monitoring, the behaviour of tight-buffered (TB) vs loose core (LC) fibre optic cables was found to differ significantly. BFS data from tight-buffered cables were found to be highly variable

with distance, appearing quite noisy as opposed to much smoother BFS profiles observed along loose core cables. The reason for the apparent noisy response of TB cables is that these cables are sensitive to both mechanical strains and temperature effects. A fibre optic cable buried in the ground in a trench is not supported uniformly along its length and is therefore subjected to variable strains associated with soil lumps, cavities, slight bends in the cable, etc. The LC cables are only sensitive to temperature changes, which are minimal underground, and therefore presented smooth profiles.

Two classes of leak tests were performed, i.e. tests in which a small volume of 40 litres of water was introduced and tests where 40 litres per hour was introduced over the period of one week. It was found that the leaks were detectable using both TB and LC cables, with the former being the more sensitive as it also responds to strain changes in addition to temperature. The BFS trendline returned to its pre-leak baseline after the leak as temperatures equilibrated, while the BFS trend in TB cables returned to a new baseline due to permanent strains caused by the leak.

### **AIM 3: Demonstrate performance of proposed leakage detection system on working pipeline**

A new 200mm uPVC potable water pipeline in Rietondale, Pretoria was instrumented with a flexible dual-core tight-buffered fibre optic cable. The operational life of the fibre optic cable used is reported to be at least 20 years when buried in the ground. As leaks on a new pipeline were unlikely, arrangements were made to impose an artificial leak of 40 litres per hour over the course of one week. The leak was clearly detectable from the BFS trends observed. The response matched the leak-induced bending moment distribution that can be expected to develop in a pipe sagging because of leak-induced soil softening.

### **AIM 4: Establish performance of fibre optic acoustic vibration detection to detect leaks**

This work was excluded from the scope of the project as explained in Chapter 6.

## **CONCLUSIONS**

The laboratory study (Report 1) demonstrated that Brillouin Frequency Shift (BFS) employed as a leak detection parameter along fibre optic cables is a potentially successful means of leak detection, capable of detecting changes in soil moisture content. In addition, it appears suitable to pinpoint the location where the moisture content change took place. The most prominent results were observed in the finer grained soils investigated in which pore water suctions and hence ground strains are greater compared to coarse grained soils.

In terms of cable types investigated, it was found that the locally produced tight-buffered (TB) telecommunication grade fibre optic cable provided the most significant output, followed by an imported strain-sensitive TB cable, with the temperature-sensitive cable loose core (LC) cable being the least sensitive. The TB telecom cable is relatively flexible, allowing it to deform due to leakage-induced ground strains. The Strain Cable is relatively stiff, but sensitive to strain changes. The Temperature Cable is nearly completely insensitive to mechanical strain changes, but is suitable to detect leak-induced temperature changes. However, these are small compared to the leakage-induced ground strain changes.

The field study on the Hillcrest campus of the University of Pretoria (Report 2) demonstrated that both loose core and tight-buffered cables were found to be suitable leak detection sensors, with the tight-buffered cables being the more sensitive to indicate leaks because, in addition to being sensitive to temperature changes, it is also sensitive to strain-induced changes. Both small water leaks of 40 litres introduced once, as well as more long-term leaks of 40 litres per hour over the course of a week could be detected from the BFS profiles logged at two-hourly intervals in the fibre optic cables.

A field study involving the installation of a dual-core flexible tight-buffered fibre optic cable along a 200mm uPVC water pipe in Rietondale, Pretoria (Report 3), showed that an artificially imposed leak of 40 litres per hour could be easily detected.

The overall conclusions of the study is that monitoring of fibre optic cables for changes in BFS represents an effective means of leak detection on water pipelines. The installation of fibre optic leak detection systems with new pipe networks offers potential to significantly reduce water losses from water leaks that may develop as the pipe networks age.

## **RECOMMENDATIONS FOR FUTURE RESEARCH AND ACTION**

Research to date has demonstrated that leaks can be detected successfully from Brillouin Frequency Shift records obtained from fibre optic cables buried next to operating potable water pipelines in the same pipe trench.

Automated software to scan Brillouin Frequency Shift records for leaks should be developed.

It is recommended that a demonstration installation of a leak detection system be installed and commissioned to showcase the technology. Steps should be taken to implement the fibre optic leak detection methodology commercially. The technology represents a significant business opportunity.

The performance of fibre optic cables as they age should be investigated. The operational life of the fibre optic cable used is reported to be at least 20 years when buried in the ground.

# Acknowledgements

The project team thanks the following reference group members for their participation in the project:

<b>Name</b>	<b>Organisation</b>
Jay Bhagwan	Water Research Commission
Nkateko Kubayi	Water Research Commission
Charmaine Dladla	Water Research Commission
Njabulo Kheswa	Umgeni Water
Nomathemba Zikhali	Umgeni Water
Mfanasibili Nkonyane	Umgeni Water
Etienne Hugo	Johannesburg Water
Neil Meyer	WRP
Jason Barry	University of Pretoria
Marco van Dijk	University of Pretoria
Trevor Westman	Formerly City of Tshwane
Brian Sonamzi	City of Tshwane

# TABLE OF CONTENTS

EXECUTIVE SUMMARY	iii
ACKNOWLEDGEMENTS	x
LIST OF FIGURES	xiv
1 INTRODUCTION	1
1.1 BACKGROUND	1
1.2 OBJECTIVES OF THE STUDY	2
1.3 SCOPE OF THE STUDY	3
1.4 METHODOLOGY	3
1.5 ORGANISATION OF THE REPORT	4
2 LITERATURE REVIEW	6
2.1 INTRODUCTION	6
2.2 WATER LOSS	6
2.2.1 NON-REVENUE WATER	6
2.2.2 PIPE LEAKAGE	7
2.2.3 LEAKAGE PROPAGATION	7
2.3 SOIL PROPERTIES RELEVANT TO FIBRE OPTIC LEAK DETECTION	8
2.3.1 EXPANSIVE AND COLLAPSIBLE SOIL	8
2.3.2 PROBLEMS ASSOCIATED WITH SOIL MOISTURE CONTENT CHANGES	9
2.4 STRUCTURAL COMPOSITION OF FIBRE OPTIC CABLES	9
2.4.1 USING FIBRE OPTIC CABLES TO MEASURE STRAIN	11
2.4.2 DISTRIBUTED FIBRE OPTIC SENSING	12
2.4.3 THE BRILLOUIN EFFECT IN FIBRE OPTIC CABLES	13
3 LABORATORY FIBRE OPTIC LEAK DETECTION STUDY	16
3.1 INTRODUCTION	16
3.2 MEASURING INSTRUMENTATION	16
3.2.1 FIBRE OPTIC CABLES TESTED	16
3.2.2 BRILLOUIN FIBRE OPTIC STRAIN INTERROGATOR	17
3.3 TESTED SOILS	18
3.3.1 COARSE SAND	18

3.3.2	FINE SAND	19
3.3.3	RED CLAYEY SOIL	20
3.4	SOIL AND CABLE HOUSING	23
3.5	EXPERIMENTAL METHODOLOGY	26
3.6	EXPERIMENTAL RESULTS	27
3.6.1	BFS PROFILE EXPLANATION	27
3.7	CALIBRATION EXERCISE UNDER MECHANICAL STRAIN	29
3.7.1	RESPONSE OF THE TELECOM CABLE	29
3.7.2	RESPONSE OF THE STRAIN CABLE	31
3.7.3	RESPONSE OF THE TEMPERATURE CABLE	33
3.8	FIBRE OPTIC CABLE BEHAVIOUR OVER 48 HOURS	35
3.9	THE EFFECT OF A LEAK ON THE BFS	40
3.10	THE INFLUENCE OF DIFFERENT SOILS ON CHANGE IN BFS	41
3.11	COMPARISON OF THE PERFORMANCE OF DIFFERENT CABLES	44
3.12	EFFECT OF TENSIONING CABLES	46
3.12.1	TELECOM CABLE	47
3.12.2	STRAIN CABLE	49
3.12.3	TEMPERATURE CABLE	50
4	FIELD INVESTIGATION ON HILLCREST CAMPUS, UNIVERSITY OF PRETORIA	52
4.1	INTRODUCTION	52
4.2	MEASURING INSTRUMENTATION	52
4.2.1	FIBRE OPTIC CABLES USED	52
4.2.2	BRILLOUIN FIBRE OPTIC STRAIN INTERROGATOR	53
4.3	FIELD SETUP	54
4.3.1	TRENCH	54
4.3.2	SOIL PROPERTIES	56
4.4	BASELINE FIELD DATA	58
4.4.1	OUTPUT FROM THE BFS INTERROGATOR	58
4.4.2	BFS IN THE TIME DOMAIN	60
4.4.3	AVERAGE BFS PROFILES AND RELATIVE BFS PROFILES	63
4.4.4	COMPARISON OF THE VARIOUS CABLES	67

4.4.4.1	72F-6C-LC-TO-STRAIN CABLE	67
4.4.4.2	6F-TB CABLE	69
4.4.4.3	4F-DC-LC CABLE	72
4.4.4.4	2F-TB CABLE	73
4.5	LEAK TEST RESULTS	75
4.5.1	Data Processing Methodology	75
4.5.1.1	Centred Moving Average	76
4.5.1.2	Zeroing Relative Profile	77
4.5.1.3	Squared Relative Profile	79
4.5.1.4	Comparison Against Expected Minimum And Maximum BFS Response	80
4.5.1.5	Repeatability of Detection	82
4.5.2	BFS Response In The Time Domain	83
4.5.3	Comparison of the Different Fibre Optic Cables	85
4.5.3.1	Strain to 72F-6C-LC	85
4.5.3.2	4F-DC-LC	87
4.5.3.3	2F-TB	88
4.5.3.4	6F-TB to 72F-6C-LC	89
5	FIELD INVESTIGATION ON ACTIVE PIPELINE – RIETONDALE, PRETORIA	90
5.1	INTRODUCTION	90
5.2	SITE LOCATION	90
5.3	FIBRE OPTIC CABLE INSTALLATION	91
5.4	LEAK TEST	92
5.5	LEAK TEST RESULTS	93
5.5.1	BASELINE MONITORING	94
5.5.2	LEAK RESPONSE	96
5.6	RECOMMENDED LEAK DETECTION PROCEDURE	99
6	LEAK DETECTION BY MEANS OF VIBRATION DETECTION	100
7	CONCLUSIONS AND RECOMMENDATIONS	101
7.1	CONCLUSIONS FROM LABORATORY STUDY	101
7.2	CONCLUSIONS FROM FIELD INSTALLATION ON HILLCREST CAMPUS	102
7.3	CONCLUSIONS FROM FIELD INSTALLATION ON ACTIVE PIPELINE	102

7.4	RECOMMENDATIONS	103
8	REFERENCES	105
	APPENDIX A: 6F-TB and 2F-TB CABLE SPEC SHEET	107
	APPENDIX B: STRAIN CABLE SPEC SHEET	111
	APPENDIX C: 72F-6C-LC CABLE SPEC SHEET	113
	APPENDIX D: 4F-DC-LC CABLE SPEC SHEET	117
	APPENDIX E: BFS INTERROGATOR SPEC SHEET	121

# LIST OF FIGURES

Figure 2-1. The structural layers comprising a fibre optic cable. Taken from Mark and Shirk (2018).	10
Figure 2-2. A graph showing the attenuation of light of different wavelengths as it travels through a fibre optic cable. Taken from Mark and Shirk (2018).	11
Figure 2-3. Mechanism whereby acoustic phonons are created by counter-propagating light waves in a fibre optic cable. Taken from A. Motil et al.	15
Figure 3-1. Particle size distribution of the coarse sand.	18
Figure 3-2. Soil-water retention curve for the coarse sand. Taken from Le Roux (2019).	19
Figure 3-3. Particle size distribution for the fine sand.	20
Figure 3-4. Soil-water retention curve for the fine sand. Taken from Garfield (2019).	20
Figure 3-5. Particle size distribution for the red clay.	21
Figure 3-6. Soil-water retention curve for the red clay.	21
Figure 3-7. Particle size distribution curves for the three soil types used for the experiment.	22
Figure 3-8. Soil-water retention curves for the three soil types used for the experiment.	22
Figure 3-9. The clamps that were made to attach to the cable to hang weights.	23
Figure 3-10. The wooden planks used to insert the fibre optic cables into the mould.	23
Figure 3-11. G-clamp used to secure wooden plank in the mould.	24
Figure 3-12. PVC pipe that was cut and fitted under the cables to prevent sharper bending than 100mm in the cables.	24
Figure 3-13 . Showing the experimental setup in the laboratory.	24
Figure 3-14. A schematic drawing (side view) of the experimental setup (dimensions in mm).	25
Figure 3-15. A plot depicting a typical BFS profile for the telecom cable.	27
Figure 3-16. BFS profiles for the telecom cable.	28
Figure 3-17. A magnified plot of the same BFS profile depicted in Figure 3-16.	29
Figure 3-18. BFS profiles of the telecom cable recorded during the calibration exercise.	29
Figure 3-19. A relative plot of the BFS profiles of the telecom cable from Figure 4.4, plotted relative to the 0kg loading curve.	30
Figure 3-20. A change in BFS vs load curve plotted for the telecom cable corresponding to a value of 12m on the length axis. There is hysteresis occurring on the unloading phase.	31
Figure 3-21. BFS profiles plotted for the Strain Cable recorded under loading during the calibration exercise.	31
Figure 3-22. A relative plot of the BFS profiles of the Strain Cable shown in Figure 3-21, plotted against the 0kg loading curve.	32
Figure 3-23. A change in BFS vs load plot for the Strain Cable during the calibration exercise. The hysteresis of the Strain Cable is less than that of the telecom cable.	32

Figure 3-24. BFS profiles for the Temperature Cable taken during the calibration exercise.	33
Figure 3-25. A relative plot of the BFS profiles of the Temperature Cable shown in Figure 4.10, plotted against the 0kg loading curve.	33
Figure 3-26. A change in BFS vs load curve for the Temperature Cable during the calibration exercise.	34
Figure 3-27. Change in BFS vs load curves for all three cables from the calibration exercise.	34
Figure 3-28. BFS profiles for the telecom cable taken over a period of 48 hours at 2-hour intervals.	35
Figure 3-29. In Figure 4.15, the axes of Figure 4.14 have been magnified to length = [9, 38] m, and BFS = [10.70, 10.77] GHz.	35
Figure 3-30. A 48-hour average BFS profile of the telecom cable.	36
Figure 3-31. A relative plot of the BFS profiles, from Figure 4.14, plotted relative to the 48-hour average profile.	36
Figure 3-32. A curve of the BFS, relative to the 48-hour average profile, vs time, for the telecom cable, showing how the BFS of the optic fibre changes as the ambient temperature varies throughout the day.	37
Figure 3-33. A BFS vs time curve for the Strain Cable.	38
Figure 3-34. A BFS vs time curve for the Temperature Cable.	38
Figure 3-35. A BFS vs time curve of an ordinate buried in soil on each cable.	39
Figure 3-36. A BFS vs time curve of an ordinate from each cable that is not buried in soil.	39
Figure 3-37. Average BFS profiles for the telecom cable.	40
Figure 3-38. A relative wetting BFS curve for the telecom cable.	41
Figure 3-39. Relative wetting BFS curves, for the telecom cable, in each of the soils tested. The telecom cable shows that there is a disturbance, but it does not indicate its magnitude	42
Figure 3-40. Relative wetting BFS curves for the telecom in each of the tested soils.	42
Figure 3-41. Relative wetting BFS curves for the Strain Cable in each of the tested soils.	43
Figure 3-42. Relative wetting BFS curves for the Temperature Cable in each of the tested soils.	43
Figure 3-43. Relative wetting BFS curves for each cable in the coarse sand. Before conducting these experiments the Strain Cable was buried between the length ordinates of 14.5m and 16.5m.	45
Figure 3-44. Relative wetting BFS curves for each cable in the fine sand. All three cables in this case registered a negative change in BFS, implying that the soil shrank when wetted.	45
Figure 3-45. Relative wetting BFS curves for each of the cables tested in the red clay.	46
Figure 3-46. Relative Wetting BFS curves, for the telecom cable, for both the tensioned and untensioned test, whilst buried in the coarse sand.	47
Figure 3-47. Relative Wetting BFS curves, for the telecom cable, for both the tensioned and untensioned test, whilst buried in the fine sand.	47

Figure 3-48. Relative Wetting BFS curves, for the telecom cable, for both the tensioned and untensioned test, whilst buried in the red clay.	48
Figure 3-49. Relative Wetting BFS curves, for the Strain Cable, for both the tensioned and untensioned test, whilst buried in the coarse sand.	49
Figure 3-50. Relative Wetting BFS curves, for the Strain Cable, for both the tensioned and untensioned test, whilst buried in the fine sand.	49
Figure 3-51. Relative Wetting BFS curves, for the Strain Cable, for both the tensioned and untensioned test, whilst buried in the red clay.	50
Figure 3-52. Relative Wetting BFS curves, for the Temperature Cable, for both the tensioned and untensioned test, whilst buried in the coarse sand.	50
Figure 3-53. Relative Wetting BFS curves, for the Temperature Cable, for both the tensioned and untensioned test, whilst buried in the fine sand.	51
Figure 3-54. Relative Wetting BFS curves, for the Temperature Cable, for both the tensioned and untensioned test, whilst buried in the red clay.	51
Figure 4-1. Bird's eye view of the 150m trench dug on the University of Pretoria Hillcrest Campus.	55
Figure 4-2. Standing point view of the trench prior to installation of the fibre optic cables.	55
Figure 4-3. Schematic diagram of the trench (not drawn to scale) depicting the three 50m segments.	56
Figure 4-4. Schematic bird's eye view diagram of the trench showing the orientation of the laid cables.	56
Figure 4-5. Particle size distribution for the red clay.	57
Figure 4-6. Soil-water retention curve for the red clay.	57
Figure 4-7. BFS profile of the cable with the 50m segment of Strain Cable spliced to it. The segment of the cable buried in the trench is highlighted by the blue rectangle.	58
Figure 4-8. Two BFS profiles taken at two different times during the day for the same cable showing how temperature variation affects the BFS output.	59
Figure 4-9. Difference between the two BFS profiles plotted in Figure 4-8.	59
Figure 4-10. A curve of the BFS plotted against time for the length ordinate $L = 240\text{m}$ along the cable to which the Strain Cable was spliced.	60
Figure 4-11. A depiction of the development of an average BFS value as time progresses at length ordinate $L = 240\text{m}$ of the 72F-6C to strain spliced cable.	61
Figure 4-12. BFS vs time plot of the 72F-6C to Strain Cable. Curves are plotted for length ordinates 240m, 280m, 340m, and 400m occurring in the 72F-6C section, and 530m, occurring in the Strain Cable section.	62
Figure 4-13. BFS vs time curves for the 72F-6C to Strain Cable, plotted from 240m to 580m, every 20m for the 72F-6C cable, and every 5m for the Strain Cable segment.	62
Figure 4-14. Normalised set of BFS vs time curves from Figure 2.7.	63

Figure 4-15. Set of BFS profiles of the 72F-6C-to-Strain Cable logged over a period of 22 hours at 2 hour intervals.	63
Figure 4-16. An average BFS profile created by averaging 12 profiles logged over a 22 hour time span at 2 hour intervals.	64
Figure 4-17. A set of average BFS profiles plotted for the 72F-6C-to-Strain Cable.	65
Figure 4-18. Set of average BFS profiles from Figure 2.11 plotted relative to the 2020/12/15 average BFS profile.	65
Figure 4-19. Average, minimum and maximum BFS value logged from 14 to 31 December 2020 for the 72F-6C-to-Strain Cable	66
Figure 4-20. Minimum and maximum BFS values logged, as per Figure 4-20, relative to the average BFS profile.	66
Figure 4-21. Set of relative BFS profiles of the 72F-6C-LC-to-Strain Cable.	67
Figure 4-22. Set of relative BFS profiles of the 72F-6C-LC-to-Strain Cable focusing on the Strain Cable section.	68
Figure 4-23. Maximum and minimum boundaries of the BFS output logged for the 72F-6C-to-Strain Cable relative to the average BFS profile.	68
Figure 4-24. Set of daily average BFS profiles for the 72F-6C-to-6F-TB cable from 15/12/2020 to 31/12/2020.	69
Figure 4-25. Set of daily average BFS profiles for the 72F-6C-to-6F-TB cable focused on the 6F-TB section.	70
Figure 4-26. Set of daily average BFS profiles relative to the 15/12/20 profile for the 72F-6C-to-6F-TB cable from 15/12/2020 to 31/12/2020.	71
Figure 4-27. Minimum-maximum envelope of the 72F-6C-to-6F-TB cable.	71
Figure 4-28. Set of daily average BFS profiles for the 4F-DC cable from 15/12/2020 to 31/12/2020.	72
Figure 4-29. Set of daily average BFS profiles relative to the 15/12/20 profile for the 4F-DC-LC cable from 15/12/2020 to 31/12/2020.	72
Figure 4-30. Minimum-maximum envelope of the 4F-DC cable.	73
Figure 4-31. Set of daily average BFS profiles for the 2F-TB cable from 15/12/2020 to 31/12/2020.	73
Figure 4-32. Set of daily average BFS profiles relative to the 15/12/20 profile for the 2F-TB cable from 15/12/2020 to 31/12/2020.	74
Figure 4-33. Minimum-maximum envelope of the 2F-TB cable.	75
Figure 4-34. Relative BFS plot generated by subtracting the 23 March baseline from the 24 March baseline.	76
Figure 4-35. A plot of the raw relative profile output as well as the 25-point moving centred average created from the raw data output.	77

Figure 4-36. A set of curves representing the raw relative BFS output profile, a 25-point CMA and a 601 point CMA.	78
Figure 4-37. 25-point CMA relative profile before being zeroed and after being zeroed.	78
Figure 4-38. Zeroed raw output and 25pt CMA profiles generated by subtracting the 601 point CMA.	79
Figure 4-39. Squared 25-point CMA relative profile.	80
Figure 4-40. Leak test result shown against the minimum and maximum expected bounds of the 72F-6C-LC to 6F-TB cable.	81
Figure 4-41. Regions of the zeroed 25-point CMA relative profile that exceeded the minimum-maximum expected BFS boundary.	81
Figure 4-42. Results of the first (24 March) and second (1 April) leak test plotted relative to the 23 <sup>rd</sup> of March baseline. The curve labelled 02-Apr is indicative that it is generated from a baseline logged on the 2 <sup>nd</sup> of April after the second leak had taken place on the 1 <sup>st</sup> of April.	83
Figure 4-43. Results of the leak test conducted on the 31 <sup>st</sup> of March output by the 6F-TB cable.	84
Figure 4-44. Time domain plot of the change in BFS at the three leak points for the two cables (72F-6C-LC and 6F-TB) as the leak test was conducted.	84
Figure 4-45. Results of the second leak test measured using the Strain to 72F-6C-LC FO cable.	86
Figure 4-46. Results of the second leak test measured using the 4F-DC-LC FO cable.	87
Figure 4-47. Results of the second leak test measured using the 2F-TB FO cable.	88
Figure 4-48. Results of the second leak test measured using the 6F-TB to 72F-6C-LC FO cable.	89
Figure 5-1. Fibre optic cable installation in Rietondale, Pretoria	91
Figure 5-2. Fibre optic cable being laid next to the uPVC water pipe	92
Figure 5-3. HDEP downpipe used to impose artificial leak shown prior to backfilling of the pipe trench.	93
Figure 5-4. BFS profiles recorded over a 24-hr cycle at 4-hourly intervals along entire monitored fibre optic cable length.	94
Figure 5-5. BFS profiles recorded over a 24-hr cycle at 4-hourly intervals along the first 140m of fibre optic cable length.	94
Figure 5-6. BFS profiles recorded over a 24-hr cycle at 4-hourly intervals along the last 140m of fibre optic cable length.	95
Figure 5-7. Variation in BFS in the absence of a pipe leak (Ch 182.68).	95
Figure 5-8. Schematic layout of fibre optic cable monitored.	96
Figure 5-9. Variation in BFS at the leak location (Ch 205).	97
Figure 5-10. BFS profiles along the fibre optic cable before during and after the leak.	98
Figure 5-11. Raw BFS profiles shortly before, during and shortly after the leak.	98
Figure 5-12. Zeroed BFS profiles shortly before, during and shortly after the leak	99

# 1 INTRODUCTION

## 1.1 BACKGROUND

Water distribution networks are the primary means by which water is supplied and transported by municipal services to the public. However, not all the water that is put into a system is used by or even reaches the consumer. A percentage of the water that goes into a water distribution system is lost and termed as Non-Revenue Water (NRW). NRW is attributed to a discrepancy between the metered water that is provided by a water distribution system and the amount of water that the public consumes. On average, NRW accounts for between 25-50% of the total volume of water supplied by the water distribution service (Pedersen et al., 2013).

NRW is categorised into unbilled authorized consumption, unauthorized consumption and real losses. Unbilled authorized consumption is made up of water usage from fire-hydrants and use of water by communities with special permission to obtain water for free. It can also be water acquired by fraudulent means, tampering with meters, or internal corruption within the management of a water distribution system authorizing the use of water without adding a cost to it. Unauthorized consumption is water that is consumed via illegal connections to a water distribution system. Metering inaccuracies (not to be confused with tampered readings) also contribute to the tally of unauthorized consumption, although this is an error in the measuring system. The largest contributor to NRW, however, are the real losses. These are losses that occur due to pipe leakage.

Leaking pipes pose a particular problem, because the majority of a pipe network is buried underground. A leaking pipe can go undetected for long periods of time. The only possible warnings of the leakage are large quantities of water appearing at the ground surface, or when surrounding infrastructure starts to become affected. However, by the time these warnings are detected, large volumes of water have already leaked out and been wasted. Furthermore, only large leaks would cause such an effect on the surrounding environment, thus smaller leaks could go undetected indefinitely.

These leaks can have an adverse effect on the surrounding environment. Changing the water content in the ground, depending on the geology, can cause swelling or collapse of the soil. This could impose unwanted stress onto nearby foundations, seep into the substructures of pavements causing damage and deformation to roads, or cause damage to a buried electrical cable. Moreover, the effort that is used to purify, store and pump additional water to account for the NRW through a system raises the costs of water distribution. These costs are ultimately paid for by the consumer. By reducing the number of pipe leaks in a distribution system large sums of money can be saved by both suppliers and consumers.

Systems are available to detect and quantify the amount of NRW present in a distribution network. However, systems that are able to pinpoint the exact location of pipe leaks are still being developed. This report discusses an experimental leak detection method that uses a Brillouin Back Scatter Fibre Optic Strain Detection System to detect leaks by measuring temperature effects and strains effects of soil near a pipe when the moisture content of the soil is changed because of a leaking pipe.

This report described the WRC study which aimed to investigate the performance of distributed strain measurement in fibre optic cables to act as a means of leak detection on water pipelines. Chapter 3 presents the result of a pilot laboratory study to investigate prospects for success under ideal laboratory conditions. Chapter 4 presents the results of a field study in which a range of fibre optic cables was investigated to determine the optimal cable type to be used in an actual leak detection system. Chapter 5 presents the results of a study to demonstrate the performance of the leak detection system on a working pipeline.

## **1.2 OBJECTIVES OF THE STUDY**

This study aims to investigate:

- Whether a Brillouin Fibre Optic Strain Detection System can be used to detect and pinpoint the location of a pipe leak point along a fibre optic cable that is buried next to a pipeline by measuring the strain (resulting from swelling or shrinking) in a soil when its moisture content is changed due to the pipe leak.
- How different types of soil, that undergo different amounts of strain when their moisture contents are changed, influence the Brillouin Frequency Shift that occurs in a fibre optic cable.
- The performance of five types of fibre optic cables as a means of leak detection on water pipelines. The cables tested fall in two classes, i.e. tight buffered and loose core. The former implies that the protective sheath around the cable is tightly bonded to the optical fibre, while the latter implies a sheath that is debonded from the optical fibre.
- Baseline data collected from the various fibre optic cables tested to assess how collected data varies over time. This is important for the establishment of a baseline against which leak-induced fibre optic readings can be distinguished from “normal” data.
- The performance of a flexible dual-core tight-buffered fibre optic cable installed parallel to a 200mm diameter uPVC potable water pipeline in the same pipe trench to act as a leak detection sensor.
- Whether leak-induced changes in Brillouin Frequency Shift (BFS) in the optical fibre can be successfully distinguished from background noise associated with daily and seasonal

changes in BFS. Such changes can be caused by daily and season temperature variation and rainfall effects.

### **1.3 SCOPE OF THE STUDY**

The first part of the study was laboratory based with field testing following in the second and third phases. Three different types of fibre optic cables with quite different properties were trialled in the tests ranging from flexible to relative stiff and from temperature insensitive to temperature sensitive. Tests were conducted in three different soils ranging from clean fine silica sand to a naturally occurring clayey soil. Tests were carried out by placing the cables in concrete beam moulds in the various soil types tested and introducing water to impose leaks while observing the associated Brillouin Frequency Shift using a suitable interrogator.

The first field investigation comprised a field study carried out on the Hillcrest Campus of the University of Pretoria in which five different types of fibre optic cables were assessed as potential sensors for leak detection. No pipe was present in the installation as it was intended to test the response of the cables to wetting up of the soil. This was achieved by imposing artificial water leaks. The cables were buried in the ground at different depths and were wetted to assess their response to leaks. Prior to the leak tests, baseline data were collected against which future leak data could be interpreted.

The final field investigation comprised a field study carried out in Rietondale, Pretoria in which a flexible dual-core tight-buffered fibre optic cable was installed parallel to a 200mm diameter uPVC potable water pipeline in the same pipe trench. The cable was monitored over a period of three months for changes in Brillouin Frequency Shift to assess whether it can serve as a means of leak detection.

### **1.4 METHODOLOGY**

The study commenced with a literature review to gain knowledge about the different aspects that would relate to a fibre optic leak detection system and to motivate why leak detection systems are necessary. These aspects included underground pipe-networks, pipe leaks, soil-water interaction and information about fibre optics and the Brillouin Frequency Shift.

Thereafter, an experimental setup was created in a laboratory and controlled tests were conducted. These tests involved pouring water into a repurposed concrete mould, housing different types of soils, with fibre optic cables buried within the soils. The Brillouin Frequency Shift profiles of the fibre optic cables, were recorded using a Brillouin Frequency Shift interrogator while the tests were being run.

The data collected from the interrogator was then processed. Analysis was performed on the data in an effort to determine if the strains that occurred in the soil due to changes in moisture content could be registered by the fibre optic cables using changes in Brillouin Frequency Shift.

The first field investigation comprised a field study carried out on the Hillcrest Campus of the University of Pretoria. It involved the excavation of a 150m long trench comprising of three sections respectively excavated to 0.5m, 1.0m and 1.5m. Five different types of fibre optic cable were buried in the trench. The cables were fitted with nine artificial leak point through which water can be introduced into the soil affecting the cables. Prior to the leak tests, the fibre optic cables were monitored using a FBS interrogator to collect baseline data against which leak data has to be interpreted. Leak tests were subsequently imposed and the response of the fibre optic cables were monitored using a BFS fibre optic interrogator.

The final investigation comprised a field study carried out in Rietondale, Pretoria. It involved the installation of a flexible dual-core tight-buffered fibre optic cable parallel to a 200mm diameter uPVC potable water pipeline in the same pipe trench. Artificial leak points were installed at selected locations through which water could be introduced into the soil to impose artificial leaks. Prior to the leak test, the fibre optic cable was monitored at two hourly intervals using a FBS interrogator to collect baseline data against which leak data could be interpreted. One month of baseline data was collected before a leak of 40 litres per hour over the duration of one week was imposed. BFS monitoring continued during and after the leak test at two-hourly intervals for two months after the leak test. The BFS records were examined and it was found that the leak event could be identified from the data.

## **1.5 ORGANISATION OF THE REPORT**

The report consists of the following chapters and appendices:

- Chapter 1 serves as an introduction to the report.
- Chapter 2 contains reference to the literature study.
- Chapter 3 describes a laboratory installation carried out.
- Chapter 4 describes the field installation carried out on the Hillcrest campus of the University of Pretoria.
- Chapter 5 describes the field installation along an operating pipeline in Rietondale, Pretoria.
- Chapter 6 presents the motivation for not carrying out the leak detection by means of vibration detection work.

- Chapter 7 contains the conclusions and recommendations of the study to date.
- Chapter 8 contains the list of references.

APPENDIX A 6F-TB and 2F-TB CABLE SPEC SHEET

APPENDIX B STRAIN CABLE SPEC SHEET

APPENDIX C 72F-6C-LC CABLE SPEC SHEET

APPENDIX D 4F-DC-LC SPEC SHEET

APPENDIX E BFS INTERROGATOR SPEC SHEET

## **2 LITERATURE REVIEW**

### **2.1 INTRODUCTION**

This chapter focuses on and reviews the research that has been conducted on the topics of Non-revenue Water and pipe leakage, the shrink-swell behaviour of soil, and fibre optic cables. Literature on Non-revenue water has been reviewed to quantify the percentage of leakage that occurs in pipe distribution networks. Water loss has detrimental effects on society. This highlights the need for the development of more sophisticated leak detection systems. Literature on soil structure, expansive soils and soil-water interaction has been researched to understand the shrink-swell behaviour of soils. This shrink-swell behavioural property of soil is the key mechanism that is used in the development of the pipe leakage detection system. Also highlighted are some of the problems that soils-water interaction poses to infrastructure. Finally, a review of fibre optic cables and the Brillouin Fibre Optic Strain Measurement Method has been conducted in order to fully understand and utilise this technology. This is necessary in order to comprehensively interpret the output that is given by a Brillouin strain measurement device employed in the leak detection system.

### **2.2 WATER LOSS**

#### **2.2.1 NON-REVENUE WATER**

Non-Revenue Water (NRW) is water that is treated and distributed by a municipal water service that is lost without generating revenue (González-Gómez et al., 2011). NRW is comprised of three components:

- unbilled authorised consumption,
- apparent losses and unauthorised consumption, and
- real losses due to pipe leakage.

Of the three categories, real losses due to pipe leakage contributes the most to the total volume of NRW. It accounts for more than 70 percent of water losses (Van Zyl and Clayton, 2007).

According to Pedersen et al. (2013) global NRW ranges between 25 to 50 percent of the water that is fed into a country's water distribution network. In 2012, Mckenzie et al. reported that the nationwide annual percentage of NRW lost by South Africa was 36.8%, 25.4% being due to pipe leakage. The financial loss due to NRW, based on the afore mentioned statistics, was calculated to be in the region of R7 billion rand per year. The money lost due to NRW has a detrimental impact on a country's economy. Therefore, reducing the percentage of NRW can greatly benefit a country. In Denmark, water losses were decreased by 30 percent as a result of the implementation of NRW reducing programmes over a 25-year period (Pederson and

Klee, 2013). Denmark currently has an average NRW percentage of 7% and the country's GDP has grown by 40 percent since the implementation of the NRW reduction programmes.

### 2.2.2 PIPE LEAKAGE

Globally, 35 percent of the water that is treated and fed into pipe networks is lost due to pipe leakage (Van Zyl et al., 2013). These real losses in water distribution networks amount to more than 32 billion m<sup>3</sup> per year. These leakages generally occur as a result of pipes that burst due to structural failure of the pipe. If a large constant flow of water is released, which migrates to the ground surface above the pipe, the leak is easy to detect. This phenomenon is known as piping. However, leakages can also occur as background leaks. These leaks are small, often dissipating water into the surrounding soil at a slow enough rate that the water does not migrate to the ground surface and the leak goes undetected. If numerous background leaks exist along a pipeline or in a network, large water losses can take place and the points of leakage may be undetectable. The only indication of leakage is the difference between the volume of water that has been introduced into the water distribution network and the metered volume of water that has been consumed.

### 2.2.3 LEAKAGE PROPAGATION

The behaviour of the zone surrounding a pipe leak point has been investigated by Van Zyl et al. (2013). The results of the research propose that the soil surrounding the leak point can be grouped into three zones, each zone exhibiting different soil-water interaction characteristics. These three zones include:

- a fluidised zone
- a mobile bed zone
- a static bed zone

In the fluidised zone, soil particles are suspended in water that is escaping from a pipe with a high velocity. Soil particles move about freely with the fluid and are transported from the orifice of the leaking pipe to the boundary surface of the fluidised zone. The size of the fluidised zone is dependent on the flow rate of the leaking pipe, while the size of the leaking orifice has no effect. Due to this fact it is speculated that the fluidised zone behaves like a hydraulic jump and energy is dissipated as water exits the pipe through the orifice and enters the soil. This is because water in a pipe flowing at a higher discharge rate would have a greater kinetic energy head component that can be dissipated into the soil creating a larger fluidised zone. It should be noted that in granular soil the fluidised zone can be smaller than in fine soil. Thus, the fluidised zone may not reach the ground surface even under high pipe flow rates. This implies that large pipe leaks can be sustained in granular soil without being detected.

The mobile bed zone surrounds the fluidised zone. It contains particles that have been deposited by the fluidised zone. These particles are closely packed and the inter-particle spaces are filled with liquid. The soil particles, however, are able to move and flow steadily toward the orifice of the pipe where they are picked up by the high velocity water and introduced into the fluidised zone again.

The static zone accounts for the soil that surrounds the mobile bed zone. This soil is unaffected by the water exiting the pipe and does not move.

## **2.3 SOIL PROPERTIES RELEVANT TO FIBRE OPTIC LEAK DETECTION**

### **2.3.1 EXPANSIVE AND COLLAPSIBLE SOIL**

Expansive and collapsible soils are soils that undergoes a change in volume when the soils' moisture content is changed (Khademi and Budiman, 2016). Expansive soils usually contain a type or multiple types of clay minerals. These clay particles have a high affinity to absorb water and expand as a result thereof. Expansive soils have swelling potentials ranging from 10 percent to 2000 percent expansion for highly active clayey soils (Ng and Menzies, 2007).

The expansive potential of a soil is dependent on various factors. These factors are categorised into properties of the soil affecting its behaviour, or physical factors which the soil is subjected to (Mokhtari and Dehghani, 2012). Physical factors include the initial water content of the soil, the drainage boundary conditions, moisture variations and vegetation growing in the soil. The soil properties influencing the expansive potential of the soil are the clay minerals present in the soil, the soil suction due to negative pore pressure, the soil plasticity and the initial dry density of the soil.

The clay mineralogy present in a soil is the main factor contributing to the expansive potential of a soil. Clay particles are plate-like in shape and have a high surface area to volume ratio, termed specific area, which means that their behaviour is dominated by surface interaction forces (Knappett and Craig, 2012). On a micro-structural level these platelets are formed by units of silicon-oxygen tetrahedrons or aluminium-hydroxyl octahedrons. Silicon-oxygen units combine by sharing oxygen ions to form silica sheets and aluminium-hydroxyl units combine by sharing hydroxyl ions to form gibbsite sheets. The silica sheet retains a net negative charge due to valency imbalance whereas gibbsite sheets are electrically neutral. Silica and gibbsite sheets bond to each other and form layered structures by stacking on top of one another. The layered structure is not strongly bonded and because of the valency imbalance on the surface of the silica sheets there is a potential for water to enter between two silica sheets and form a hydrogen bond. Other chemicals, such as potassium and magnesium, can replace the silicon or aluminium atoms by isomorphous substitution. This creates further charge imbalances

which can either increase or decrease the sheet's affinity for water. This process, by which water enters between clay platelets, is what gives rise to the swelling nature of a clayey soil.

Collapse of soils due to wetting also poses a threat when a soil's moisture content is changed. Soils that are compacted at dry of optimum conditions will inevitably collapse upon wetting (Li et al., 2016). This is attributed to the metastable open flocculated structure that is attained when soil is compacted in a dry of optimum state. The collapse is triggered by the loss in shear strength that exists between the particles as the matric suction is reduced due to an increase in moisture content. The volume change of collapsible soils is due to a change in either, or both, net stress and matric suction, with soils experiencing their maximum settlement as their degree of saturation approaches 100 percent.

### **2.3.2 PROBLEMS ASSOCIATED WITH SOIL MOISTURE CONTENT CHANGES**

Pipe leakages, depending on the intensity of the leakage, can significantly alter the moisture content within a soil. Because of this, soil expansion poses a threat to various types of infrastructure. Due to the swell-shrink nature of expansive soils, stresses and deformations can be imposed onto building foundations, the substructures of pavements and buried pipelines. This is due to a phenomenon called the soil heave that acts on these structures during soil expansion (Khademi and Budiman, 2016). Differential settlement of structures can occur if the soil under selected sections of a structure shrinks as its water content is reduced, while other sections of the soil retain the same moisture content undergoing no volume change. These stresses and deformations, if large enough, can cause cracking of concrete and brickwork in buildings, pipe breaks and failure of pavements. Li et al. (2013) have reported that the estimated annual costs of damage due to expansive soils in the United States, China and the United Kingdom are US\$15 billion, US\$15 billion and £400 million, respectively.

Another potential problem of changes in soil moisture content is that the shear strength of a soil is dependent on the degree of saturation. Soils that exist under infrastructure can be unsaturated with part of their shear strength being due to the matric suction that exists between soil particles. Vanapalli et al. (1996) developed a mathematical relationship for determining the shear strength of an unsaturated soil using Soil Water Characteristic Curves and the Mohr-Coulomb Effective Stress State Theory. The mathematical model showed that soils exhibit their lowest values of shear strength when they are fully saturated.

## **2.4 STRUCTURAL COMPOSITION OF FIBRE OPTIC CABLES**

Fibre optic cables are thin hollow glass cables that are able to receive an input light signal, transfer it along their length and deliver the same signal as an output to an optical readout device (Mark and Shirk, 2018). An optic fibre transmission system consists of:

- an optical transmitter,
- an optical receiver,
- the fibre optic cable and
- connectors

The optical transmitter and receiver work in tandem with each other. The transmitter converts an electrical signal into an optical signal and sends it through the fibre optic cable as an infrared light signal. The optical receiver then interprets the light signal that it receives from the transmitter, converting it back from a light signal to an electrical signal.

The fibre optic cable is made up of three layers, the core, cladding and coating. The core is a hollow tube made of silica glass through which the optical signal travels. The cladding is the second layer surrounding the core and is made of silica glass as well. The cladding layer has a lower refractive index (the ratio of the speed of light travelling through a medium to the speed that light travelling through a vacuum) than the core layer. The light travelling through the core is thus reflected off the core-cladding interface back into the core layer. The cladding layer thus serves to guide the light through the cable by the process of total internal reflection, enabling the light signal to travel along the cable through the core without escaping. The coating is the outermost layer which protects the fibre optic silica core and cladding from damage and also prevents unwanted light from entering into the core.

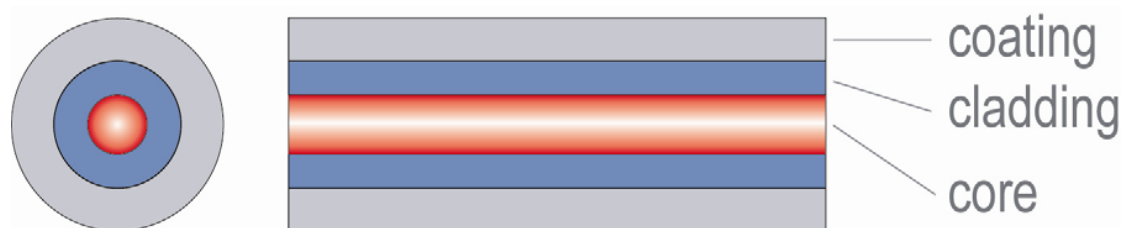


Figure 2-1. The structural layers comprising a fibre optic cable. Taken from Mark and Shirk (2018).

The connectors join the fibre optic cable to the transmitter and the receiver. They can also be used to join unconnected cables together. Two types of connections are available, fusion splicing and physical connectors. Fusion splicing involves welding together two ends of a fibre optic cable. The advantage of this method is that there is very little insertion loss (loss of the light signal as it moves through a connector) as light moves through a splice. However, this welded material is fragile and must be reinforced to prevent damage. Physical connectors are placed onto an open end of a fibre optic cable and behave like plugs. The male and female adapters can be plugged into one another at any time to connect two separate cables together, or a connector can be plugged into a transmitter or receiver as a temporary connection. The end of the cable housed by the connector is robust and protected from the external environment. Connectors can be plugged in and out of each other and switched numerous times without damaging the fibre optic cable being housed inside. The disadvantage of a

physical connector is the higher insertion loss that is experienced as light passes through it compared to a spliced connection. It is thus important to ensure that the fibre optic lead in a physical connector is cleaned properly before it is plugged into another connection.

An important occurrence to note is the gradual drop in strength of the light signal as it travels through the fibre optic cable. This is called attenuation. The attenuation is measured in dB/km and is a function of the wavelength of the light signal. Experimentation has shown that a wavelength of 1550nm is optimal as it ensures the smallest attenuation of the light signal as it travels through the cable (Mark and Shirk, 2018). If too much attenuation of the optic signal strength occurs as it travels along the cable, then the signal that enters the receiver will be uninterpretable. To circumvent this problem, signal amplifiers can be placed along the length of the cable to rejuvenate the signal strength where critical amounts of attenuation have taken place.

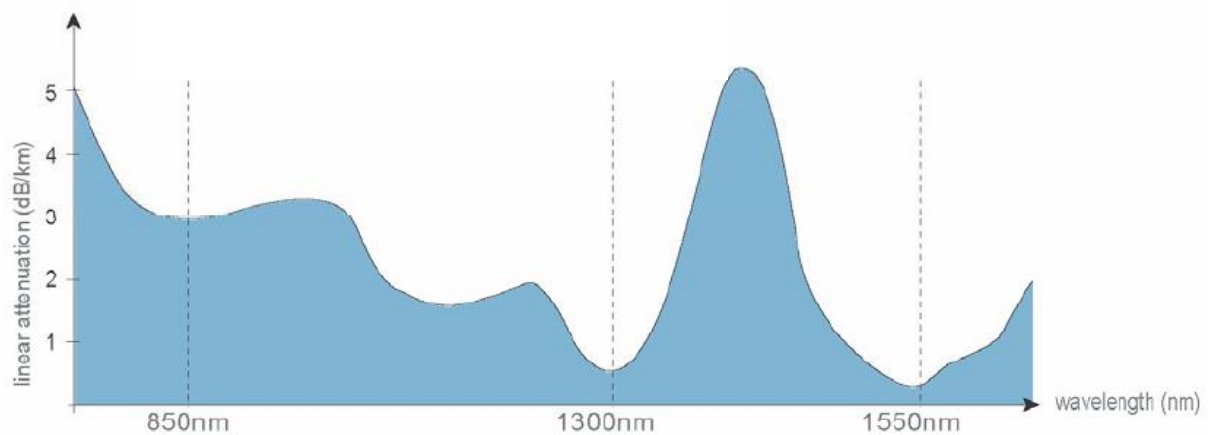


Figure 2-2. A graph showing the attenuation of light of different wavelengths as it travels through a fibre optic cable. Taken from Mark and Shirk (2018).

Fibre optic cables have been used as a telecommunication medium since the 1960s when the advancement in laser technology and the creation of the low-loss optic fibre (fibre optic cables made from silica with low light attenuation potentials) made fibre optic telecommunication economically viable (Grattan and Sun, 1999). This was due to their ability to transmit information at higher bandwidths over longer distances than alternatives such as copper. Experimentation with fibre optics in the 1970s led to the development of techniques that use fibre optic cables as strain measurement devices.

#### 2.4.1 USING FIBRE OPTIC CABLES TO MEASURE STRAIN

When a segment of a fibre optic cable is subjected to a mechanical stress in the longitudinal or lateral direction, the segment experiences strain which changes the physical properties of the optic fibre (Motil et al., 2015). Fibre optic readout devices, called interrogators, are able to

measure the changes in these physical properties. The changes in these measured quantities can be used to back calculate the values of strain that occur in the fibre optic cable.

One of these affected properties is the average refractive index of the cable (the ratio of the speed of light travelling through a medium to the speed of light travelling through a vacuum) whose change can be quantified to calculate the strain experienced by the cable. Another property affected by strain is the speed of acoustic sound wave propagation through the cable. By measuring the change in acoustic wave propagation speed through a cable, the strain that the cable undergoes can be calculated by determining what strain is required to cause the change in acoustic wave propagation speed. A technique which directly measures the change in length of the cable is the Bragg Fibre Grating measurement technique. A periodic UV light pattern is shone through the cable which inscribes permanent refractive index gratings onto the inside surface of the cables. When an input light signal is shone into the cable, these gratings reflect the input light back with a specific period dependent on the refractive index of the grating. When the cable is strained the return period is altered. The change in return period is used to quantify the strain imposed on the cable.

The use of fibre optic cables as strain meters is advantageous as they are lightweight and easy to attach to the measurand, having little or no effect on it. They are able to withstand harsh working environments and are immune to radiation and electromagnetic interference. This is because the optic cables are transmitting light and do not conduct an electric current (Grattan and Sun, 1999). Furthermore, measurement of strain in fibre optic cables is made simple by the fact that the cable acts as the sensor and it relays the sensed data back to the interrogator (Motil et al., 2015).

#### 2.4.2 DISTRIBUTED FIBRE OPTIC SENSING

An important application of the use of fibre optic cables is distributed fibre optic sensing (Grattan and Sun, 1999). Distributed fibre optic sensing is a measurement technique that allows strain measurements to be taken at any point along the entire length of the cable. The fibre optic readout devices, that send a light signal through the cable and receive a response signal back, must be designed to take readings that are spatially discriminated along the length of the cable. This means that the readout device, based on the data received from the response signal, is able to determine the strain that the fibre experiences at a specific distance along its length, and furthermore, is able to do this for any point along the cable's length.

The parameters that define the performance of a distributed fibre optic sensing system are the resolution, spatial resolution, dynamic range and distance range (Galindez-Jamiy and Lopez-Higuera, 2012). The resolution is the smallest detectable change in the quantity being measured that the interrogator is able to pick up. The spatial resolution is the smallest distance between two points along the fibre optic cable over which a single change can be detected.

The dynamic range is defined as the loss in optical link between the interrogator and the measurand, due to attenuation, within which the interrogator is able to make a meaningful measurement. The distance range is the distance over which the fibre optic cable is able to give measurements within a stated uncertainty range.

Distributed fibre optic sensing techniques employ optical time domain or frequency correlation techniques to function (Galindez-Jamioy and Lopez-Higuera, 2012). This technique was originally used to determine the locations of faults in cables (Grattan and Sun, 1999). The location of the fault was calculated by knowing how long a pulse, having a certain wavelength, took to propagate through a cable. This technique was extrapolated to determine the location of a measurand interaction with a fibre optic cable to create a sensing system. Distributed fibre optic sensing uses linear and non-linear effects that take place in the silica layers of the fibre which exhibit distinctive responses to changes in external measurands. The non-linear effect that will be discussed in this chapter is the Brillouin effect.

### 2.4.3 THE BRILLOUIN EFFECT IN FIBRE OPTIC CABLES

The Brillouin effect is a non-linear phenomenon that takes place due to the interaction between an electromagnetic wave and the molecular structure of the matter with which the electromagnetic wave interacts (Galindez-Jamioy and Lopez-Higuera, 2012). In the presence of an electric field materials have a tendency to become compressed and thus the density of that region of material changes. This is called the electrostriction effect. A light wave is a wave of electromagnetic radiation which generates an electric and a magnetic field perpendicular to each other as the light wave travels. As an incident wave of light travels over matter the electric field generated by the light wave causes the matter to become condensed where the electric field is strongest. This occurrence is illustrated in Figure 2.3. This modulation of matter that has been condensed and matter of normal density, is called an acoustic phonon.

The occurrence of the acoustic phonon generates a periodic modulation in the refractive index of the material, the refractive index being changed where the material has been condensed. The acoustic phonon provokes backscattering of light in the same manner as a Bragg grating. Energy is needed for the formation of the acoustic phonon which is derived from the incident light wave. Part of this energy is absorbed by the material in forming the acoustic phonon, while the remainder of the energy is emitted as a backscattering light wave of lower frequency than the incident light wave. The difference in the frequency of the incident light wave causing the acoustic phonon formation and the backscattered light is called the Brillouin Frequency Shift (BFS) (Motil et al., 2015).

The value of the BFS is dependent on the acoustic phonon and the structure of the medium in which it develops (Galindez-Jamioy and Lopez-Higuera, 2012). When the medium material is subjected to an external factor, such as a stress or a change in temperature, the density of the

material that is subject to the external factor will change and the material will strain. This change in material density will result in a change in the BFS from the original BFS due to the material being affected by the external stress or change in temperature. The change in BFS can be used to back calculate the strain that the material underwent.

The Brillouin effect can be used to create distributed fibre optic sensors that range over 100km. Standard telecommunication fibre optic cables can be used as sensors as the Brillouin effect can be induced in any material. The typical BFS in fibre optic cables is of the order of 10-11 GHz. The Brillouin scattering process can be induced in fibre optic cable in two ways: spontaneous Brillouin scattering and stimulated Brillouin scattering. In spontaneous Brillouin scattering an incident light wave is introduced into a fibre optic cable through only one cable end. The incident light produces acoustic phonons which backscatter light in the opposite direction to the direction of travel of the incident light. This backscattered light has been downshifted due to the Brillouin effect. In stimulated Brillouin scattering, light is introduced into both ends of the cable. These waves are called the forward-propagating pump wave and the backward-propagating probe wave. The pump wave and the probe wave have different frequencies. The electric fields of the two light waves superimpose and where strong electric fields occur constriction of the fibre optic cable material takes place creating an acoustic phonon. The acoustic phonons then backscatter downshifted light in the direction of the probe light wave (Galindez-Jamioy and Lopez-Higuera, 2012).

The BFS that occurs in the fibre optic cable is dependent on the material structure of the silica in the cable. When the cable is attached to a measurand, and part of the measurand undergoes strain due to an external stress (for example, water entering the soil from a leaking pipe), a portion of the cable will strain with the measurand. On a microstructural level the density of silica in the affected portion of the cable will change due to the strain. This will cause the BFS in the strained region of the cable to differ from the unstrained BFS that the cable would otherwise experience. The value of the difference between the strained and unstrained BFS is used to back calculate the strain that the cable, and in turn the measurand, undergoes.

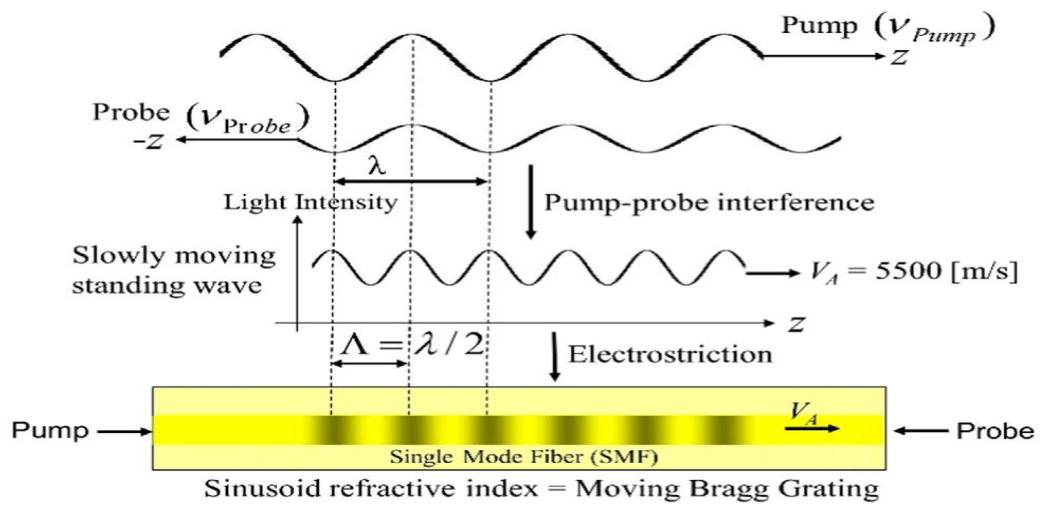


Figure 2-3. Mechanism whereby acoustic phonons are created by counter-propagating light waves in a fibre optic cable. Taken from A. Motil et al.

## **3 LABORATORY FIBRE OPTIC LEAK DETECTION STUDY**

### **3.1 INTRODUCTION**

This chapter discusses the experimental setup implemented to simulate underground pipe leakages. The measuring instrumentation used, the different soils in which leakages were simulated and how the soil was housed will be discussed. The testing methodology will be explained.

- The instrumentation used included three different fibre optic cables, a BFS strain interrogator and a fibre optic multi-channel four-way splitter.
- Three different types of soil were used. A coarse silica sand, a fine silica sand and a red clayey soil.
- The soil and cables were housed and tested in the laboratory in a 2m long concrete mould.

### **3.2 MEASURING INSTRUMENTATION**

#### **3.2.1 FIBRE OPTIC CABLES TESTED**

The experimental setup was designed around the use of fibre optic cables to detect the strain induced in a soil when the soil moisture content changes. Three different fibre optic cables were used the experimental setup:

- a standard telecommunication cable (17m long),
- a cable designed specifically to be used as a mechanical strain sensor (100m long),
- a cable sensitive only to temperature change (100m long).

The standard telecommunication cable was made up of six optic fibres running through a sheath of soft rubber. At one end of the cable, four optic fibre ends were spliced to connector cables attached to physical connectors that could be plugged into the BFS interrogator. At the opposite end of the same cable, two pairs of optic fibres were spliced to form two continuous fibres that looped out of and back into the end of the cable. Thus, in these two fibre pairs, an optic signal entered the fibre through a connector and propagated forward through the length of the cable. The signal then travelled through the looped splice at the opposite end, propagated back through the cable again and exited the fibre through the other connector (refer to Figure 3.13). This caused the output BFS profiles for this cable to be mirrored about the looped splice at the end of the cable (refer to Figure 4.1). The optic fibres were not attached to the inside of the rubber-sheathing. However, friction was present between the optic fibre and the sheath. This implied that if the rubber-sheathing underwent strain, the optic fibre inside might not have undergone the same amount of strain as the sheath.

The mechanical strain sensor cable consisted of a single optic fibre running through a hard, stiff plastic sheath. In this cable the optic fibre was securely attached to the plastic coating along the cable length. This ensured that the strain experienced by the plastic sheath would directly transmit onto the optic fibre so that accurate strain outputs would be measured by the cable. At each end of this sensor cable, the optic fibre was spliced to connector cables attached to physical connectors. When the connectors were plugged into the BFS interrogator, the cable formed a continuous loop. Thus, the optic signal propagated in one direction through the cable in this configuration. The splices connecting the optic fibre to the connector cables had been encased in a stiff protective surround.

The temperature sensitive cable consisted of two optic fibres running through a stiff plastic sheath. The optic fibres and the sheath were mechanically isolated from each other, thus the strain experienced by the plastic sheath would not be transmitted onto the optic fibre. Therefore, the only mechanism by which the optic fibre could strain was through thermal expansion or contraction. As with the mechanical strain sensor cable, the temperature sensitive cable had all four of its optic fibres ends spliced to connector cables attached to connectors, and optic signals propagated in one direction only through the cable.

Throughout the remainder of this report (all literature and Figures), the telecommunications cable, mechanical Strain Cable and Temperature Cable will be referred to as the telecom cable, Strain Cable and Temperature Cable, respectively.

### 3.2.2 BRILLOUIN FIBRE OPTIC STRAIN INTERROGATOR

The strain interrogator used in the experimental setup was a fibrisTerre fTB series fibre-optic sensing system. In addition, the interrogator was connected to a fibrisTerre optic fibre multi-channel splitter. The three different fibre optic cables could therefore be connected to the interrogator at the same time. The interrogator model uses Stimulated Brillouin Scattering to determine the BFS at a specific point along the length of a fibre optic cable. To perform distributed sensing, the interrogator employs Brillouin optical frequency domain analysis to create a BFS profile of the entire cable length. A software package, fTView, was used to control the interrogator and interpret the results.

The BFS profile is created as follows:

- The interrogator first determines the length of the cable it is monitoring by injecting an optical signal into one end of the optic fibre and measuring the time it takes for the signal to be received at the other end.
- The interrogator then performs a process called a frequency sweep. In this process two optic signals, of different frequencies, are injected into the optic fibre, one into each end. The two optic signals are injected into the fibre at different times so that they coincide with each other at a specific ordinate along the fibre length. When the

optic signals coincide, Stimulated Brillouin Scattering occurs at that point. The downshifted light travels back to the interrogator and the BFS is logged for the ordinate. The interrogator repeats this process every 5cm along the cable length and can measure BFS in a cable up to 30km in length.

- Once the BFS has been logged for the entire length of the cable the interrogator sends the logged data to fTView and a BFS profile can be plotted.

fTView is able to export BFS profiles to a text file format, which can then readily be imported into a numerical analysis package, such as Excel.

### 3.3 TESTED SOILS

To bury the cables, three different types of soils were used. A coarse sand, a fine sand and a clayey soil. This was done to investigate how soils, with different particle size distributions (PSD), would affect the BFS output that the cables would produce. PSDs were created by passing samples from each of the soils through sieves of different sizes. The percentage of soil that was retained on each sieve was calculated, comparing the volume of soil on the sieves and the total volume of the soil sample.

Soils with finer particles tend to undergo larger amounts of strain and generate large changes in suction when their moisture contents are changed. Soils with larger particles tend to undergo lesser amounts of strain as they do not produce changes in suction pressure as large as fine grained soils when their moisture contents are changed.

#### 3.3.1 COARSE SAND

The coarse sand used was centrifuge modelling sand composed of silica.

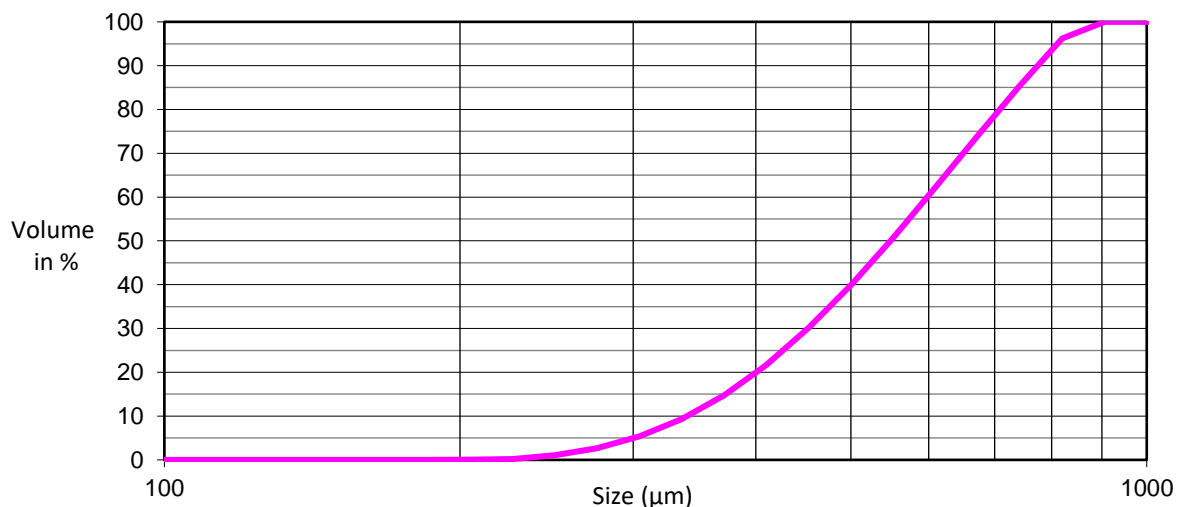


Figure 3-1. Particle size distribution of the coarse sand.

The particles making up the coarse sand are all larger than 200 $\mu\text{m}$  and smaller than 900 $\mu\text{m}$ . This soil was thus expected to have a low affinity for water, thus large suction would not be expected to be generated as the saturation ratio ( $S_r$ ) of the soil is decreased.

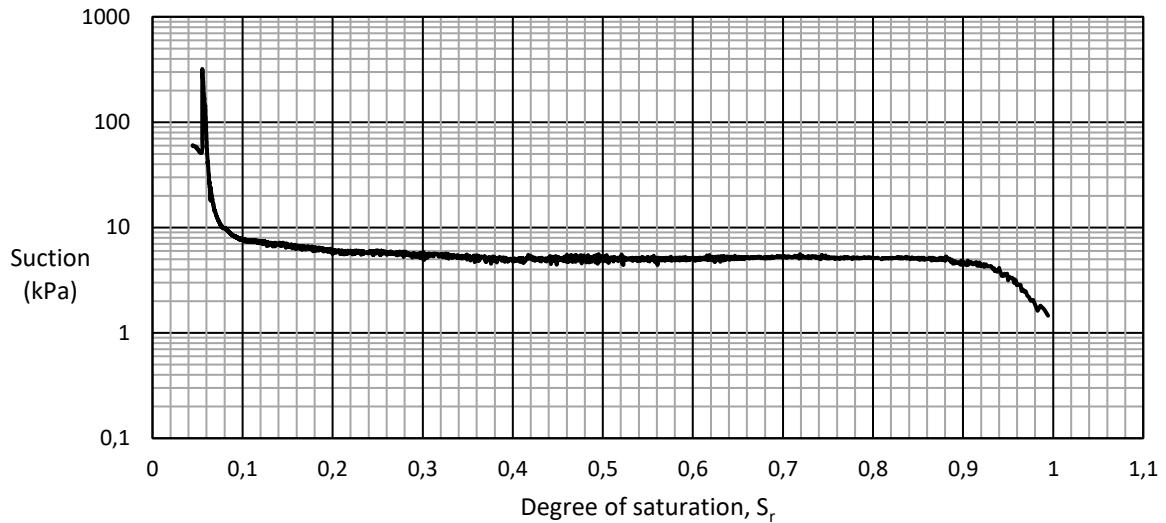


Figure 3-2. Soil-water retention curve for the coarse sand. Taken from Le Roux (2019).

Figure 3.2 is a plot of the coarse sand's soil-water retention curve (SWRC) showing the suction pressure that the soil generates given a specific degree of saturation ( $S_r$ ). The SWRCs were measured using tensiometers. A tensiometer measures the suction pressure of the water in a soil sample as the  $S_r$  of the soil is decreased. As can be seen, the coarse soil generates non-uniformly increasing suction as the  $S_r$  is decreased from 1 to 0.9. The generated suction remains fairly constant until the  $S_r$  becomes 0.2 where it begins to increase gradually. At a  $S_r$  value of 0.08 the suctions increase rapidly before cavitation occurs at a  $S_r$  of 0.058. Cavitation of the tensiometers occurs at the  $S_r$  at which the tensiometers measuring the suction dried out due to the moisture content of the soil becoming too low.

### 3.3.2 FINE SAND

The fine sand used was also a centrifuge modelling sand composed of silica.

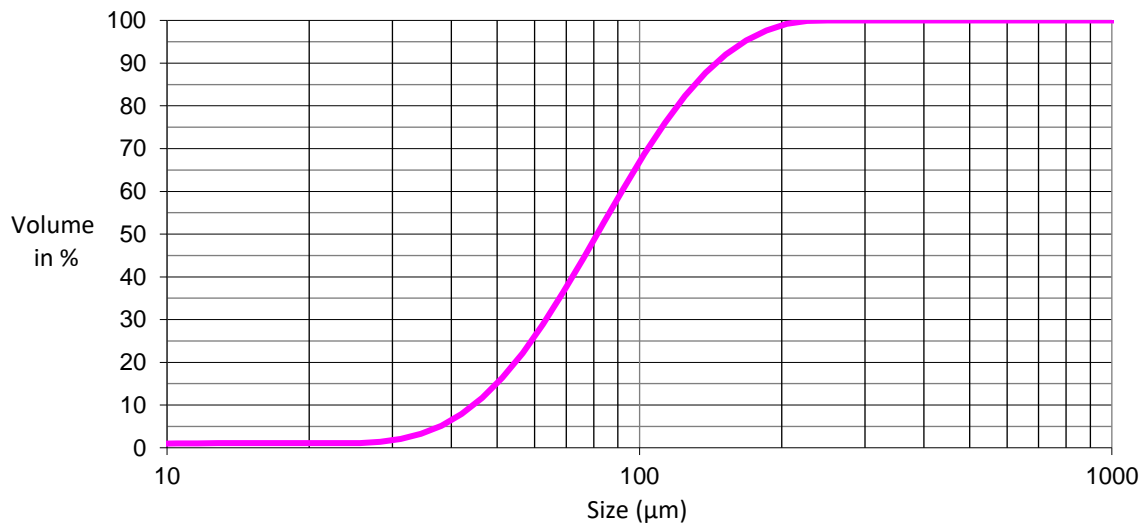


Figure 3-3. Particle size distribution for the fine sand.

As can be seen in Figure 3.3, 99% of the particle size distribution lies within 20 $\mu\text{m}$  and 200 $\mu\text{m}$ . Fine particles would thus be expected have a high affinity for water and would generate a large amount of suction pressure, but not as much as a clayey soil with even finer particles.

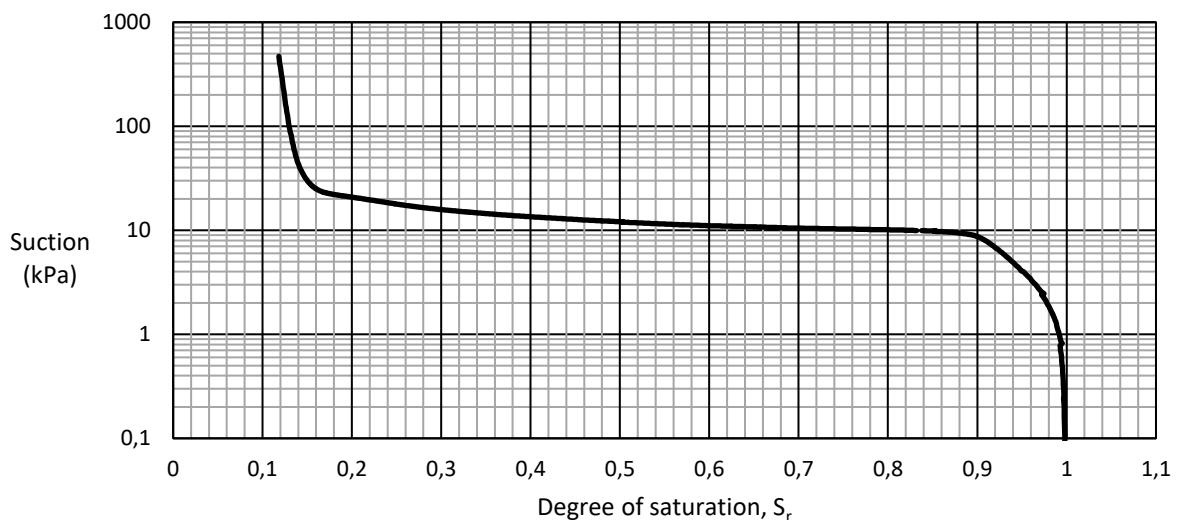


Figure 3-4. Soil-water retention curve for the fine sand. Taken from Garfield (2019).

According to the SWRC of the fine sand, Figure 3.4, suction pressure begins to be generated rapidly as the  $S_r$  falls below 1, until a  $S_r$  value of 0.88. Hereafter the suction pressure increases gradually as the  $S_r$  is reduced, until a  $S_r$  of 0.16. Here the suction pressure begins to increase rapidly until cavitation pressure is reached at a  $S_r$  value of 0.12.

### 3.3.3 RED CLAYEY SOIL

The red clayey soil used was taken from The University of Pretoria, LC de Villiers Campus where 2km of the telecom cable was buried for later field testing once the laboratory work had been completed.

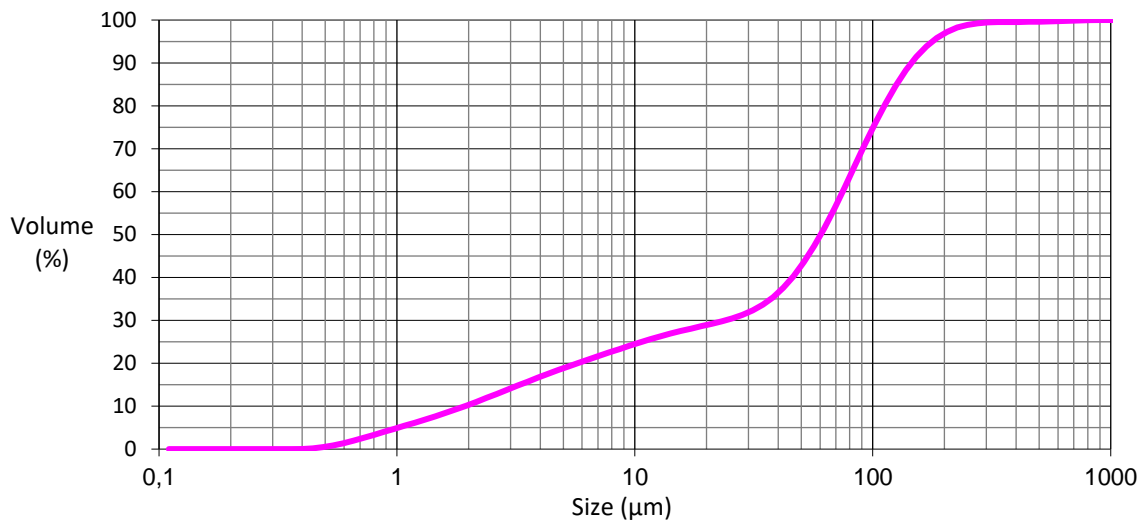


Figure 3-5. Particle size distribution for the red clay.

As can be seen in Figure 3.5, the red clay is comprised of 75% particles that are smaller than 100μm. Furthermore 25% of the particles range between the sizes of 0.5μm and 10μm. This soil can therefore be expected to have a high affinity for water and a change in moisture content will induce large changes in suction pressures. This can be seen in the SWRC below.

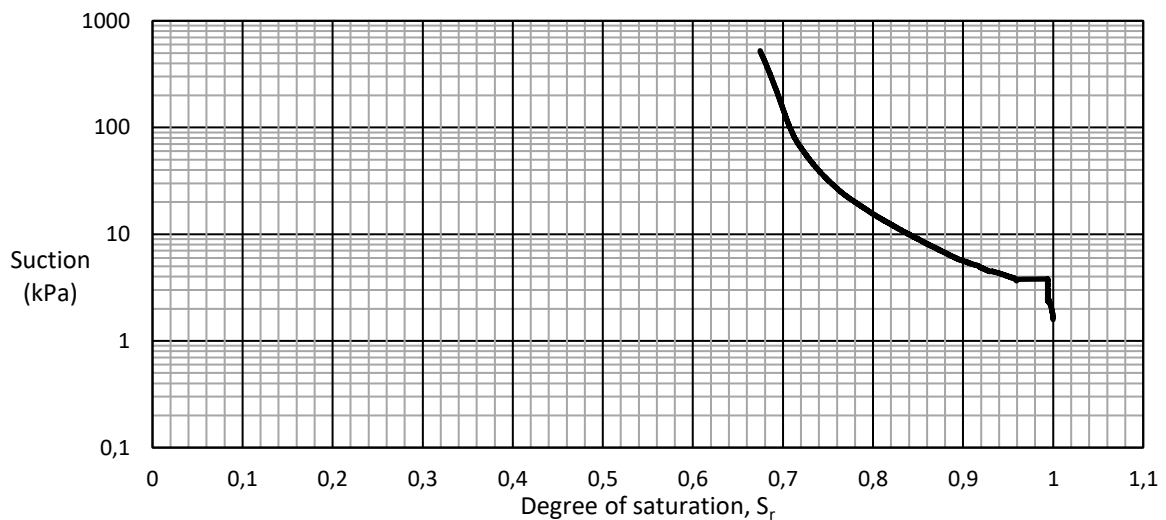


Figure 3-6. Soil-water retention curve for the red clay.

At a degree of saturation of 1 the soil already begins to generate suction pressures. At a  $S_r$  of 0.96 larger suction pressures start to be generated until the cavitation pressure is reached at a  $S_r$  of 0.67.

Figures 3.7 and 3.8 below provide the PSDs and the SWRCs for the three testing soils grouped together so that the soil properties in question can be compared.

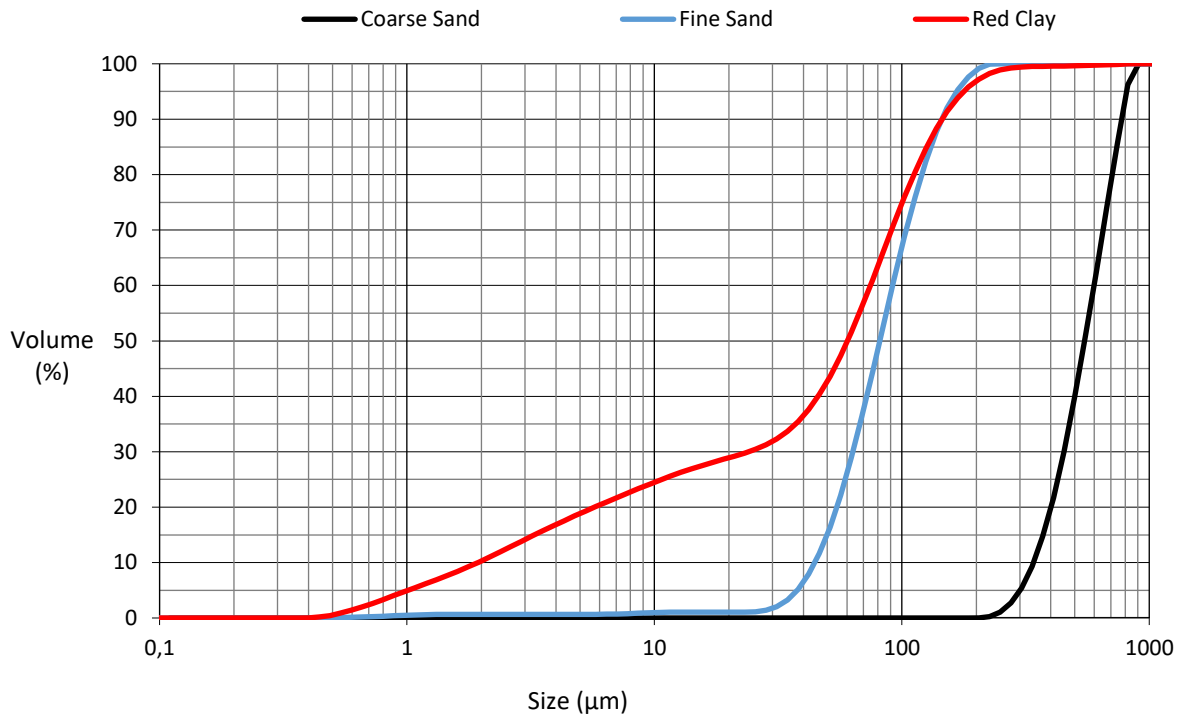


Figure 3-7. Particle size distribution curves for the three soil types used for the experiment.

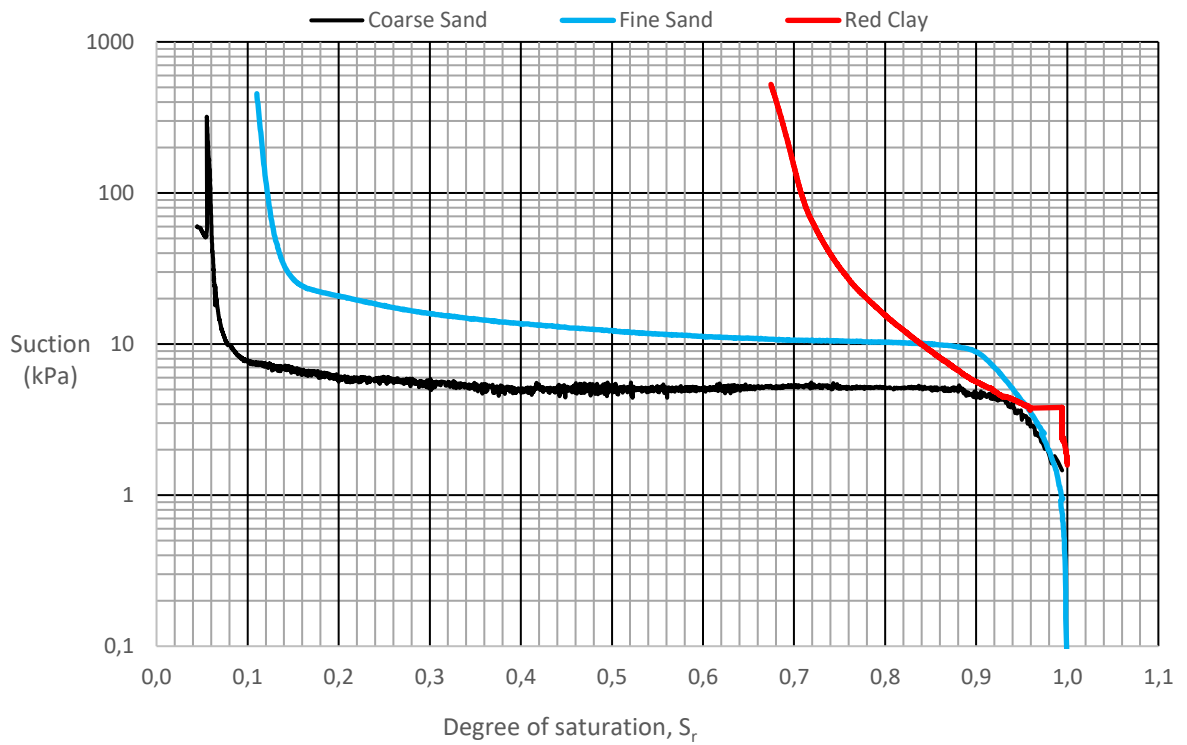


Figure 3-8. Soil-water retention curves for the three soil types used for the experiment.

### 3.4 SOIL AND CABLE HOUSING

To create an environment where the three cables could be buried in different types of soil, a 2000 x 220 x 150mm concrete mould was modified to allow the fibre optic cables to run through the soil without being affected at the mould boundaries. To achieve this, the ends of the mould were replaced with wooden planks. Two planks were cut to a size of 150 x 250mm. Thereafter, three holes were drilled through at a spacing of 37.5mm, and a height of 100mm from the plank bottom to allow the three cables to pass through, as can be seen in Figure 3.9. This ensured that the cables would run straight, at a constant level, through the mould. This cable system mimicked how a cable would be laid in the ground congruent with a pipeline. The planks were clamped in the mould using a G-clamp as can be seen in Figure 3.11.

Six clamps were made in order to perform tests with both tensioned and non-tensioned cables, as shown in Figure 3.10. Three clamps were used to brace the cable against a wooden plank at one mould end. The other three clamps were attached to the cables as they exited the mould on the opposite side. Weights were hung on these clamps to tension the cables. The clamps were made from small blocks of plastic. The blocks, 40 x 10 x 10mm in dimension, had a hole drilled through each side to allow a bolt to pass through. Two blocks were then bolted together. A hole was drilled through the middle of the blocks where the faces meet in order to feed a cable between the two blocks.

In addition to being able to hang weights, it was also important to prevent the cable from undergoing excessive bending at the edge of the mould. A minimum bending radius of 100mm was required to prevent unwanted BFS from taking place at the site of bending and to ensure that the signal did not undergo too much attenuation. To negate this problem, a PVC pipe of radius larger than 100mm was fitted just under the holes where the cables exited the mould, as can be seen in Figure 3.12. The cables were thus prevented from bending with a radius smaller than 100mm.



Figure 3-10. The wooden planks used to insert the fibre optic cables into the mould.



Figure 3-9 .The clamps that were made to attach to the cable to hang



Figure 3-11. G-clamp used to secure wooden plank in the mould.



Figure 3-12. PVC pipe that was cut and fitted under the cables to



Figure 3-13. Showing the experimental setup in the laboratory.

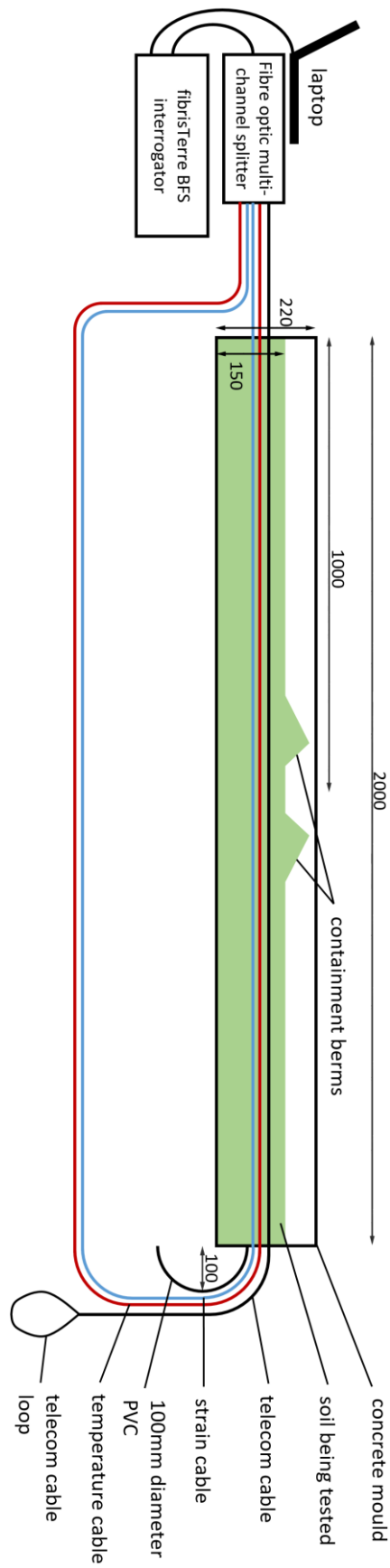


Figure 3-14. A schematic drawing (side view) of the experimental setup (dimensions in mm).

The fibre optic cables depicted in this figure are at different levels. This was done to depict each different cable housed in the mould. In the actual experimental setup the cables were at the same level (100mm) in the mould.

### **3.5 EXPERIMENTAL METHODOLOGY**

To determine how the three cables would react to external stresses being applied to them, a loading-unloading cycle was imposed onto each of the cables. While the cables were threaded through the concrete mould, they were systematically loaded and unloaded by placing weights on the clamps attached to the cables hanging over the PVC pipe, as shown in Figure 3.12. First BFS profiles were recorded for the three cables while they were not loaded. Thereafter, each cable was loaded with a 2kg weight and BFS profiles were recorded with the cables under tension. This process was repeated using 4kg and 6kg loads, which made up the loading phase of the cycle. Thereafter BFS profiles were consecutively logged for 4kg, 2kg and 0kg loads, constituting the unloading phase of the cycle.

Six leak simulations were performed in total. Two simulations were performed on each type of soil. The two tests performed on each soil type included a non-tensioned test and a tensioned test. During the non-tensioned tests, the cables were buried in the soil with no axial load applied to them. In the tensioned tests, a 2kg weight was used to apply an axial load to each cable. This was done to determine how the cables would respond to a pipe leak if they were buried with residual in situ axial tension, or buried under no tension.

To simulate pipe leakages, the following procedure was used:

- Each cable was put under tension using a 2kg weight placed on the clamp hanging over the PVC pipe. The concrete mould was then filled with soil 200mm deep. Thus the cables were buried 100mm from the bottom of the mould and covered by 100mm of soil. This ensured that the cables would run straight in the soil, devoid of kinks that might impede the pathway of the optical signal as it travelled through the mould.
- Thereafter the 2kg weights were either removed, or left hanging on the cables, depending on whether a tensioned or non-tensioned test was being performed.
- Once the cables were buried, BFS profiles were taken for each cable every two hours over a 24-hour period. These profiles constituted the baseline of the cables against which subsequent readings could be compared.
- Two small containment berms were made in the centre of the mould, as depicted in Figure 3.13, between which water could be poured to simulate water leaks. The containment berms ensured that the water poured would not simply run to the sides over the surface of the soil, but be concentrated into one region.

- To simulate a leak, two litres of water was poured between the embankments. Thereafter BFS profiles were recorded at ten minutes intervals over ninety minutes for each cable in order to observe the soil movement as the water propagated through the soil.
- BFS profiles were then logged for each cable every two hours for 24 hours to obtain baseline readings for the wet soil

### 3.6 EXPERIMENTAL RESULTS

This section serves to discuss the outcomes of the experiments that were performed and explain why the results were obtained by linking the results to the fundamental principles laid out in chapter two.

The general layout of the BFS profile generated by the interrogator is explained in order to familiarise the reader with its structure.

The results of the calibration exercise will be discussed, followed by the basic behaviour of the fibre optic cables over a 48-hour cycle. Thereafter, the effect of changing the soils' moisture content on the BFS of a fibre optic cable, the influence of differing soil types, the use of different fibre optic cables and pre-tensioning of cables will be discussed.

#### 3.6.1 BFS PROFILE EXPLANATION

Figure 3-15 is a graph of the BFS plotted against the cable length for the telecom cable.

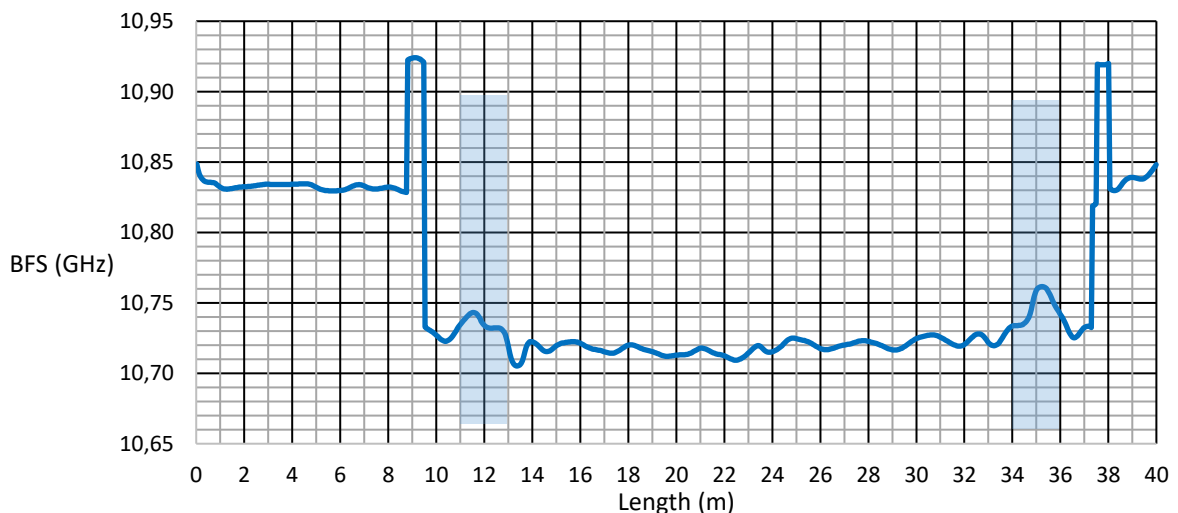


Figure 3-15. A plot depicting a typical BFS profile for the telecom cable.

The BFS occurring throughout the length of the cable is not constant, due to the non-uniform material properties of the silica comprising the optic fibre. The shaded block over the BFS profile signifies the region of the cable that was buried in soil.

In Figure 3-15 the segments from 0m to 8.5m and 38m to 40m, where the BFS is at a value between 10.75GHz and 10.85GHz, the cable that is being read is the connector cable that is plugged into the interrogator. The sudden jumps in BFS that occur from 8.5m to 9.5m and 7.5m to 38m indicate the position of the splices that connect, in this case, the telecom cable to the connector cables. The section of the graph between the splice jumps from 9.5m to 37.5m is the BFS along the telecom cable optic fibre.

The BFS profile of the telecom cable segment, and even the connector cable, is not uniform. This is due to the material properties of the fibre optic cable varying along the length of the fibre. The shape of the baseline BFS profile, however is not important. What is important is the change in BFS that is measured relative to a baseline BFS reading. Figure 3-16 illustrates this argument.

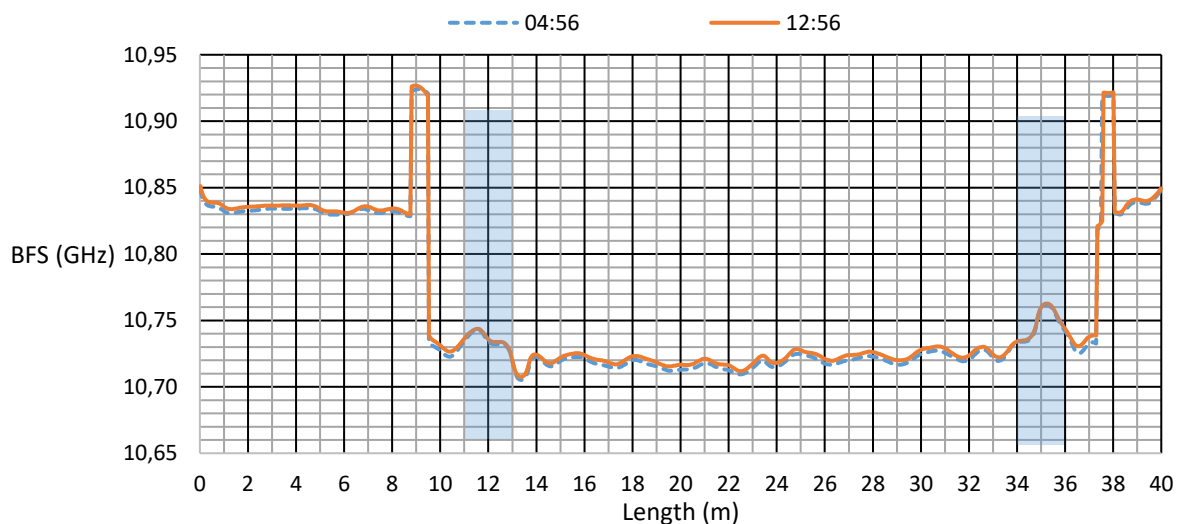


Figure 3-16. BFS profiles for the telecom cable.

One BFS profile was taken at 4:56 in the morning, the other was taken at 12:56 in the afternoon on the same day.

The BFS profiles plotted above in Figure 3-16 for the telecom cable were taken at 04:56 in the morning and 12:56 in the afternoon. These two times are on opposite ends of the daily temperature range. Due to the fact that the fibre optic cable will undergo thermal expansion and contraction, the fibre will strain with a change in temperature causing the BFS to change as well. By magnifying the plot, it can be seen that the BFS profile has shifted upward, relative to the 4:56 plot, due to the increase in ambient temperature from 4.56 to 12.56.

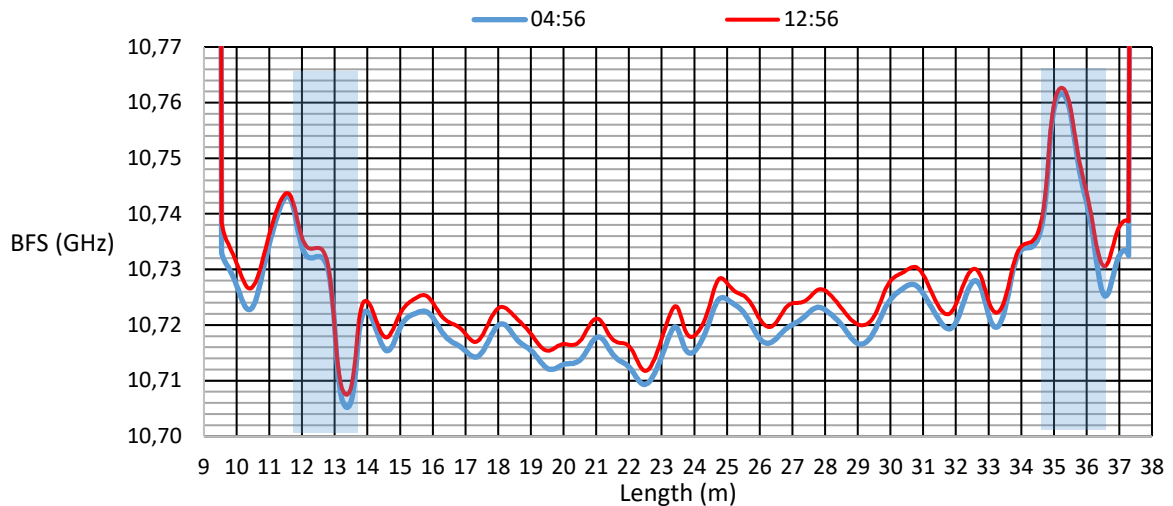


Figure 3-17. A magnified plot of the same BFS profile depicted in Figure 3-16.

The BFS axis has been limited to values between 10.7GHz and 10.75GHz. The length axis has been limited to values between 9m and 38m, where the splices occur.

It is important to note that the upshifted BFS profile (12:56) has the same shape as the reference profile (04:56). However, if a localised disturbance takes place, then only a portion of the BFS profile changes shape. The rest of the profile remains unchanged. By comparing a BFS profile, containing a localised disturbance, against a baseline profile, strain in the fibre optic cable can be detected due to the change in BFS between the two profiles.

### 3.7 CALIBRATION EXERCISE UNDER MECHANICAL STRAIN

#### 3.7.1 RESPONSE OF THE TELECOM CABLE

Placing a load on the fibre optic cable will cause the cable to strain, either elastically, or plastically, depending on whether the yield strength on the cable is reached under the given load. When the optic fibre is strained, the BFS of the fibre, at the localised point of strain, will change proportionally to the amount of strain that is applied.

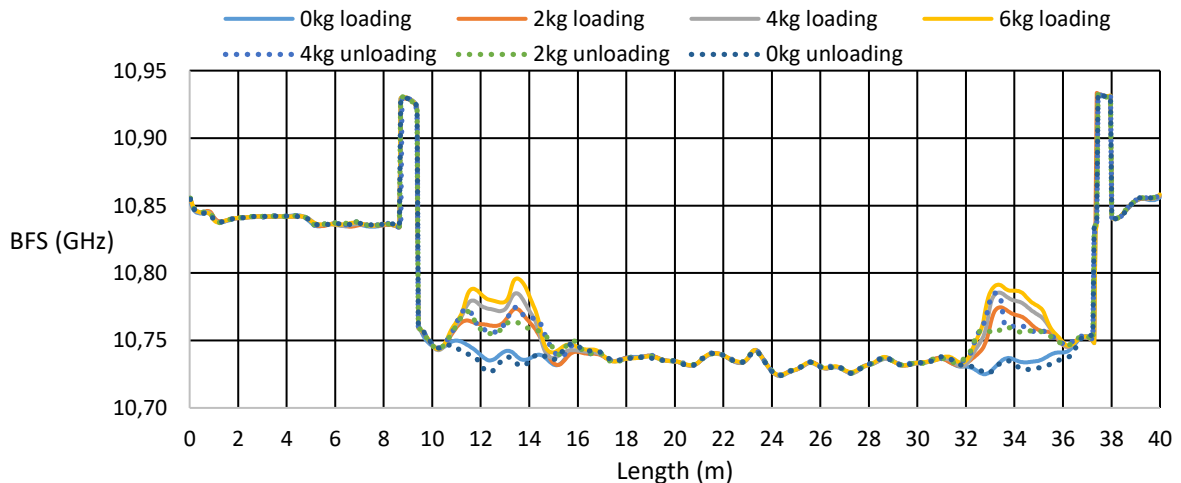


Figure 3-18. BFS profiles of the telecom cable recorded during the calibration exercise

The cable was loaded in increments of 2kg, from 0kg to 6kg, and then unloaded from 6kg to 0kg.

Only the segment of the cable that experiences tension registers a change in BFS. The unaffected segments output the same BFS, whether another segment is experiencing strain or not. The graph between 9.5m and 37.5m is mirrored about 23.5m, due to the configuration of the telecom cable (see Figure 3.13).

Figure 3-18 shows the BFS profiles of the telecom cable during the calibration exercise. The BFS changes over localised segments where the fibres are experiencing stress, and in turn strain, while the BFS does not change for cable length that has no load applied to it. By plotting the different BFS profiles against a baseline, a relative BFS graph can be obtained. Figure 3-19 shows the BFS profiles plotted relative to the 0kg loading profile. It also shows the position of where the cable is buried in the mould as well as the overhanging clamped segment.

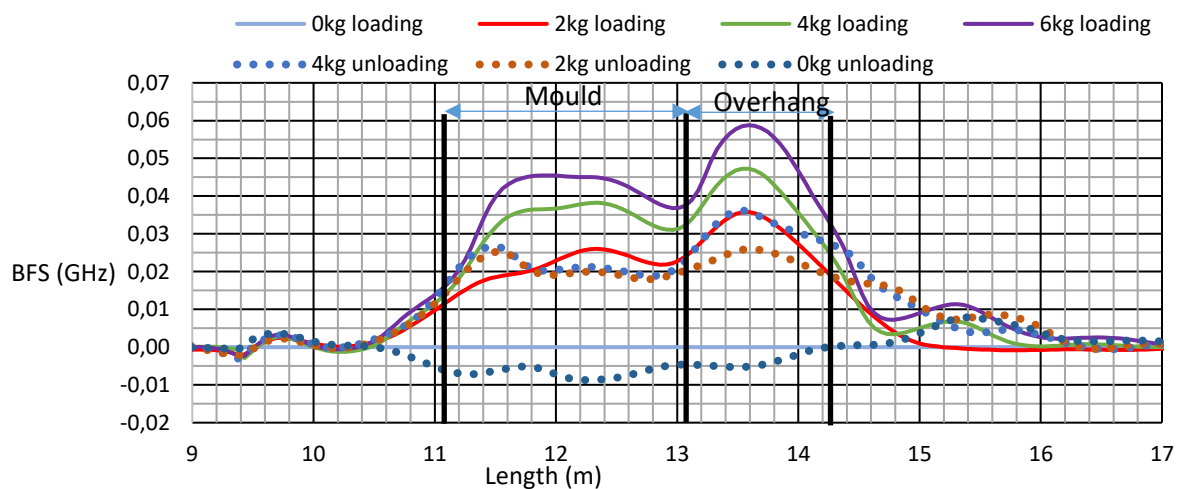


Figure 3-19. A relative plot of the BFS profiles of the telecom cable from Figure 4.4, plotted relative to the 0kg loading curve.

This graph therefore shows the change in BFS when the cable is tensioned, relative when the cable is not tensioned. The positions of the mould and the overhanging segment have been indicated on the graph.

The relative plot, Figure 3-19, is most useful to determine points that are experiencing strain. Due to the strange shapes that BFS profiles can assume, and the wide frequency range over which BFSs take place for different cable types, it can be difficult to distinguish points along a cable that are undergoing strain. By normalising the BFS profile against a reference point, the shape of the BFS profile can be negated and points of localised strain can be much easier to detect.

Furthermore, an array of BFS readings occurring at a single point along a fibre can be isolated to investigate how an external factor is influencing the BFS. In Figure 3-20 a graph of the load

vs BFS has been plotted to determine what happens to the BFS when the cable is subjected to a tensile load. Since the BFS is linked to strain, Figure 3-20 can be viewed as a load-deformation curve.



Figure 3-20. A change in BFS vs load curve plotted for the telecom cable corresponding to a value of 12m on the length axis. There is hysteresis occurring on the unloading phase.

### 3.7.2 RESPONSE OF THE STRAIN CABLE

Figure 3-21 shows the BFS profiles of the Strain Cable during the calibration exercise. As stated before, it is difficult to detect the strain that the cable is experiencing by just observing the raw BFS profile output.

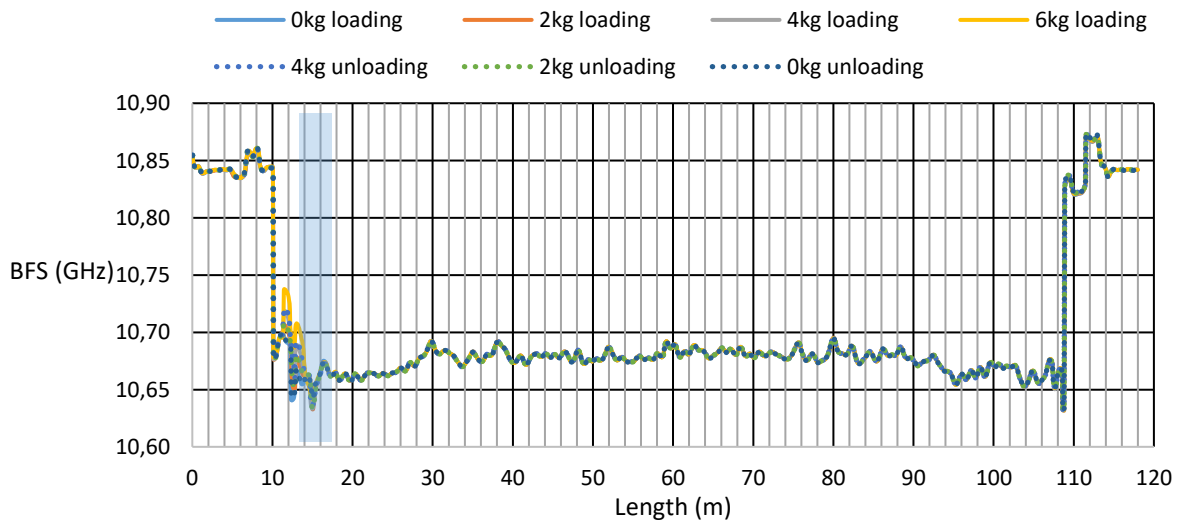


Figure 3-21. BFS profiles plotted for the Strain Cable recorded under loading during the calibration exercise.

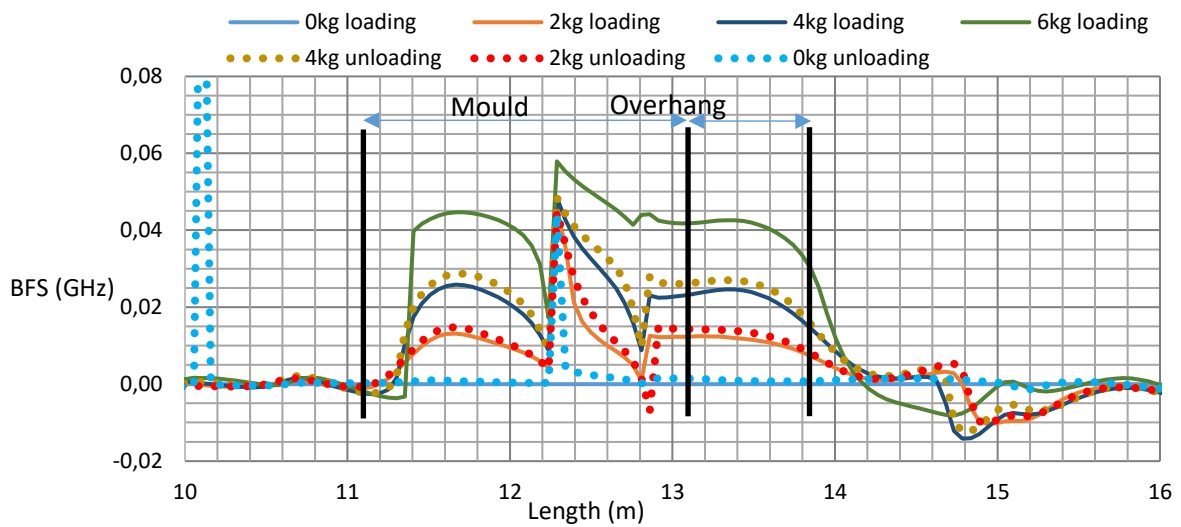


Figure 3-22. A relative plot of the BFS profiles of the Strain Cable shown in Figure 3-21, plotted against the 0kg loading curve.

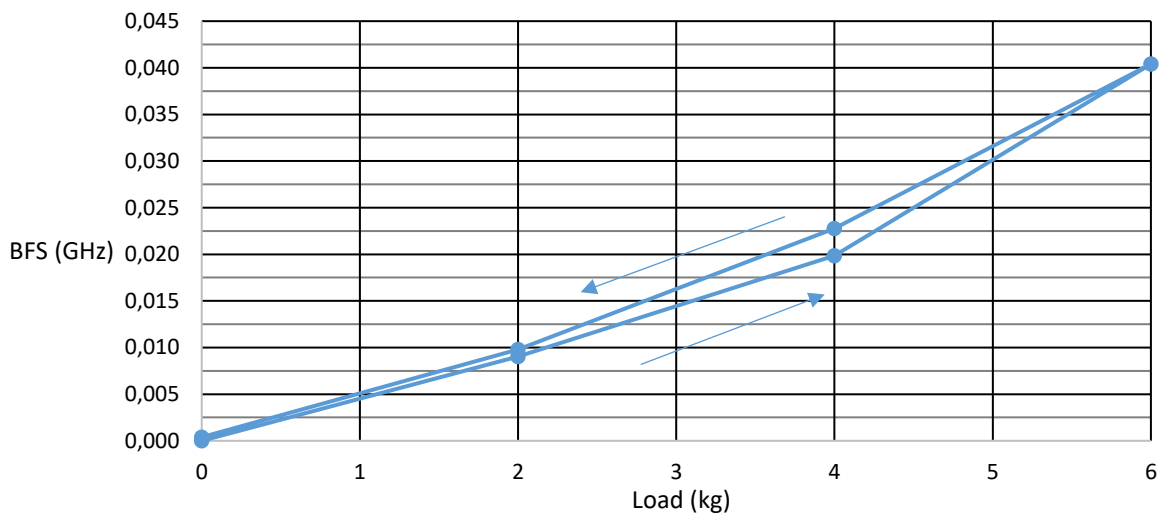


Figure 3-23. A change in BFS vs load plot for the Strain Cable during the calibration exercise. The hysteresis of the Strain Cable is less than that of the telecom cable.

Figure 3-23 it can be seen that, compared to the telecom cable BFS vs load plot (refer to Figure 3-20), there is less hysteresis between the loading and unloading cycles. This is due to the fact that the optic fibre, inside the Strain Cable, is fixed to the sheath. Therefore, the Strain Cable is able to give more precise BFS readings as the cable undergoes strain.

### 3.7.3 RESPONSE OF THE TEMPERATURE CABLE

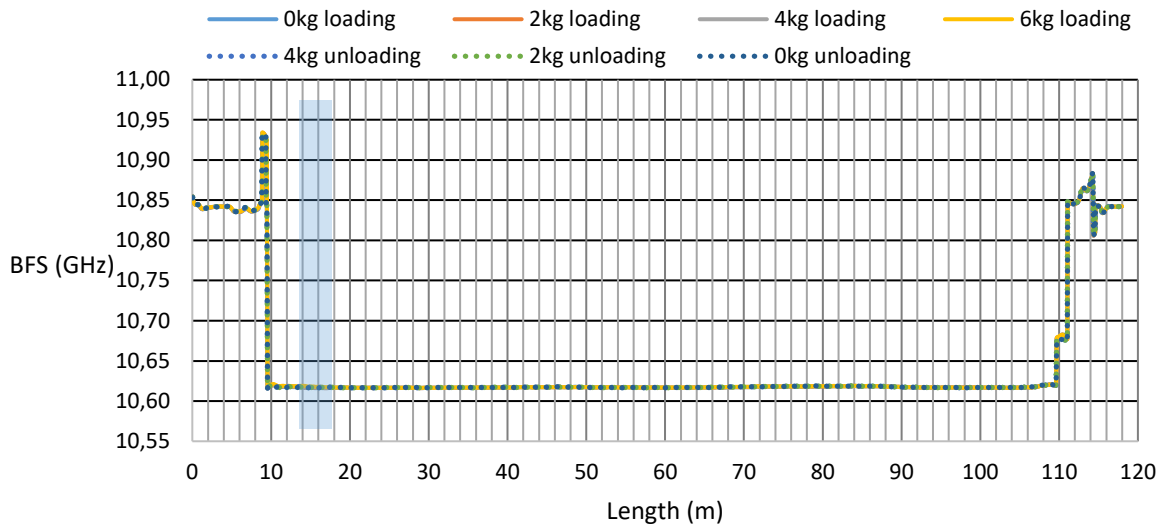


Figure 3-24. BFS profiles for the Temperature Cable taken during the calibration exercise.

The Temperature Cable BFS profiles, as seen in Figure 3-24 above, appear to be fairly constant along the length of the cable between the splices. This is due to the optic fibre being separate from the sheath inside the cable. The fibre is therefore able to slide around freely inside the sheath and even itself out throughout the cable length. Changes to the BFS profile, due to the changing load, cannot be seen on this plot as would be expected from a cable that is sensitive to temperature change only.

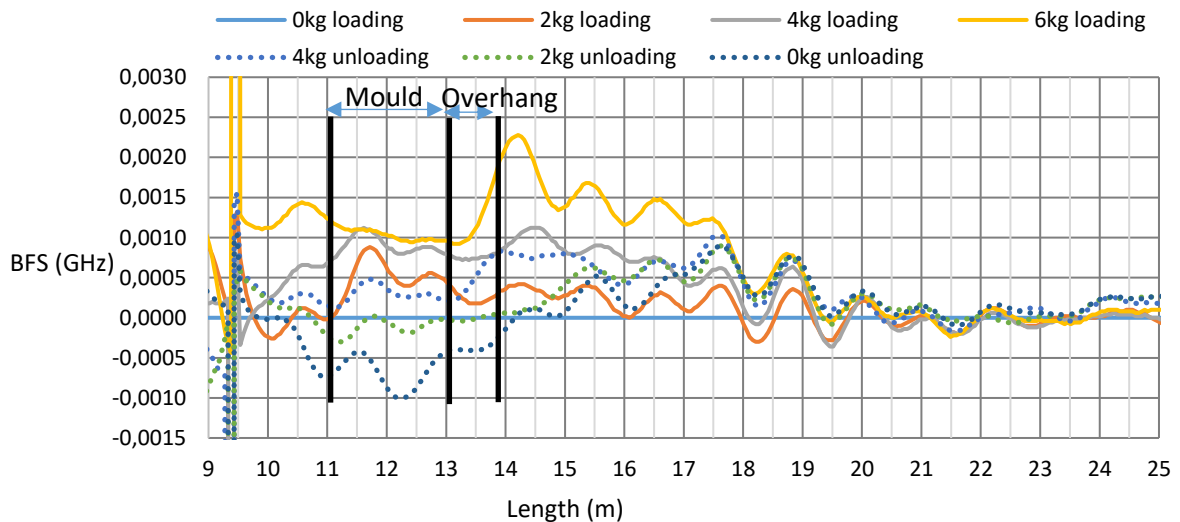


Figure 3-25. A relative plot of the BFS profiles of the Temperature Cable shown in Figure 4.10, plotted against the 0kg loading curve.

It is interesting to note that the BFS of the cable also changes for a few metres surrounding the disturbance as well. In Figure 3-23 it can be seen that relative to the 0kg loading profile, loading on the Temperature Cable does affect the BFS.

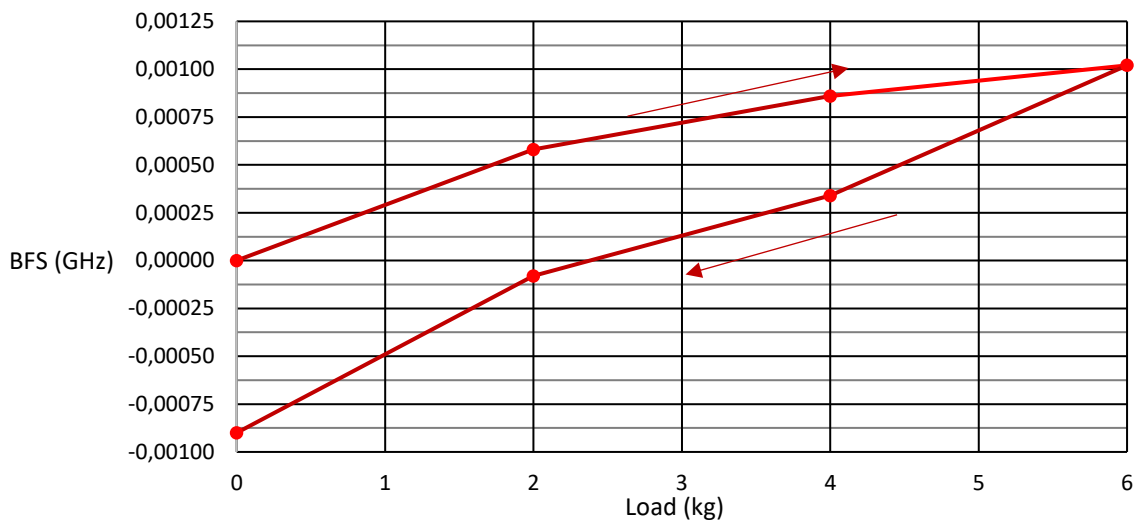


Figure 3-26. A change in BFS vs load curve for the Temperature Cable during the calibration exercise.

Considering Figure 3-26, it is evident that the optic fibre inside the sheath is straining as the cable is being loaded. However, the magnitude by which it is being strained is more than an order of magnitude smaller than the telecom and Strain Cables. The Temperature Cable outputs a maximum change in BFS of 0.001GHz when loaded with 6kg, whereas the telecom and Strain Cable output maximum changes in BFS of 0.045GHz and 0.04GHz under 6kg loading, illustrating how well the core of the Temperature Cable is mechanically isolated from its sheath. By plotting the three loading curves together it becomes clear that the strain imposed on the Temperature Cable's optic fibre is very slight.

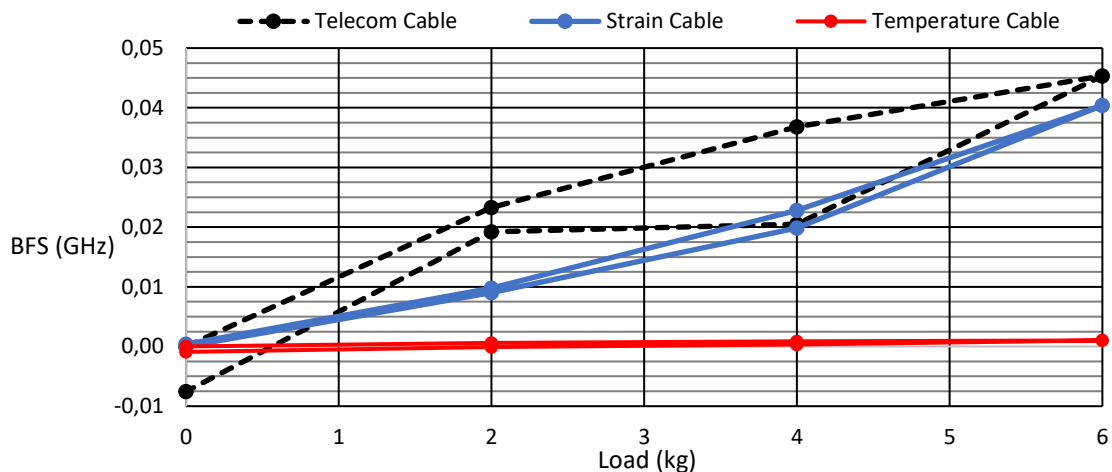


Figure 3-27. Change in BFS vs load curves for all three cables from the calibration exercise.

An incorrect interpretation of Figure 3-27 would suggest that the Temperature Cable is many times stiffer than the telecom and Strain Cable. However, the smaller BFS for the Temperature Cable under loading is due to the fibre straining very slightly. This is attributed to a small amount of friction between the fibre and the sheath.

### 3.8 FIBRE OPTIC CABLE BEHAVIOUR OVER 48 HOURS

In order to assess the suitability of the optic fibres to act as leak detection sensors, the performance of the optic fibres had to be assessed over time in the absence of a leak. The most obvious impact on performance would be daily temperature fluctuation. It was therefore decided to examine how the cables behaved over a 48-hour period, BFS profiles were taken for all three cables at two-hour time intervals for 48 hours. The resulting BFS plot can be seen below.

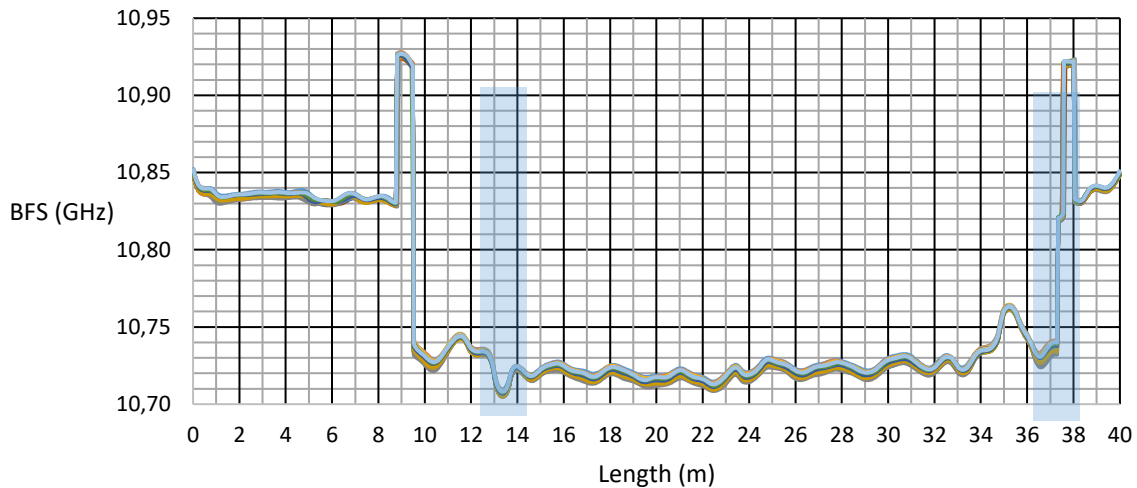


Figure 3-28. BFS profiles for the telecom cable taken over a period of 48 hours at 2-hour intervals.

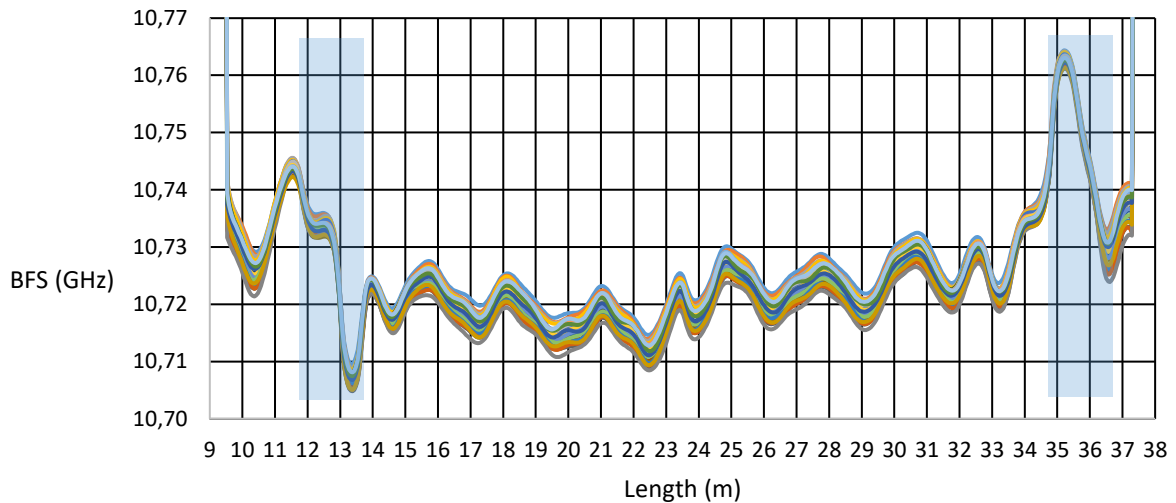


Figure 3-29. In Figure 4.15, the axes of Figure 4.14 have been magnified to length = [9, 38] m, and BFS = [10.70, 10.77] GHz.

The range over which the BFS shifts up and down is bound by the BFS corresponding to the warmest and coolest temperatures experienced throughout the day.

Looking at the magnified plot, Figure 3-29, it is evident that the BFS fall within a specified range. This range is defined between a minimum BFS when the cable temperature is at its

lowest and a maximum BFS when the cable temperature is highest, corresponding to temperature fluctuation throughout the day. In order to develop a baseline against which other BFS profiles could be compared, the BFS profiles were averaged over the 48-hour period to create an average BFS profile.

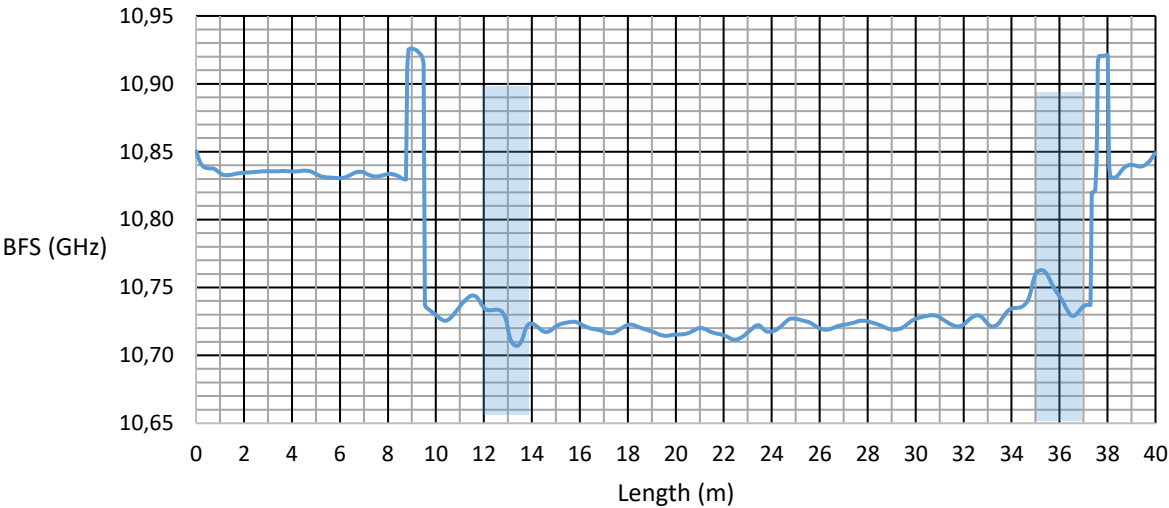


Figure 3-30. A 48-hour average BFS profile of the telecom cable.

This curve is created by averaging each array of BFS values, recorded over 48 hours, for every ordinate along the cable length.

Plotting the BFS profiles over the 48 hours relative to the average BFS profile, shown in Figure 3-30, yields Figure 3-31.

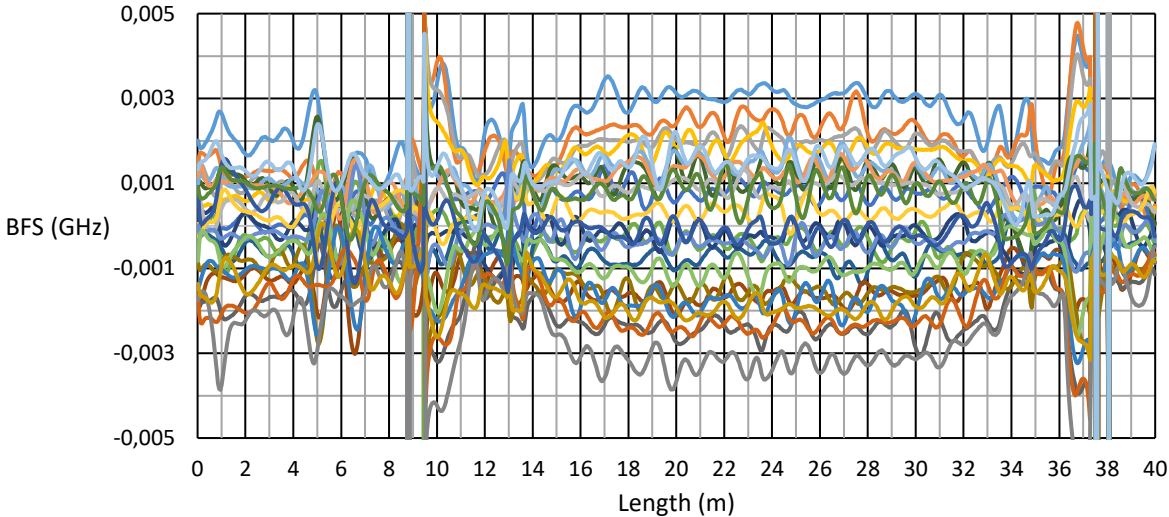


Figure 3-31. A relative plot of the BFS profiles, from Figure 4.14, plotted relative to the 48-hour average profile.

Figure 3-31 shows that temperature changes are able to induce BFS changes in the fibre. However, to determine how changes in temperature change the BFS, a BFS vs time plot can be created for a given point along the cable length. The Figures below show how the BFS

changes, in each cable, with time due to the temperature fluctuation throughout the day. The solid lines represent points along the cable which are not buried in soil. The dashed lines represent points along the cable which are buried in the soil.

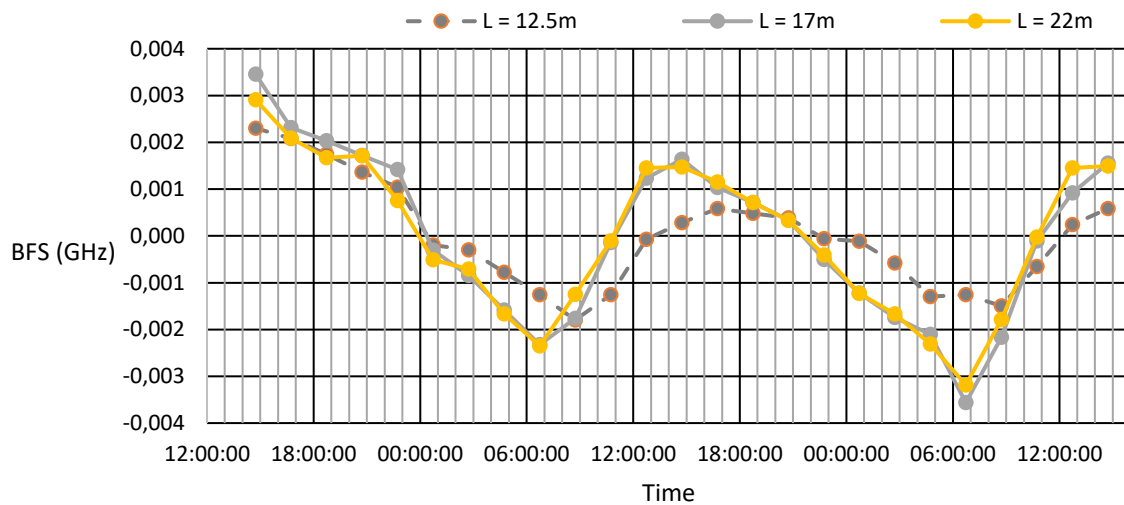


Figure 3-32. A curve of the BFS, relative to the 48-hour average profile, vs time, for the telecom cable, showing how the BFS of the optic fibre changes as the ambient temperature varies throughout the day.

The dashed line represents a point along the cable length where it is buried ( $L = 12.5\text{m}$ ). It is interesting to note that the telecom cable curve for the buried segment lags behind the unburied segments. Furthermore, the buried segment experiences a smaller change in BFS at the warmest and coolest times of day as opposed to the unburied segments.

The BFS follows a shape similar to that of a sinusoidal wave with a period of 24 hours. If BFSs over a 24 hour period are averaged, the sinusoidal shaped curve can be negated and a single BFS value can be used to represent a 24 hour cycle for each ordinate along a cable. A drawback of this methodology is that a single unwanted disturbance to the cable can ruin an average value.

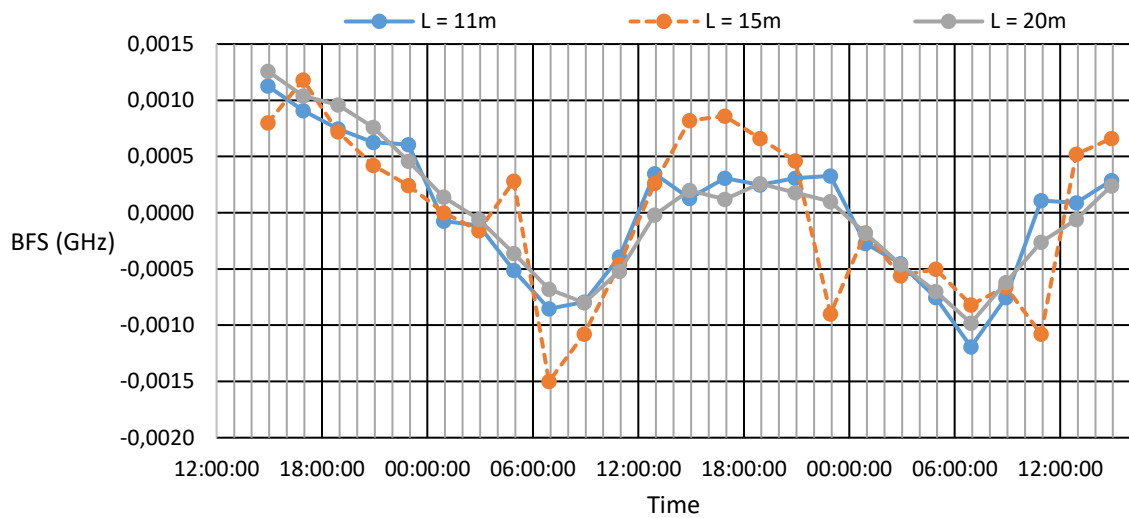


Figure 3-33. A BFS vs time curve for the Strain Cable.

The buried segment of the Strain Cable outputs a fair amount of noise, as it can be seen straying from BFS vs time curve for the unburied segments.

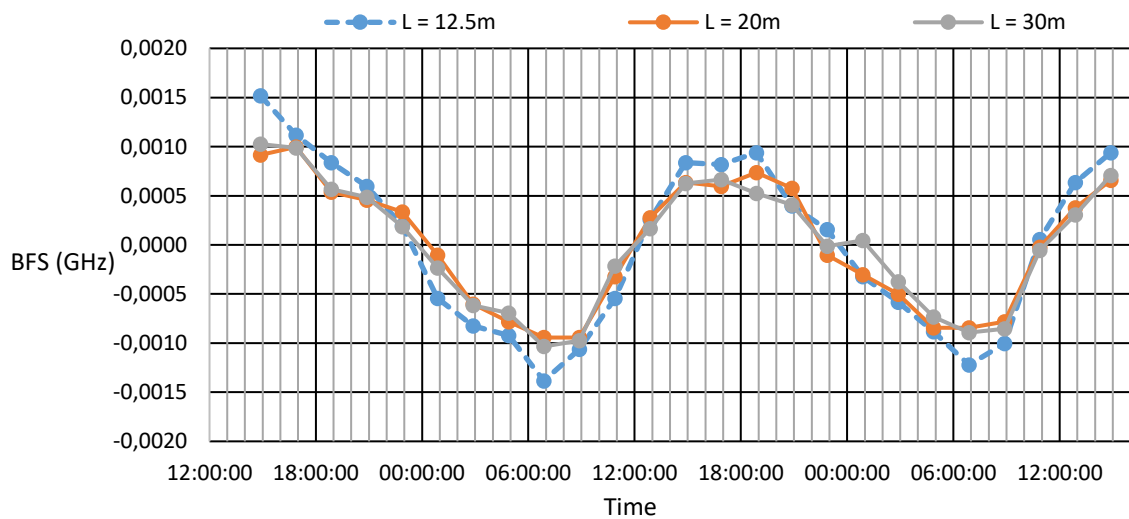


Figure 3-34. A BFS vs time curve for the Temperature Cable.

The buried segment of the Temperature Cable behaves identically to the unburied segments, unlike the telecom and Strain Cables.

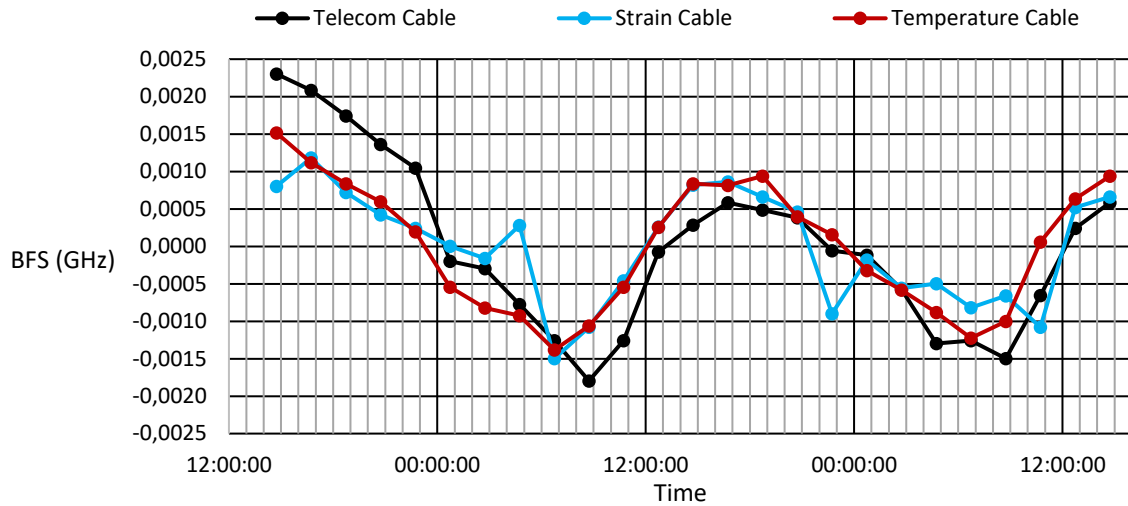


Figure 3-35. A BFS vs time curve of an ordinate buried in soil on each cable.

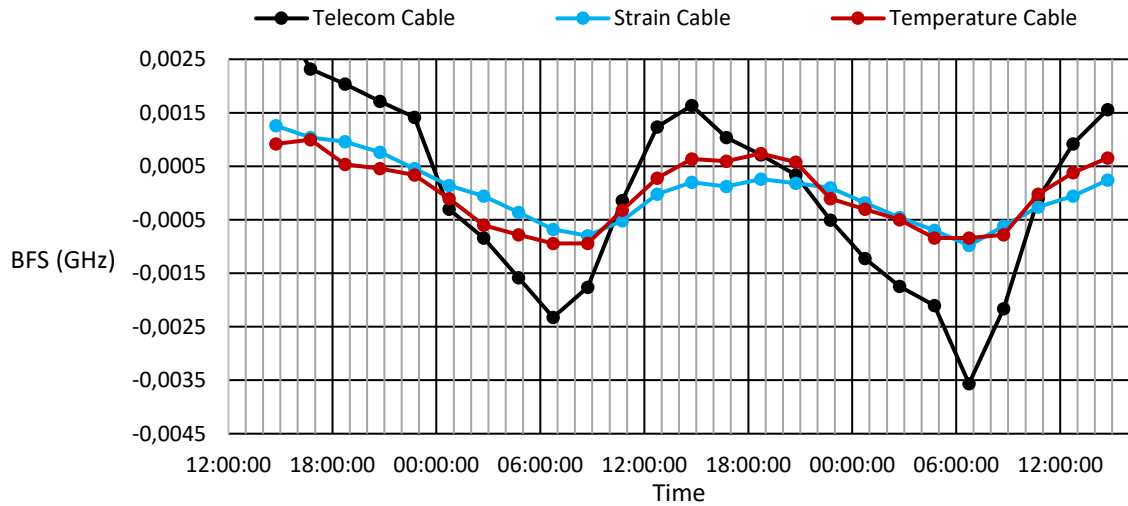


Figure 3-36. A BFS vs time curve of an ordinate from each cable that is not buried in soil.

Comparing Figure 3-35 and Figure 3-36, it can be seen in Figure 3-35 that each cable undergoes changes in BFS, and hence strains, of similar magnitude when buried in soil. When the cables are not buried, i.e. exposed to the atmosphere, the telecom cable undergoes greater changes in BFS, due to temperature changes, than the Strain and Temperature Cables. This may be attributed to the fact that the cables, when buried, strain with the soil when it strains due to temperature change. When the cables are not buried the coefficient of thermal expansion of the fibre optic cable governs the strain that the cables experience due to temperature change.

Plotting BFS profiles against an average profile will form the foundation upon which further data processing is developed.

### 3.9 THE EFFECT OF A LEAK ON THE BFS

When a pipe begins to leak, the change in moisture content of the soil will cause the soil to undergo strain due to matric suction that will be generated in the soil as a wetting front advances from the leak location. The experiment performed was done with the aim of determining if these strains could be detected by the fibre optic cables. BFS profiles were logged for 24 hours. Water was then poured into the mould, containing the soil in which the cables were buried. Thereafter, BFS profiles were again recorded for a further 24 hours. Figure 3-37 shows the averaged BFS profiles of the telecom cable, between the splices, before and after the soil was wetted.

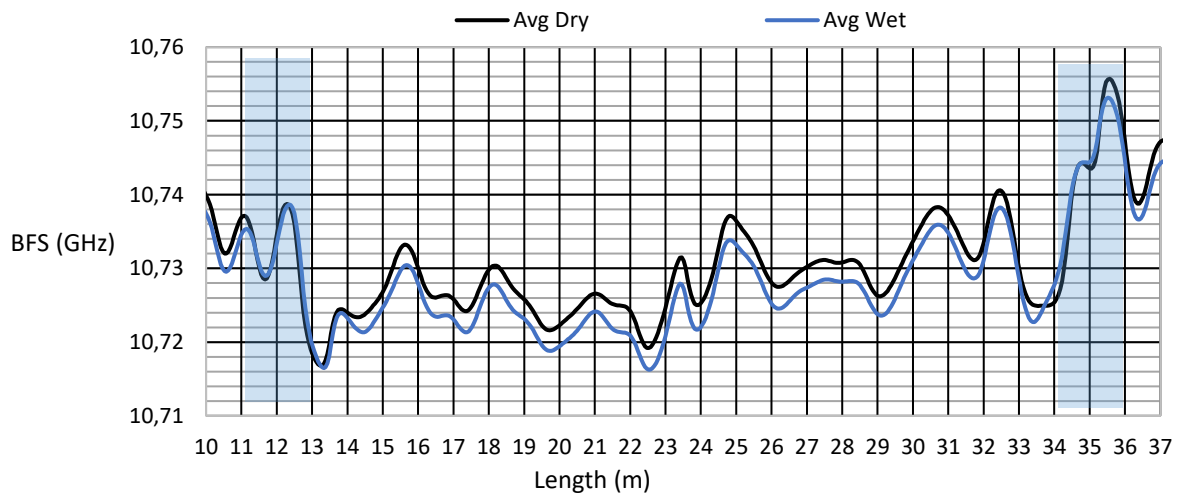


Figure 3-37. Average BFS profiles for the telecom cable.

The Avg Dry curve is a 24-hour average profile from before the soil in the mould was wetted. The Avg Wet curve is a 24-hour average profile from after the soil in the mould was wetted.

In Figure 3-37 it is evident that there is a clear difference between the dry average and the wet average BFS profile. This is possibly attributed to the 24 hours after wetting being a colder cycle than before the wetting. From this plot no disturbance can be easily detected. Plotting the average wet profile relative to the average dry profile, however, shows a clear disturbance occurring between 11m and 14m. Seeing that the mould lies between 11m and 13m, this indicates that the cable segment buried in the soil has strained. On the opposite end of the graph, a disturbance is also detected between 33.5m and 35.5m. Due to the configuration of the telecom cable, as discussed in chapter 3, the BFS is mirrored about the 23.5m ordinate. Thus, the disturbance detected between 33.5m and 35.5m also corresponds to where the cable is buried in soil.

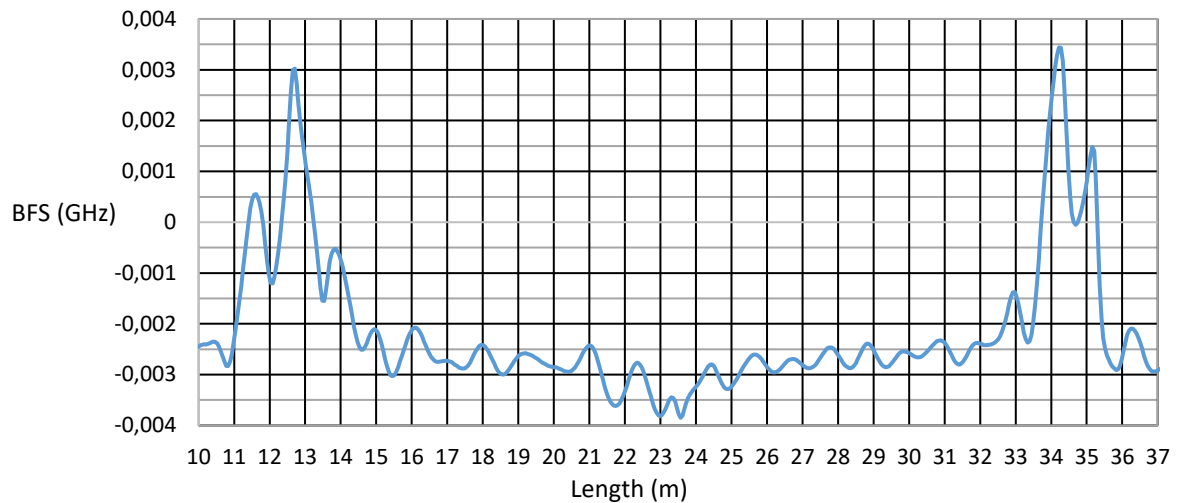


Figure 3-38. A relative wetting BFS curve for the telecom cable.

Figure 3-38 is created by subtracting the Avg Dry profile from the Avg Wet profile. (Avg Wet – Avg Dry). The segments of the curve that stand out from the rest of the plot indicate where a segment of the cable detected a disturbance. In this case the disturbance is the strain in the soil due to a change in moisture content.

### 3.10 THE INFLUENCE OF DIFFERENT SOILS ON CHANGE IN BFS

Due to the different particle size distributions, and different soil-water retention characteristics, the three soils will experience different amounts of strain when their moisture contents are changed. The coarse sand would be expected to undergo the least amount of strain, due to it being composed mostly of larger particles. The red clay would be expected to strain the most, due to the very fine particles present, resulting in the largest matric suctions (see Figure 3-8). The fine sand would be expected to produce strains of magnitude somewhere between the coarse sand and the red clay. This is because the fine sand has particle distribution and soil-water retention properties that lie between that of the coarse sand and the red clay.

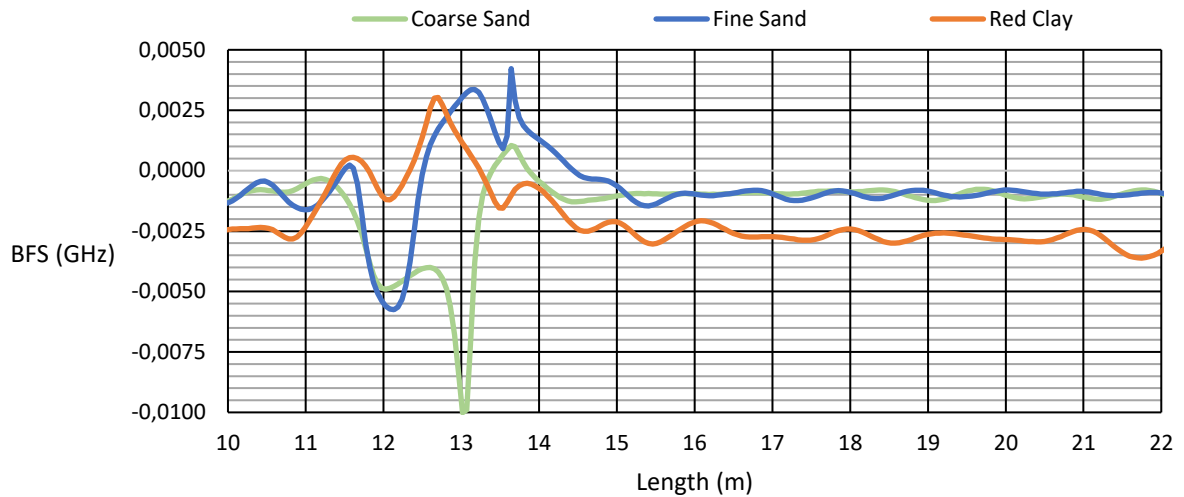


Figure 3-39. Relative wetting BFS curves, for the telecom cable, in each of the soils tested. The telecom cable shows that there is a disturbance, but it does not indicate its magnitude

Referring to the results for the telecom cable, Figure 3-39 and Figure 3-40, the red clay caused a positive change in BFS, while the coarse and fine sand both caused negative changes in BFS. The reason for this is because the red clay swelled when wetted and the coarse and fine sand both shrank. This result is congruent with the behaviour of soils, as clays readily absorb water and swell as a result thereof. Soils, especially sands, which do not contain clayey particles tend to collapse when wetted and thus shrink. According to the plot, however, the red clay swelled less than what the coarse and fine sand shrank. Furthermore, the coarse and fine sand both shrank by the same amount. This could indicate that the telecom cable, although it is able to detect disturbances, does not excel at giving an accurate indication of the amount of strain a measurand is experiencing, because its sheath is not rigidly attached to its core.

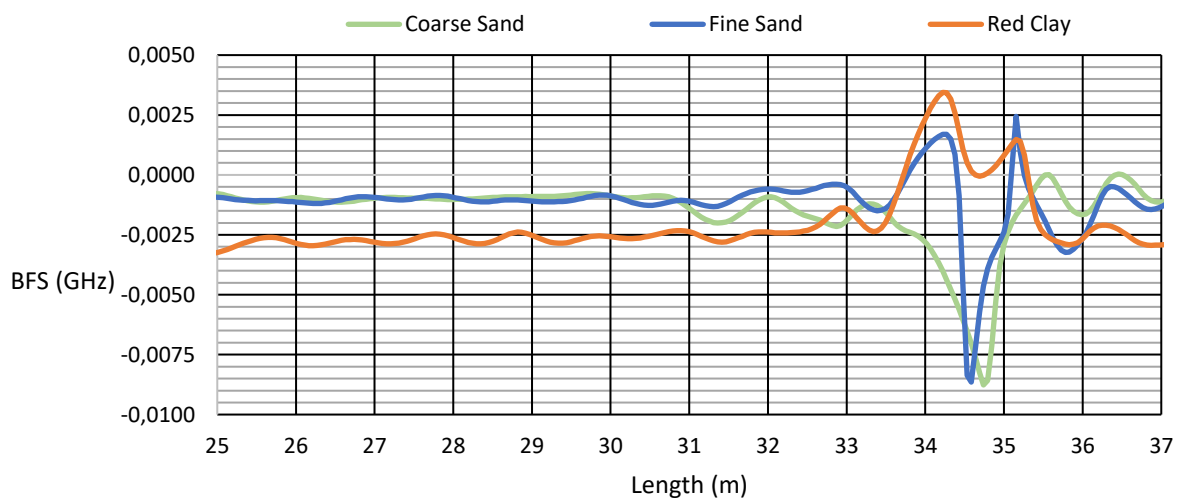


Figure 3-40. Relative wetting BFS curves for the telecom in each of the tested soils.

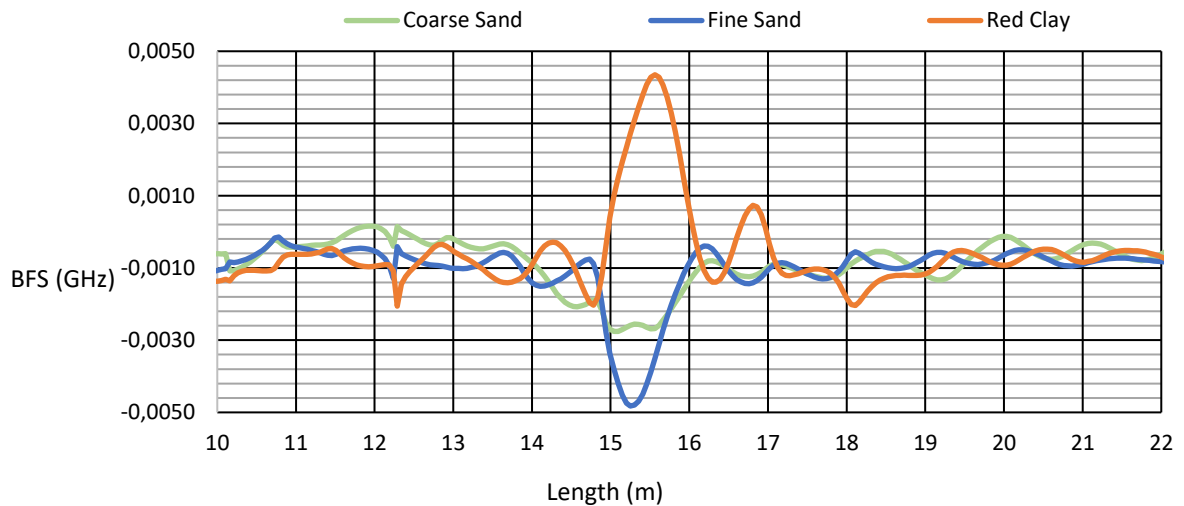


Figure 3-41. Relative wetting BFS curves for the Strain Cable in each of the tested soils.

The Strain Cable shows that there is a disturbance, i.e. the soil is straining due to being wetted, and it gives a good indication of the magnitude of the disturbance taking place.

The results of the Strain Cable, Figure 3-41, are consistent with those of the telecom cable, Figure 3-39 and Figure 3-40. However, the Strain Cable seems to be more capable at not only detecting the strains in the soil, but also providing a good indication of the magnitude and sense of the strain experienced. According to the Strain Cable's results the red clay swelled, and underwent the greatest amount of strain, the fine sand shrank, with the second largest magnitude, and the coarse sand shrank, experiencing the smallest amount of strain out of the three soils as expected.

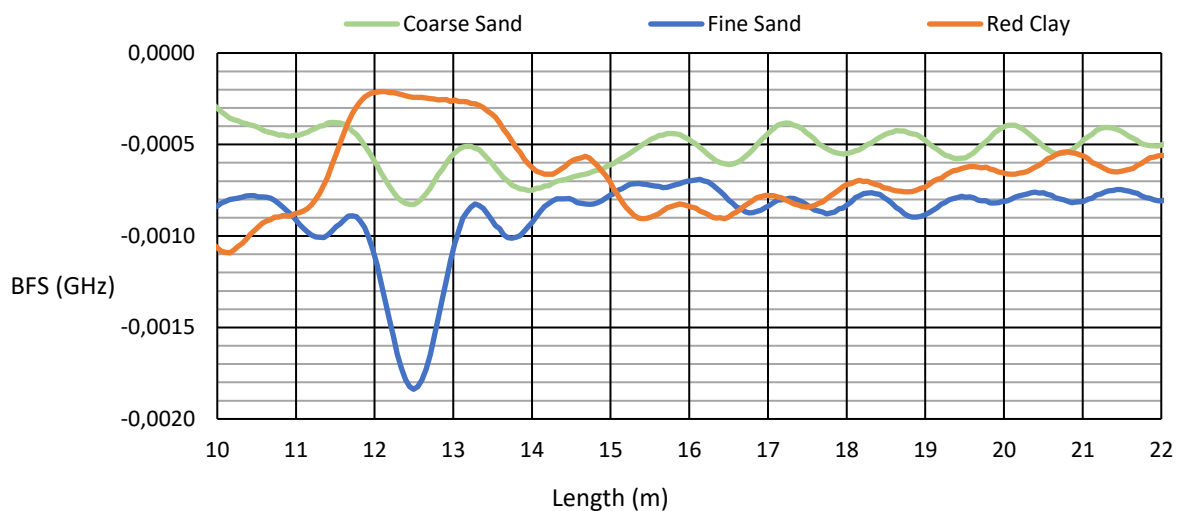


Figure 3-42. Relative wetting BFS curves for the Temperature Cable in each of the tested soils.

The Temperature Cable only detects a disturbance in the fine sand and red clay. These two soils undergo the largest strain when their moisture contents are changed. In the coarse sand, the Temperature Cable does not convincingly show that it had detected any disturbance.

The results of the Temperature Cable, as shown in Figure 3-42, correlate with the results achieved during the calibration exercise, shown in Figure 3-26. The strains detected by the Temperature Cable are slight compared to those of the telecom and Strain Cables. The Temperature Cable did not even appear to have detected any disturbance whilst buried in the coarse sand. The clay and fine sand had a visible effect on the Temperature Cable due to the larger suction pressures that they are able to generate relative to the coarse sand. These suction pressures would have imposed some small amount of friction onto the fibre, through the sheath, which resulted in very small strains being detected.

Looking at the plotted results comparing the change in BFS for the three types of soil, it is clear that the different soils all behave differently when wetted. In each plot a localised disturbance, i.e. a change in BFS, can be seen spanning over 1m to 2m where the soil has been wetted. The disturbance is preceded and followed by the cable flat line readings where no disturbances are detected.

### **3.11 COMPARISON OF THE PERFORMANCE OF DIFFERENT CABLES**

To compare the performance of the different cables, the relative wetting BFS curves, for each cable, were compared keeping the type of soil in which they were buried the same.

Looking at the results of the coarse sand Figure 3-43, it is immediately evident that the telecom cable has been strained. The Strain Cable has undergone a much smaller amount of strain, relative to the telecom cable, and the Temperature Cable does not appear to have detected any change in moisture content. The large amount of strain that the telecom cable has experienced is indicative that the telecom cable is better suited to detecting changes in moisture content in coarse grained soils than the Strain Cable. This is due to the fact that the telecom cable is significantly less stiff than the Strain Cable. Thus, a strain in the measurand (the soil) will impose a larger strain onto the telecom cable as opposed to the Strain Cable.

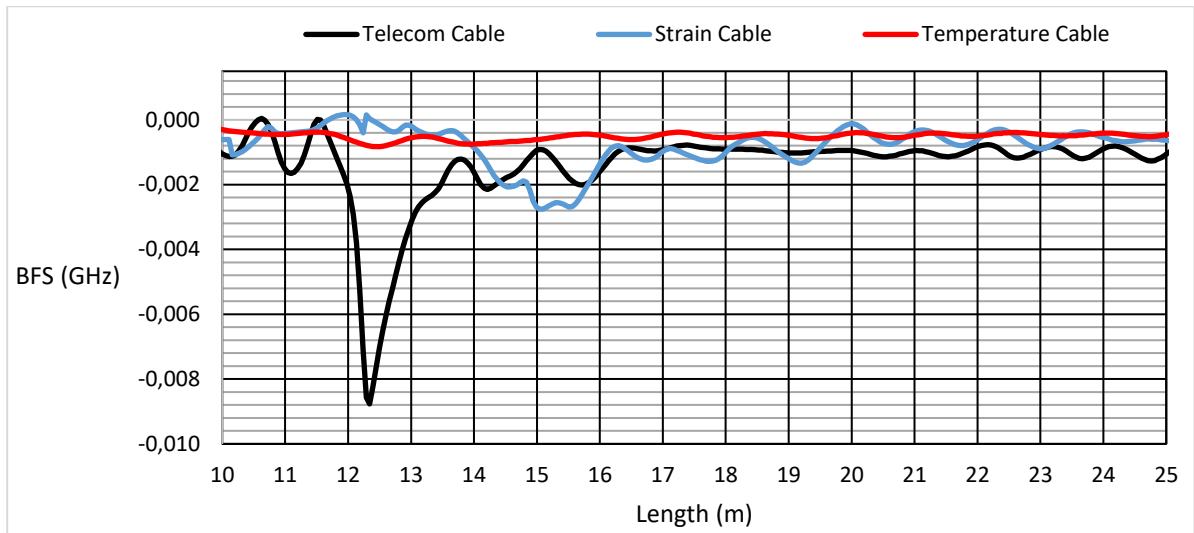


Figure 3-43. Relative wetting BFS curves for each cable in the coarse sand. Before conducting these experiments the Strain Cable was buried between the length ordinates of 14.5m and 16.5m.

As can be seen in Figure 3-43, the changes in BFS of the cables do not lie within the same length boundaries. This shows that the cables are able to pinpoint the location of the change in soil moisture content. The telecom cable undergoes a large change in BFS when the coarse sand is wetted. The Strain Cable undergoes a lesser change in BFS and the Temperature Cable does not register any change in BFS. The telecom and Strain Cables both register a negative change in BFS. This indicates that the coarse sand shrank when wetted.

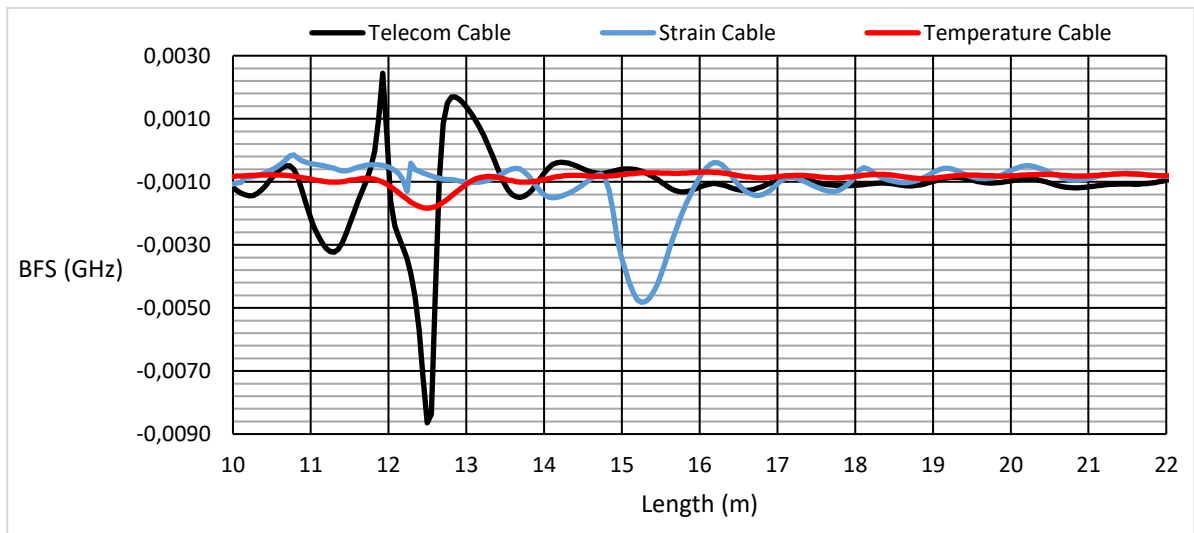


Figure 3-44. Relative wetting BFS curves for each cable in the fine sand. All three cables in this case registered a negative change in BFS, implying that the soil shrank when wetted.

The telecom cable again registered the largest change in BFS. The Strain Cable registered a larger change in BFS than the coarse sand. The Temperature Cable registered a change in BFS, but of much smaller magnitude than either the telecom or Strain Cable.

The results of the fine sand, Figure 3-44, correlate well with those of the coarse sand. The telecom cable underwent the largest amount of strain, followed by the Strain Cable. In this test the Temperature Cable also registered a change in BFS, indicating that it detected strain in the soil, but of a much smaller magnitude than the Strain or Temperature Cable. Comparing the telecom cable with itself in the coarse sand test, it can be seen that the telecom cable experienced very similar changes in BFS, and thus strain, when buried in both the fine and coarse sand. As it was pointed out earlier, the telecom cable is not well suited to giving an accurate measurement of the amount of strain the soil experienced. The Strain Cable registered roughly twice the amount of strain in the fine sand as it did in the coarse sand. This reiterates the fact that the Strain Cable is capable of detecting strains and giving a good indication of their magnitudes.

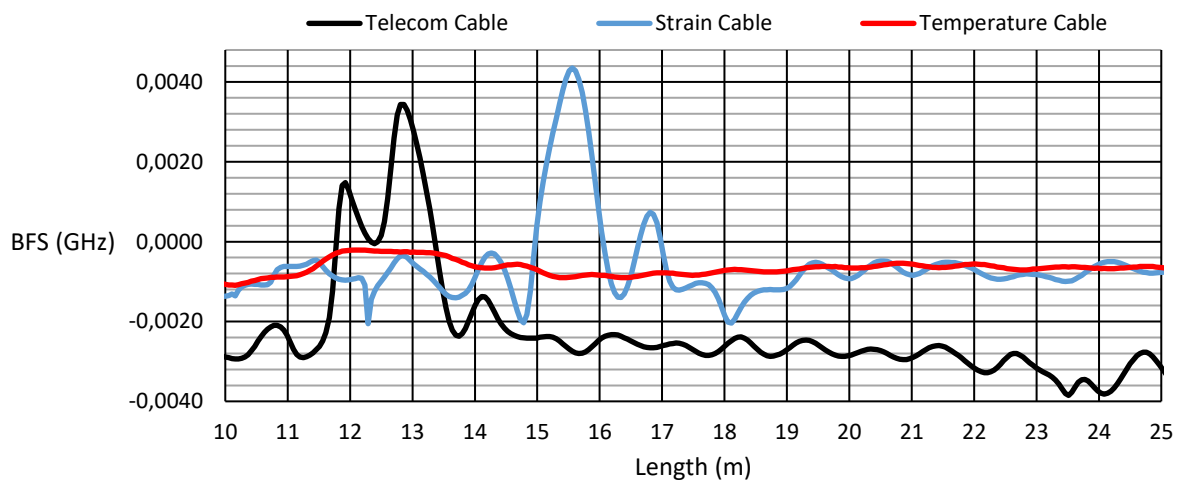


Figure 3-45. Relative wetting BFS curves for each of the cables tested in the red clay.

The telecom and Strain Cables registered very similar changes in BFS in the clay. The Temperature Cable again registered a slight change in BFS. Each cable registered a positive change in BFS, meaning that the clay swelled when wetted.

During the red clay test (results shown in Figure 3-45) all three cables registered change in BFS that was positive, confirming that the clay did indeed swell when it was wetted, unlike the sands which shrank. In this case the telecom and Strain Cables both output changes in BFS of similar magnitudes. In addition, both of these cables' change in BFS were distinct and clearly visible. The change in BFS of the Temperature Cable was again much smaller in magnitude than the telecom and Strain Cable, and took place over a larger segment than in the fine sand.

### 3.12 EFFECT OF TENSIONING CABLES

All preceding plots have used the results of cables that were not tensioned during testing. In this section, how the different cables perform in the different soils, whilst the buried cable

segment is tensioned using a 2kg weight is discussed. This was done to assess whether a leakage detection system will give improved performance if a normal amount of tension is placed on the sensing cable during installation.

### 3.12.1 TELECOM CABLE

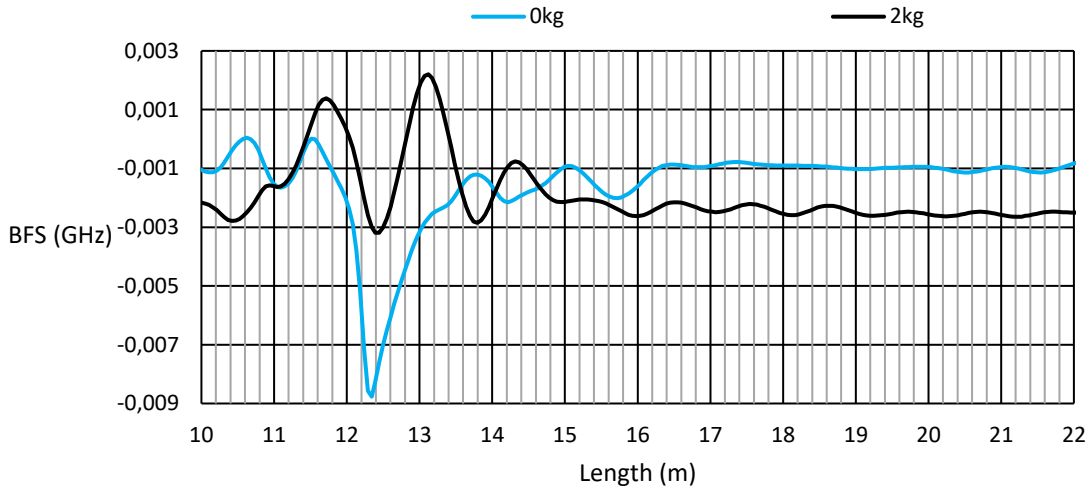


Figure 3-46. Relative Wetting BFS curves, for the telecom cable, for both the tensioned and untensioned test, whilst buried in the coarse sand.

Figure 3-46 shows that, for the coarse sand, the change in BFS of telecom cable was positive when it was loaded. The reason for this is because the cable experienced creep while loaded with the 2kg weight. Due to the creep the cable underwent positive strain. Thus, the average wet BFS profile, for the 24 hours after the wetting of the soil, for the buried cable segment, would have been slightly above the average dry BFS profile. However, the BFS dip at 12.4m, on the **2kg** plot, registered the change in BFS due to the soil being wetted, as for the **0kg** plot.

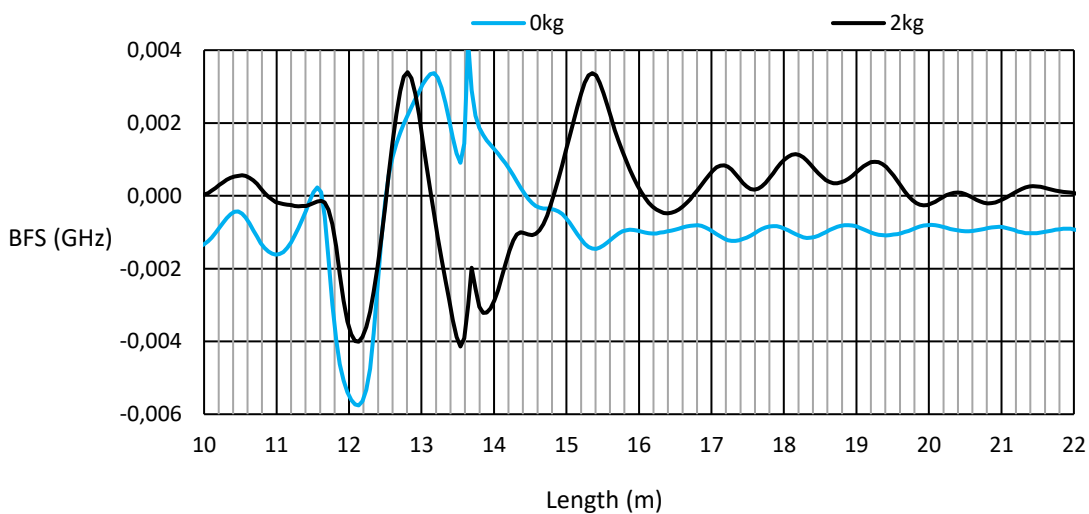


Figure 3-47. Relative Wetting BFS curves, for the telecom cable, for both the tensioned and untensioned test, whilst buried in the fine sand.

From the plot of the fine sand results, Figure 3-47, it can be seen that, for the **2kg** plot, the BFS between 12.5m and 14.5m has shifted down, relative to the **0kg** plot. This may be attributed to slippage occurring inside the cable. The weight hanging on the sheath was loaded with the 2kg for the 24 hours before wetting the soil, but the optic fibre inside the sheath may have slipped in the opposite direction to the load. Therefore, the optic fibre was longer before the wetting test than after the wetting test, hence, the negative change in BFS. The tensioned cable still detected the soil's strain at 12m. However, the change in BFS of the tensioned cable was less than that of the non-tensioned cable.

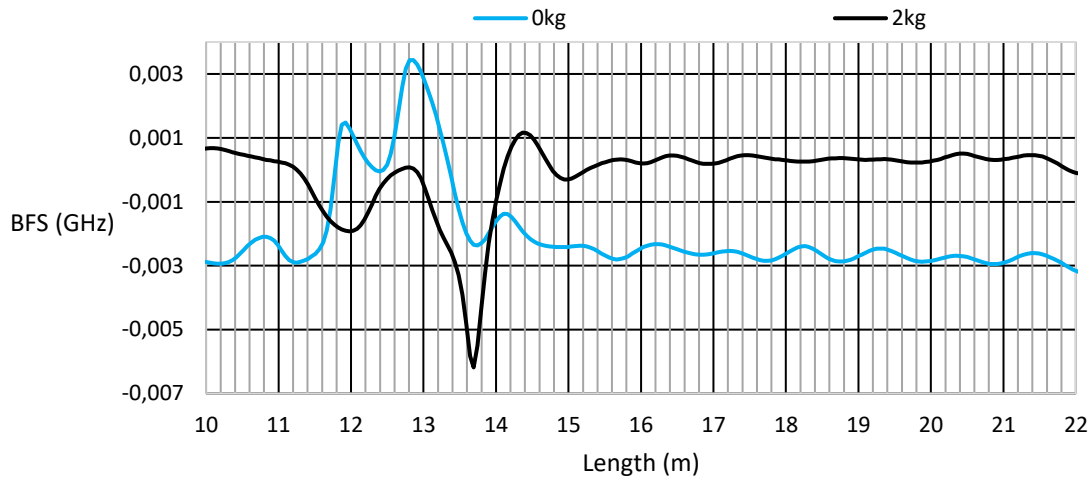


Figure 3-48. Relative Wetting BFS curves, for the telecom cable, for both the tensioned and untensioned test, whilst buried in the red clay.

As with the fine sand test, it appears that slippage happened between the optic fibre and the sheath for the clay test, Figure 3-48. At 12.8m, the tensioned cable seemed to detect the strain in the soil, but the change in BFS due to the strain was not as pronounced as the non-tensioned cable, as for the fine sand test.

The two problems encountered in the tension test were therefore creep and internal slippage of the optic fibre relative to the sheath.

### 3.12.2 STRAIN CABLE

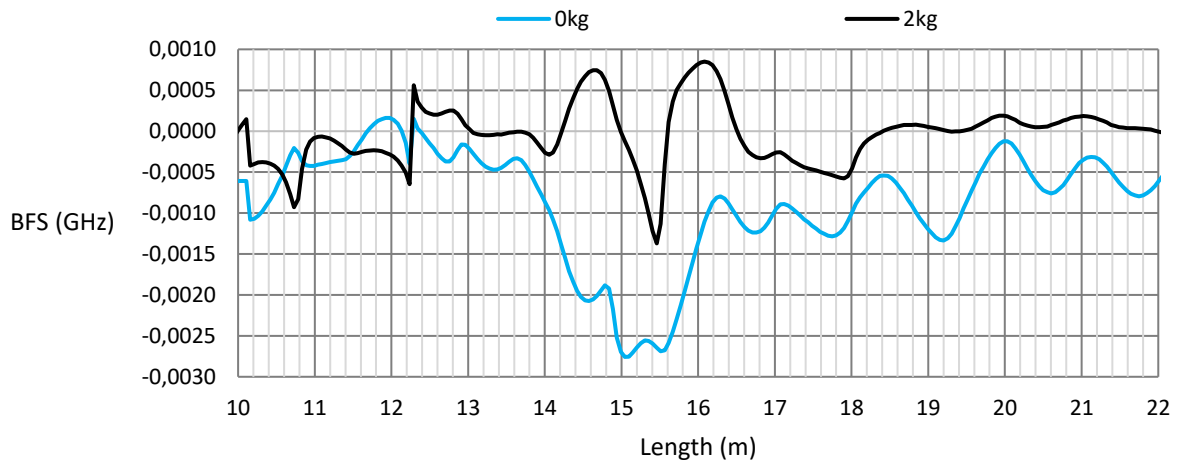


Figure 3-49. Relative Wetting BFS curves, for the Strain Cable, for both the tensioned and untensioned test, whilst buried in the coarse sand.

According to Figure 3-49, the Strain Cable seemed to have undergone creep during the tensioned test, the **2kg** plot showing a slight increase in BFS relative to the flat line reading. The cable under tension did register a negative change in BFS, due to the soil being wetted, at 15.4m. This change in BFS, for the tensioned cable, was very similar to that of the non-tensioned cable. However, due to the creep imposed by the **2kg** weight, the soils strain due to wetting on the **2kg** plot is not as pronounced as the strain registered on the **0kg** plot.

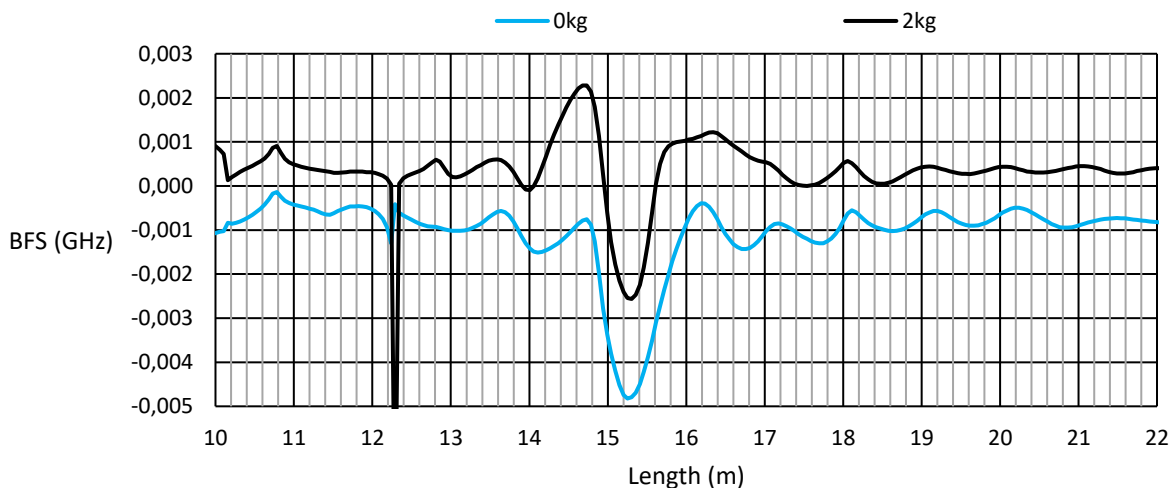


Figure 3-50. Relative Wetting BFS curves, for the Strain Cable, for both the tensioned and untensioned test, whilst buried in the fine sand.

The results of the fine sand test, Figure 3-50, show that the tensioned cable has undergone creep, but it has still succeeded in detecting the strain of the soil due to wetting. The change in BFS, due to the soil being wetted, for both the 0kg and 2kg plots are quite similar, the tensioned cable registering a slightly smaller change in BFS.

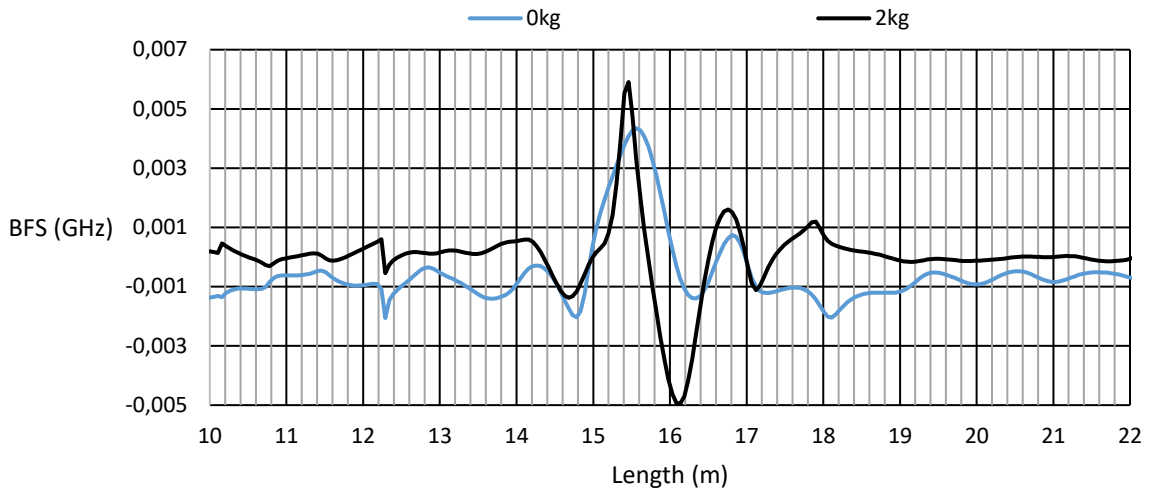


Figure 3-51. Relative Wetting BFS curves, for the Strain Cable, for both the tensioned and untensioned test, whilst buried in the red clay.

According to the red clay test results, Figure 3-51, there appears to have been slippage rather than creep, due to the occurrence of a dip at 16m on the **2kg** plot. It is interesting to note that the change in BFS, due to wetting, of the tensioned cable is slightly greater than that of the change in BFS of the non-tensioned cable. This result goes against the general trend of tensioned cable outputting smaller changes in BFS when the soil is wetted.

### 3.12.3 TEMPERATURE CABLE

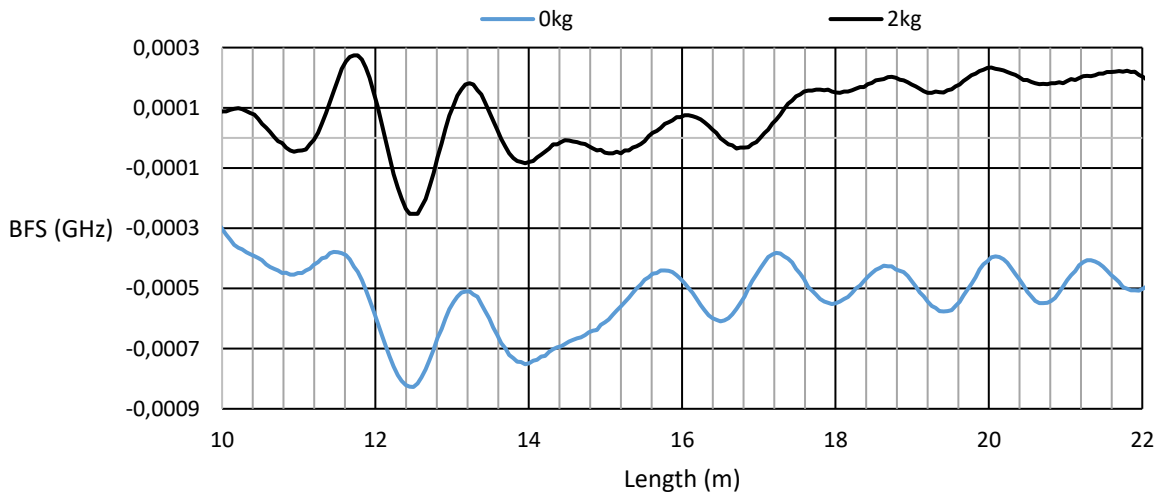


Figure 3-52. Relative Wetting BFS curves, for the Temperature Cable, for both the tensioned and untensioned test, whilst buried in the coarse sand.

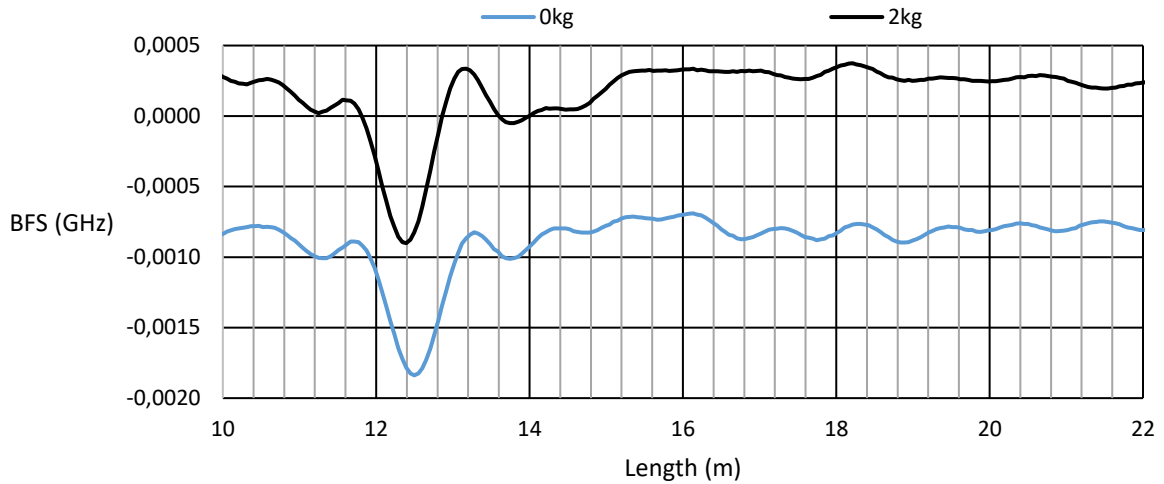


Figure 3-53. Relative Wetting BFS curves, for the Temperature Cable, for both the tensioned and untensioned test, whilst buried in the fine sand.

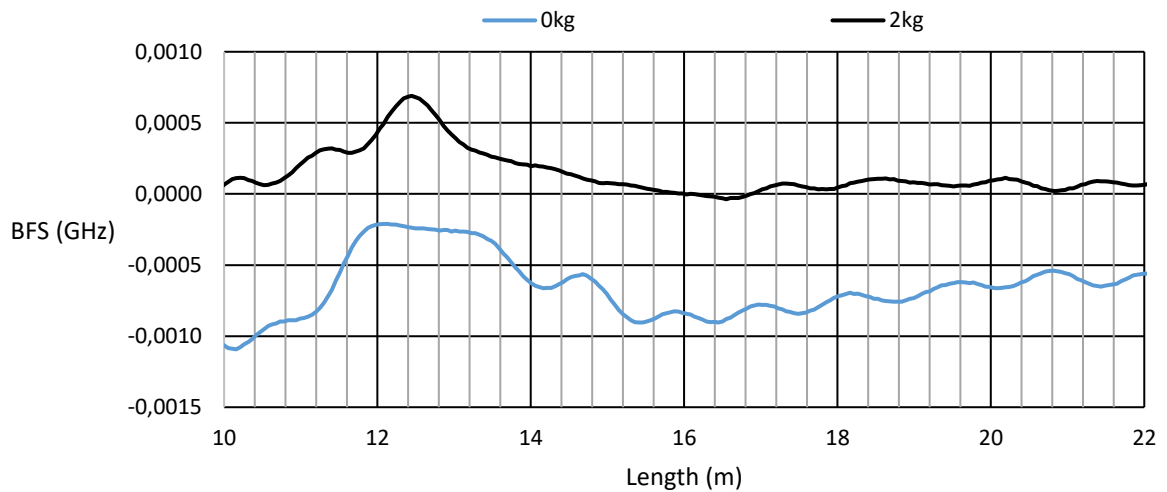


Figure 3-54. Relative Wetting BFS curves, for the Temperature Cable, for both the tensioned and untensioned test, whilst buried in the red clay.

The results of the Temperature Cable as seen in Figure 3-52, Figure 3-53 and Figure 3-54, seem to indicate that the Temperature Cable is unaffected by whether the cable is tensioned or not. This is because the cable is designed to be insensitive to mechanical strain. When the sheath is loaded it simply slips over the optic fibre, as the optic fibre inside is not fixed to the sheath.

# 4 FIELD INVESTIGATION ON HILLCREST CAMPUS, UNIVERSITY OF PRETORIA

## 4.1 INTRODUCTION

This chapter discusses the experimental setup that was created on the Hillcrest campus of the University of Pretoria to simulate effects of a water leak on a fibre optic cable buried in the ground, i.e. the environment that a pipeline would be placed into. The purpose of this fieldwork is to determine the optimal type of fibre optic cable for use in a fibre optic leak detecting system which would operate by detecting strain along the length of a fibre optic cable buried in a pipe trench alongside a water pipeline. The measuring instrumentation and the testing methodology used are presented.

The instrumentation used included five different fibre optic cables, a BFS (Brillouin Frequency Shift) strain interrogator and a fibre optic multi-channel four-way splitter. The five cables were buried in a trench that was 150m long, with fibre optic cables running in from the one end of the trench, turning around at the opposite end of the trench, and exiting from the same end in which they entered.

## 4.2 MEASURING INSTRUMENTATION

### 4.2.1 FIBRE OPTIC CABLES USED

Five different fibre optic cables types were used in the experimental setup to investigate what type of cable is best suited to be used as a leak detection sensor. The five different cable types included four different telecommunication cables, and one cable specifically designed to measure mechanical strain. The primary difference between the five types of cables is that each cable has a different protective sheath that houses the optic fibres contained within them. The most important difference between the classes of cables tested is that some of them were made to have the optical fibres free-sliding within the protective surround (referred to as loose core (LC) cables, while others had a tight surround (referred to as tight buffered (TB) cables). The five cables were:

- An Aerial Self Support (industrial strength) 72-fibre, 6-core cable with loose cores (72F-6C-LC)
- A 6-fibre Tight Buffered Field Deployable Cable (6F-TB)
- A 4-fibre Dual Purpose Drop Cable (4F-DC-LC)
- A 2-fibre Tight Buffered Field Deployable Cable (2F-TB)
- A BRUsens strain V9 cable (strain-TB)

The 72F-6C-LC cable is a multicore cable designed for telecommunication networks with many branches over great distances. The structural composition of the cable is as follows: a Polyethylene sheath houses and protects 6 tubes that surround a glass reinforced plastic strength member. Within these tubes there are 12 optic fibres surrounded by a lubricant. This ensures that the optic fibres are not tensioned or compressed, hindering the passage of optical signals carried by the fibres. The advantage of using such a cable is the ability to create a branched network of cables leading out from and back to the 72F-6C cable. However, the lubricant surrounding the fibres significantly reduces the transfer of longitudinal stress from the sheath to the optic fibres, which may impair the ability of the cable to perform as a leak detection sensor.

The 6F and 2F tight buffered cables are cables designed for re-usable, temporary or mobile point to point links in military applications. The sheath housing the fibre is composed of Hytrel, a strong, flexible, cut resistant rubber like material suitable for harsh environments. The optic fibres housed inside are surrounded by yarn, and there is no gel present to provide lubrication between the sheath and the fibres. This implies that the fibres would be sensitive to external effects as the transfer of strains from the sheath onto the fibre would not be hindered. This would be advantageous in leak detection applications as a change in stress state in the soil would be imposed into the fibre via the sheath. However, this type of cable would be more prone other to unwanted disturbances that could affect the baseline behaviour of the cable.

The 4F cable is comprised of a high density Polyethylene sheath that houses 4 optic fibres surrounded by a lubricant and yarn to provide extra tensile resistance. Like the 72F-6C-LC cable, because of the lubricant the external effects from the sheath would be expected to be less pronounced upon the fibres housed inside. However, the effects of unwanted disturbances acting on the cable would be less pronounced as well which may be beneficial in establishing the baseline behaviour of the cable.

The Strain Cable, as its name suggests, is a cable specially designed to measure strain. This is achieved by formulating perfect contact between the fibre and the sheath. The sheath is made of Nylon Plastic (PA) which is directly attached to a steel tube interlocked with a buffer and transfer layer the surrounds the optic fibre. Thus, any strain that is imposed onto the sheath will be transferred to the optic fibre.

#### 4.2.2 BRILLOUIN FIBRE OPTIC STRAIN INTERROGATOR

The strain interrogator used in the experimental setup was a fibrisTerre fTB series fibre-optic sensing system. In addition, the interrogator was connected to a fibrisTerre optic fibre multi-channel splitter. Four of the five different fibre optic cables could therefore be connected to the interrogator at the same time. The interrogator model uses Stimulated Brillouin Scattering to determine the BFS at a specific point along the length of a fibre optic cable. To perform

distributed sensing, the interrogator employs Brillouin optical frequency domain analysis to create a BFS profile of the entire cable length. A software package, fTView, was used to control the interrogator and interpret the results.

The BFS profile is created as follows:

The interrogator first determines the length of the cable it is monitoring by injecting an optical signal into one end of the optic fibre and measuring the time it takes for the signal to be received at the other end. The interrogator then performs a process called a frequency sweep. In this process two optic signals, of different frequencies, are injected into the optic fibre, one at each end. The two optic signals are injected into the fibre at different times so that they coincide with each other at a specific ordinate along the fibre length. When the optic signals coincide, Stimulated Brillouin Scattering occurs at that point. The downshifted light travels back to the interrogator and the BFS is logged for the specific ordinate. The interrogator repeats this process every 5cm along the cable length and can measure BFS in a cable up to 30km in length.

Once the BFS has been logged for the entire length of the cable the interrogator sends the logged data to fTView and a BFS profile can be plotted. FTView is able to export BFS profiles to a text file format, which can then readily be imported into a spreadsheet package, such as Excel.

## **4.3 FIELD SETUP**

### **4.3.1 TRENCH**

To mimic the environmental conditions that a buried pipeline would be subject to, a 150m trench was excavated on the University of Pretoria's Hillcrest campus in three 50m sections in August 2020. The range of fibre optic cables investigated in this study were laid long the base of the trench. The three trench sections were excavated to depths of 0.5m, 1.0m and 1.5m respectively. The three different depths were chosen to investigate how varying depths would affect the temperature variation experienced by each cable. Temperature variation is an important factor in establishing the baseline behaviour of a cable over time. The cable would be expected to undergo more pronounced temperature variation if buried closer to the surface, and less temperature variation when buried deeper underground. An aerial view of the trench can be seen in Figure 4-1 and Figure 4-2.

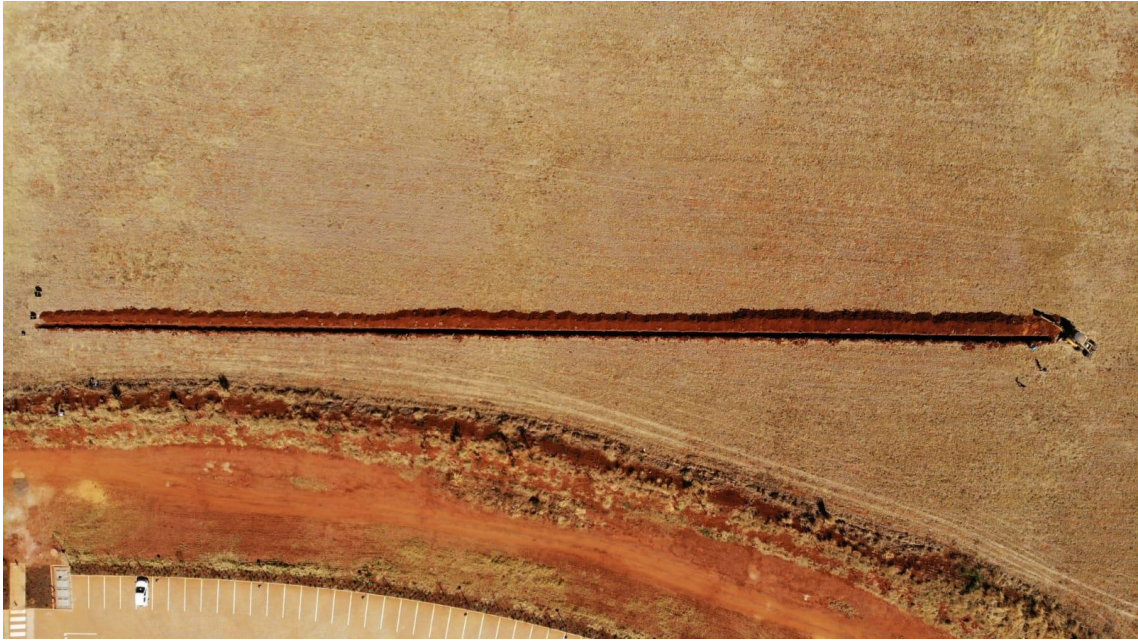


Figure 4-1. Bird's eye view of the 150m trench dug on the University of Pretoria Hillcrest Campus.



Figure 4-2. Standing point view of the trench prior to installation of the fibre optic cables.

Within the three 50m segments standpipes were inserted into the soil leading down to the level of the fibre optic cables. These standpipes are to serve as points of introduction for water into the soil to simulate pipe leaks during the leak test phase of the experiment. Three stand pipes, spaced 15m apart were installed in each of the three trench sections. These standpipes are depicted in the schematic diagram shown in Figure 4-3.

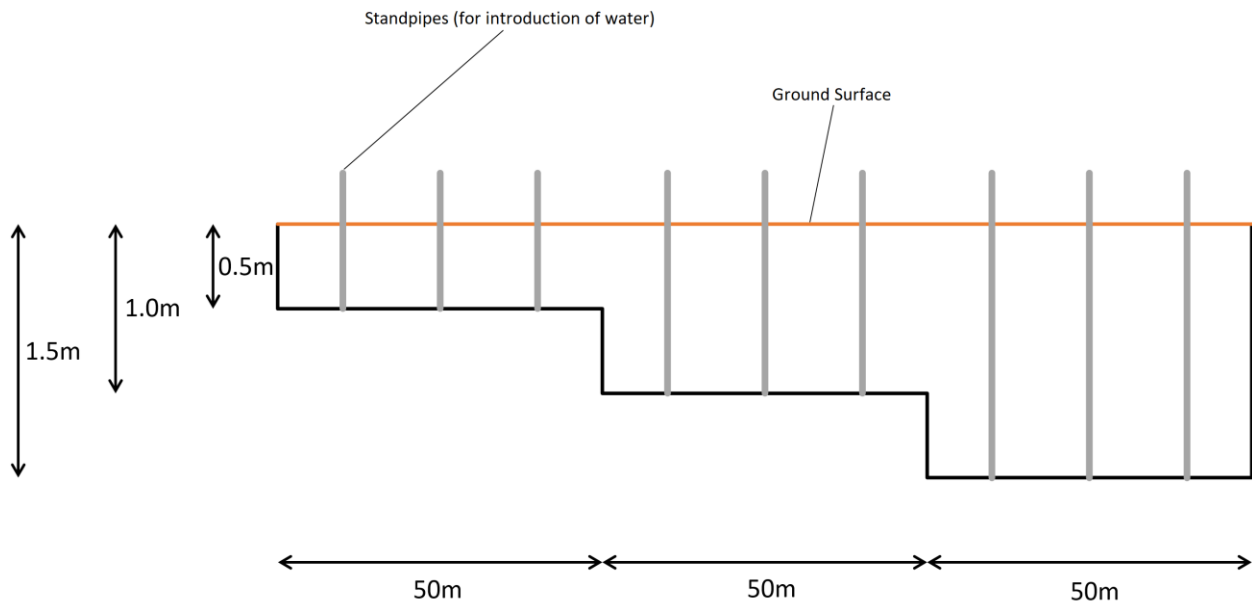


Figure 4-3. Schematic diagram of the trench (not drawn to scale) depicting the three 50m segments.

The layout of the cables is illustrated in Figure 4-4 which shows a schematic diagram of the cables' layout in the trench.

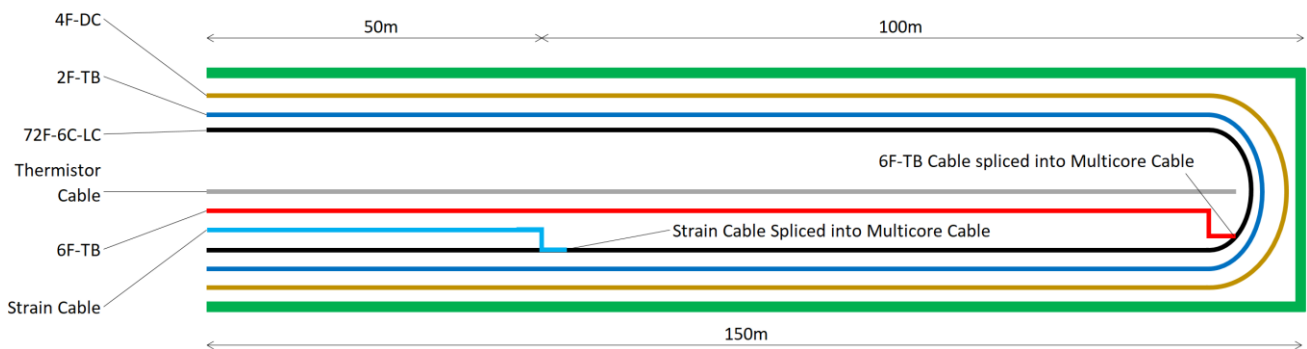


Figure 4-4. Schematic bird's eye view diagram of the trench showing the orientation of the laid cables.

As can be seen in Figure 4-4 the cables were laid along the trench in both directions, entering in at the shallow end (0.5m depth), running the length of the trench to the deep end (1.5m depth) and then looping around, running back along the trench and exiting at the shallow end. The ends of the cable segments buried in the trench were spliced to a single multicore cable leading to the BFS interrogator housed in the server room of the Engineering 4 building approximately 150m away.

Due to limited availability of the lengths of the Strain Cable and the 6F-TB cable, on 50m of Strain Cable and 150m of 6F-TB cable were spliced into two of the fibres of the 72F-6C-LC cable.

#### 4.3.2 SOIL PROPERTIES

The soil in which the trench was dug on the LC de Villiers Campus is a red clayey soil. Clayey soils are highly sensitive to soil moisture content changes as they are more likely to undergo

volume changes during moisture content fluctuation than coarser soil types. Therefore, they are supposedly best suited as a soil for housing fibre optic cables to be used as leak detection sensors as clays will be able to impose great strains onto the cables buried within them.

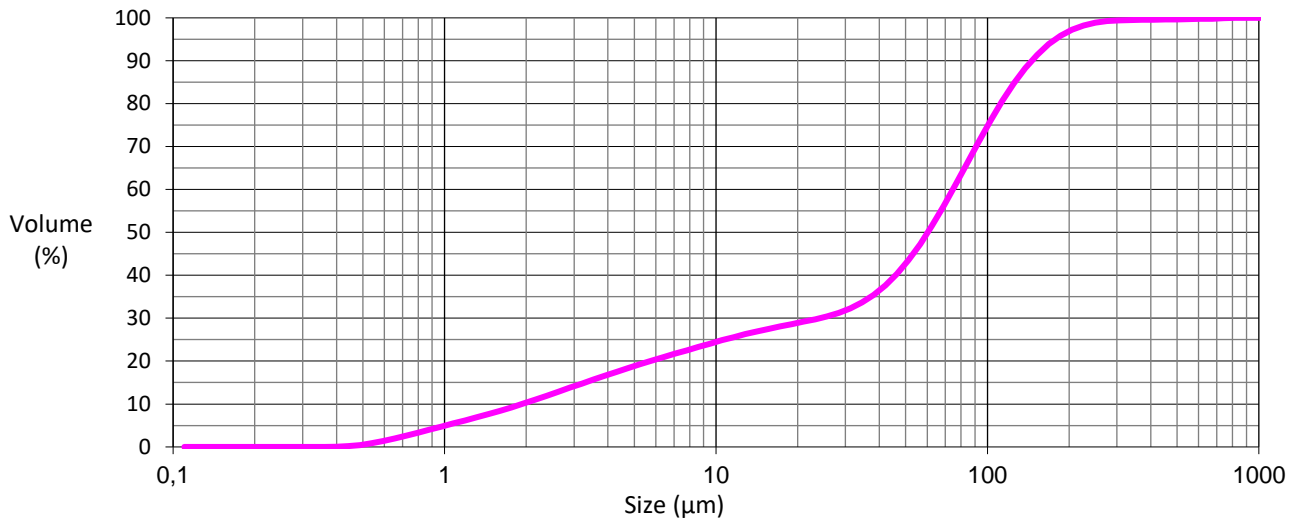


Figure 4-5. Particle size distribution for the red clay.

Figure 4-5 presents the particle size distribution of the soil. As can be seen in Figure 4-5, the red clay is comprised of 75% particles that are smaller than 100µm. Furthermore 25% of the particles range between the sizes of 0.5µm and 10µm. This soil can therefore be expected to have a high affinity for water and a change in moisture content will induce large changes in suction pressures. This can be seen in the soil water retention (SWRC) below.

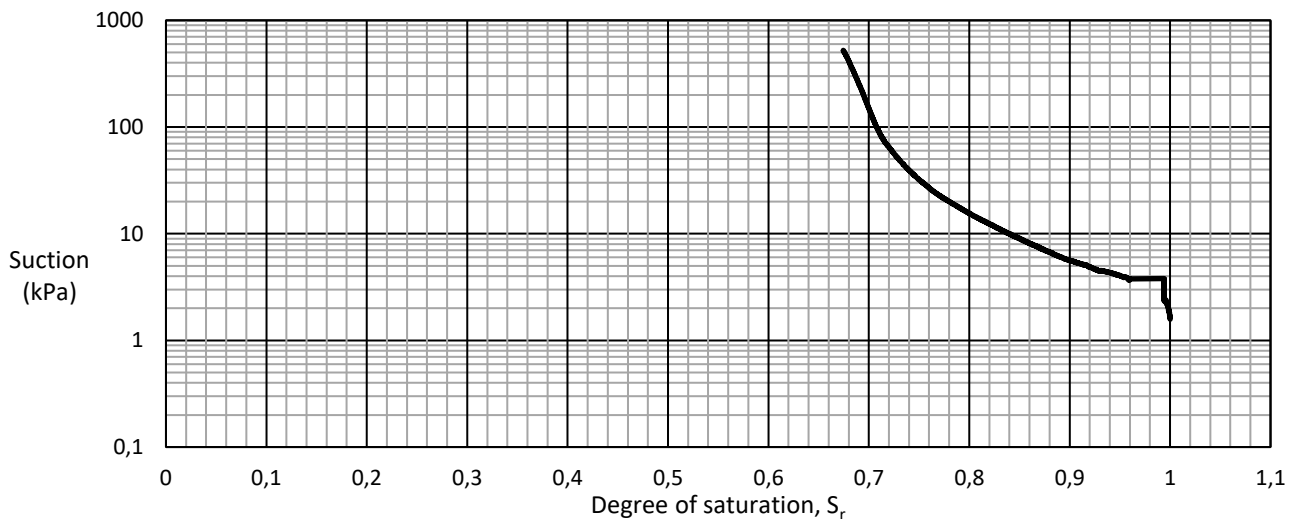


Figure 4-6. Soil-water retention curve for the red clay.

From a degree of saturation ( $S_r$ ) below 1 the soil already begins to generate suction pressures. At a  $S_r$  of 0.96 larger suction pressures start to be generated until the cavitation pressure is reached at a  $S_r$  of 0.67. The SWRC below  $S_r = 0.67$  is therefore not available, but suction values below this value would increase with a further reduction in  $S_r$ .

## 4.4 BASELINE FIELD DATA

The baseline field data, the analysis and the findings thereof are discussed in this chapter. An overview of the output from the BFS interrogator is presented, and thereafter an interpretation and method of analysis of the output are developed. The analysis method discussed in this chapter is focused on establishing the baseline behaviour of a fibre optic cable buried underground over the two-week monitoring period for which data is available.

### 4.4.1 OUTPUT FROM THE BFS INTERROGATOR

A typical output of a BFS interrogator is shown in Figure 4-7.

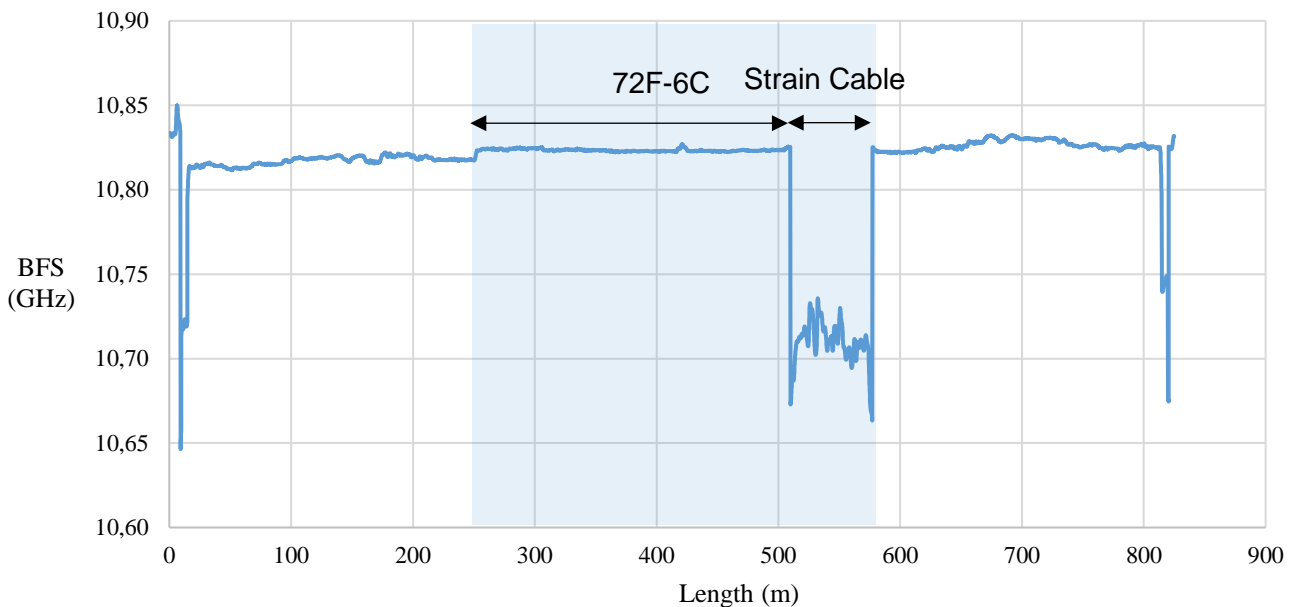


Figure 4-7. BFS profile of the cable with the 50m segment of Strain Cable spliced to it. The segment of the cable buried in the trench is highlighted by the blue rectangle.

The profile shows the BFS in Giga Hertz measured along the length of the optic fibre at a moment in time. In each BFS plot discussed in this report the midpoint of the profile corresponds to the location where the cable was looped about 180° at the end of the deep end (1.5m) of the trench. The section of the fibre optic cable shaded in blue represents the part of the cable buried in the trench, while the remainder represents the communications cable linking to the interrogator which was housed in the server room of the nearby Engineering 4 building. Only the section shaded blue is therefore relevant in this study.

Each BFS profile logged for a given optical fibre is different, due to fluctuations in ambient temperature around the cable. This phenomenon is demonstrated in Figure 4-8, where two BFS profiles registered 12 hours apart are shown together. In Figure 4-8 the two profiles seem to lie one on top the other for the majority of the profile, save for the two instances seen around 200m and 600m. The difference between the two profiles can be more explicitly seen by

subtracting one profile from another. Figure 4-9 shows a plot of the difference between the two profiles plotted in Figure 4-8, namely the 00:48 profile subtracted from the 12:48 profile.

The two regions in Figure 4-8 and Figure 4-9 where the difference between the profiles was pronounced are segments of the cable which are surrounded by air and not by soil. The segments at the sides of the profiles correspond to sections that are running in underground ducts leading to the server room housing the BFS interrogator, but are not part of the area of interest.

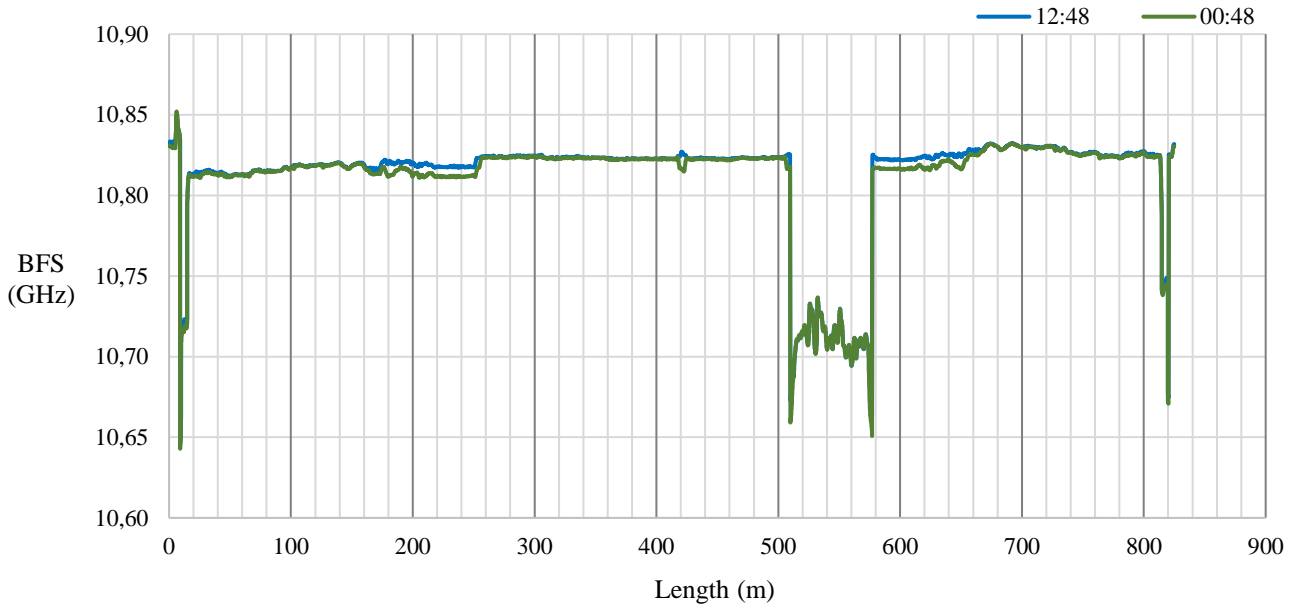


Figure 4-8. Two BFS profiles taken at two different times during the day for the same cable showing how temperature variation affects the BFS output.

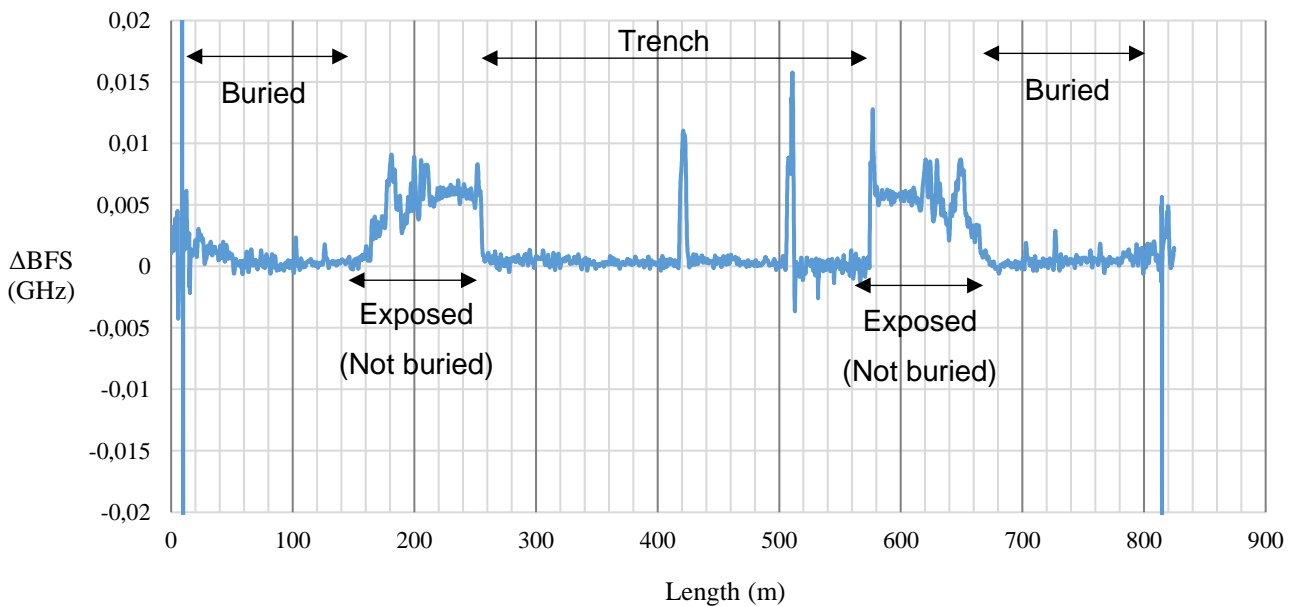


Figure 4-9. Difference between the two BFS profiles plotted in Figure 4-8.

#### 4.4.2 BFS IN THE TIME DOMAIN

It was illustrated above that the BFS measured along the length of an optical fibre changes over time. In order to determine a baseline against which data from a leak test is to be compared, it is important that the fluctuation in BFS be understood for the different types of optical fibres investigated. By shifting the focus from plotting the BFS of the cable along its entire length to plotting the BFS of a specific length ordinate in the time domain, a plot such as that shown in Figure 4-10 can be created. The BFS vs Time curve was plotted using the BFS readings taken at the length ordinate  $L = 240\text{m}$  from the Strain Cable. The variation of the BFS with time as the ambient temperature changes is an unwanted occurrence and it would be useful to eliminate the variation of the BFS output.

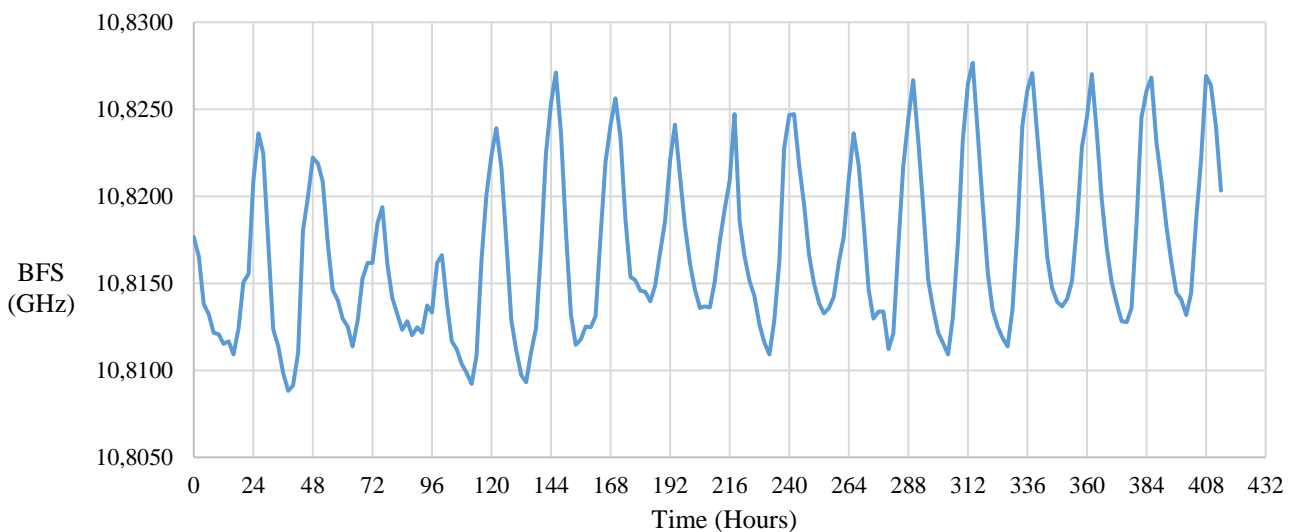


Figure 4-10. A curve of the BFS plotted against time for the length ordinate  $L = 240\text{m}$  along the cable to which the Strain Cable was spliced.

In order to circumvent the problem of variable BFS readings based on the ambient temperature the average BFS reading, with respect to time can be calculated, starting at the beginning of the available data, and ending with the last available data point. The way the average BFS value develops as time progresses can be demonstrated in Figure 4-11.

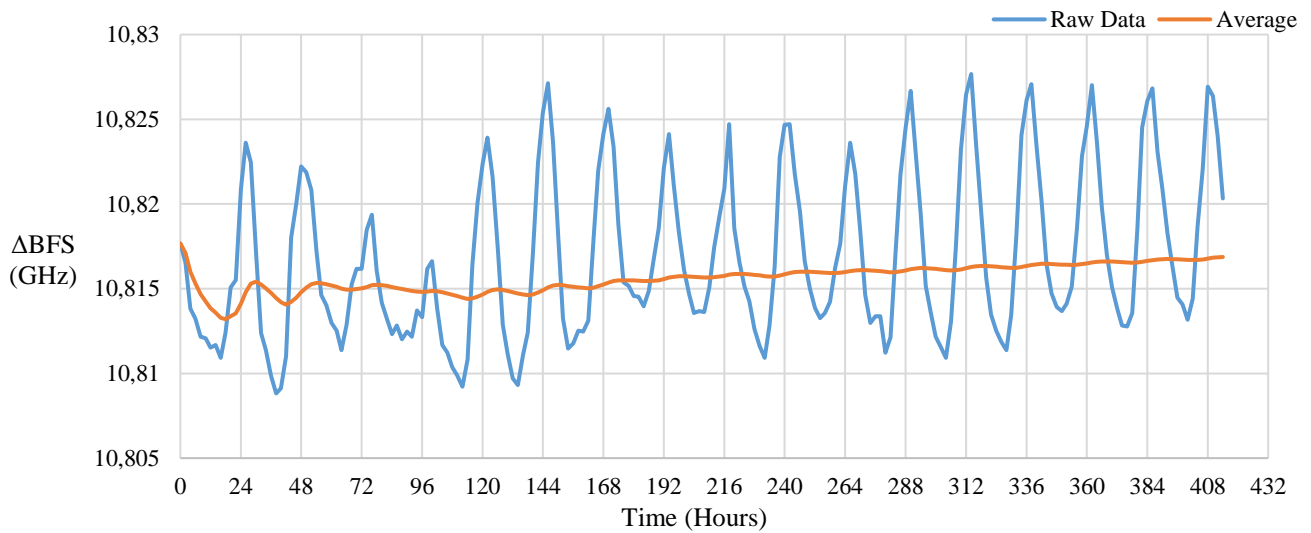


Figure 4-11. A depiction of the development of an average BFS value as time progresses at length ordinate  $L = 240\text{m}$  of the 72F-6C to strain spliced cable.

The data and the development of the average BFS value shown in Figure 4-11 occur over the course of 17 days, from the 14<sup>th</sup> to the 31<sup>st</sup> of December 2020. As time progresses the average BFS curve becomes flatter, thus the more time and data is available for the development of and average BFS value, then ideally the more established the value will be. This means that the average BFS value is less likely to be affected by outlying data. The value becomes stable.

Referring back to Figure 4-9 the length ordinate  $L = 240\text{m}$  is in the non-buried segment of the cable. This is the reason why this segment of the optic fibre shows a much greater change in BFS output 12 hours apart. A fibre optic cable undergoes greater temperature variation when it is in an air medium above ground as opposed to being underground. The soil lying 0.5m below the ground will undergo less temperature variation that the environment at ground level because it is protected from the ambient temperature change by 0.5m of soil. This is demonstrated in Figure 4-12, showing BFS profiles recorded at 280m (0.5m depth), 340m (1.0m depth) and 400m (1.5m depth) in the 72F-6C-LC cable and in the Strain Cable at 530m (0.5m depth) respectively.

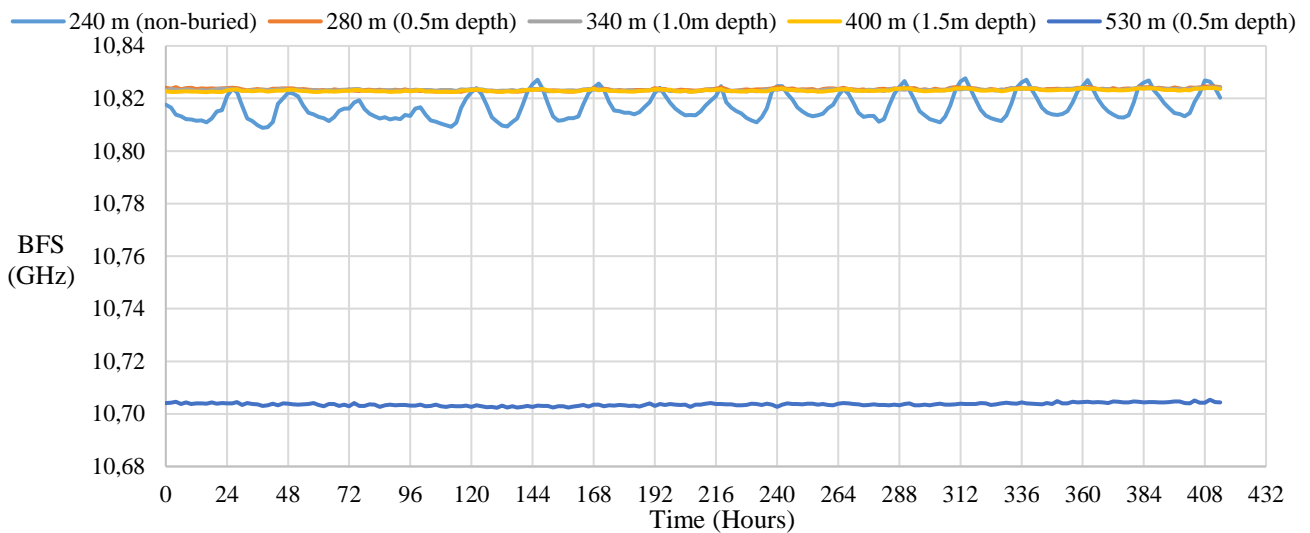


Figure 4-12. BFS vs time plot of the 72F-6C to Strain Cable. Curves are plotted for length ordinates 240m, 280m, 340m, and 400m occurring in the 72F-6C section, and 530m, occurring in the Strain Cable section.

In Figure 4-12 the BFS vs time curves labelled 320m and 530m are taken from segments of the 72F-6C and the Strain Cable, respectively, which are buried in the trench. The BFS vs time plots from length ordinates where the cable is buried are clearly distinguishable from BFS vs time curves plotted for ordinates that are not buried. The cables within the trench experience less BFS variation over time relative to non-buried cables, and this indicates that the cables within the trench undergo less temperature variation as they are separated from the ambient environment by the soil. A set of BFS vs time curves is shown in Figure 4-13 for the 72F-6C-to-Strain Cable.

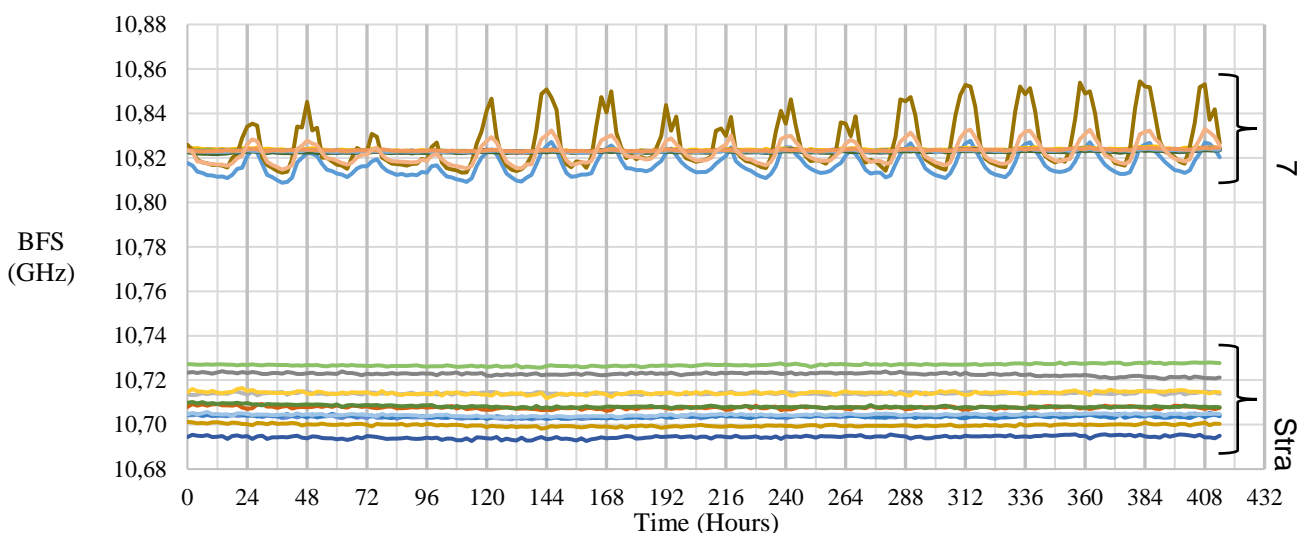


Figure 4-13. BFS vs time curves for the 72F-6C to Strain Cable, plotted from 240m to 580m, every 20m for the 72F-6C cable, and every 5m for the Strain Cable segment.

It is notable that the BFS of the Strain Cable is different to that of the 72F-6C cable. This is because the BFS is also a function of the material composition of the glass of which the fibre

is composed. Thus, the BFS of the 72F-6C-LC and the Strain Cable are different due to the different structural make-up of the optic fibres. This is where the process of developing an average BFS value for each length ordinate, explained in Figure 4-11, becomes useful. By calculating an average BFS value for each length ordinate with respect to time, each BFS vs time curve can be normalised relative to its own respective average BFS value. By normalising the set of curves shown in Figure 4-13, Figure 4-14 can be generated.

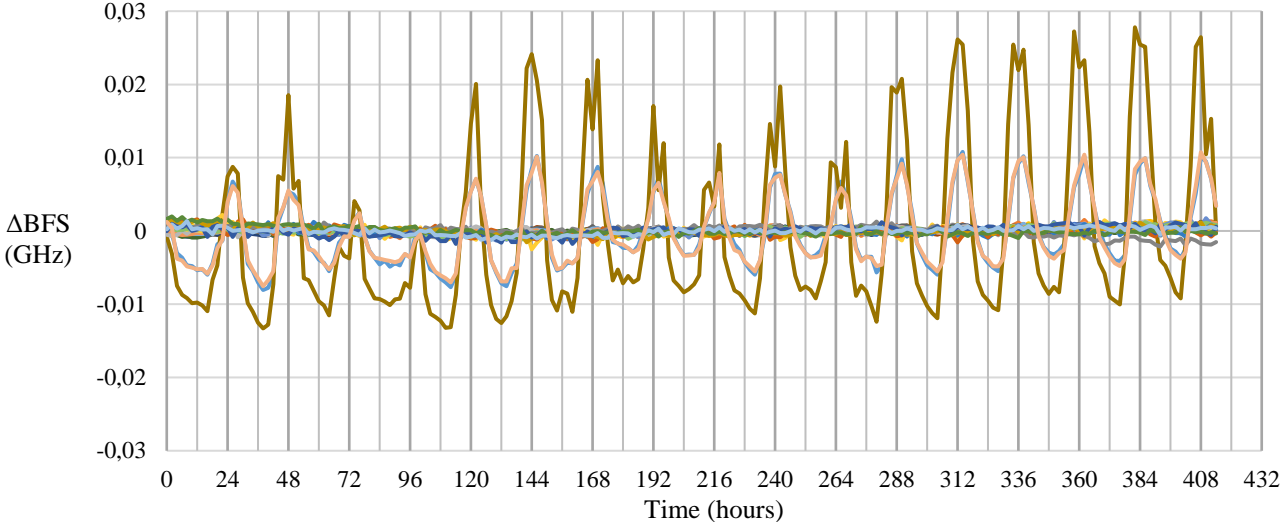


Figure 4-14. Normalised set of BFS vs time curves from Figure 4-13.

4.4.3 AVERAGE BFS PROFILES AND RELATIVE BFS PROFILES

Consider the set of BFS profiles shown in Figure 4-15 showing BFS for the 72F-6C-LC-to-Strain Cable logged over a period of 22 hours at 2 hour intervals.

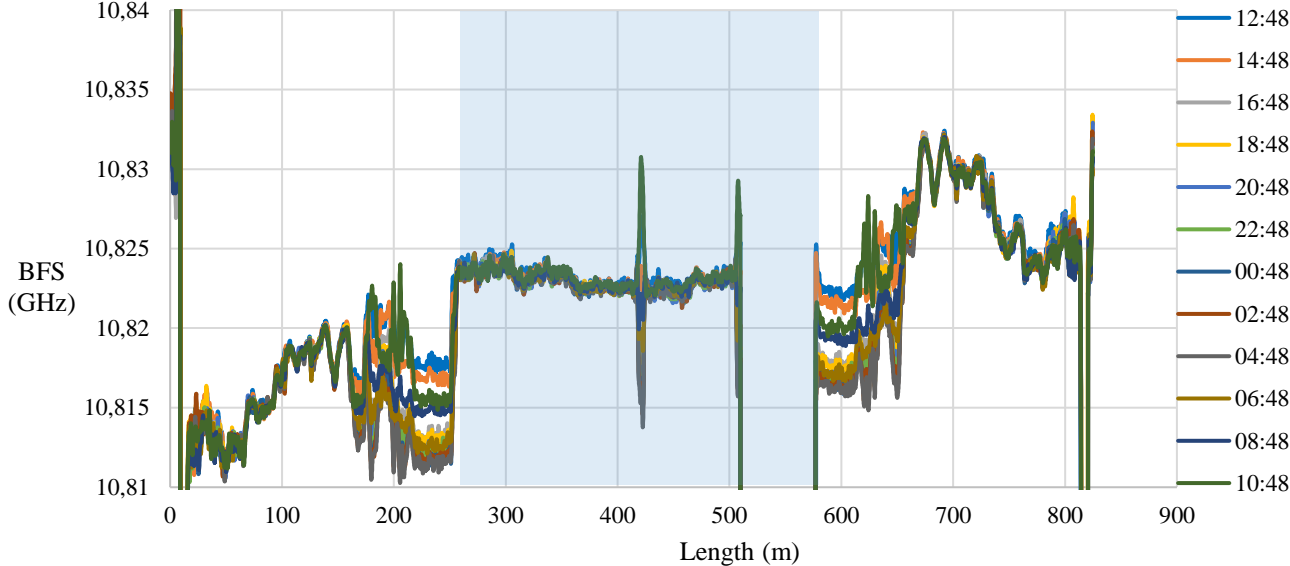


Figure 4-15. Set of BFS profiles of the 72F-6C-to-Strain Cable logged over a period of 22 hours at 2 hour intervals.

As has been demonstrated in Section 4.4.2 this set of BFS profiles can be condensed into a single average BFS profile, by averaging the BFS readings with respect to time for each length ordinate. In doing so a profile such as can be seen in Figure 4-16 can be generated.

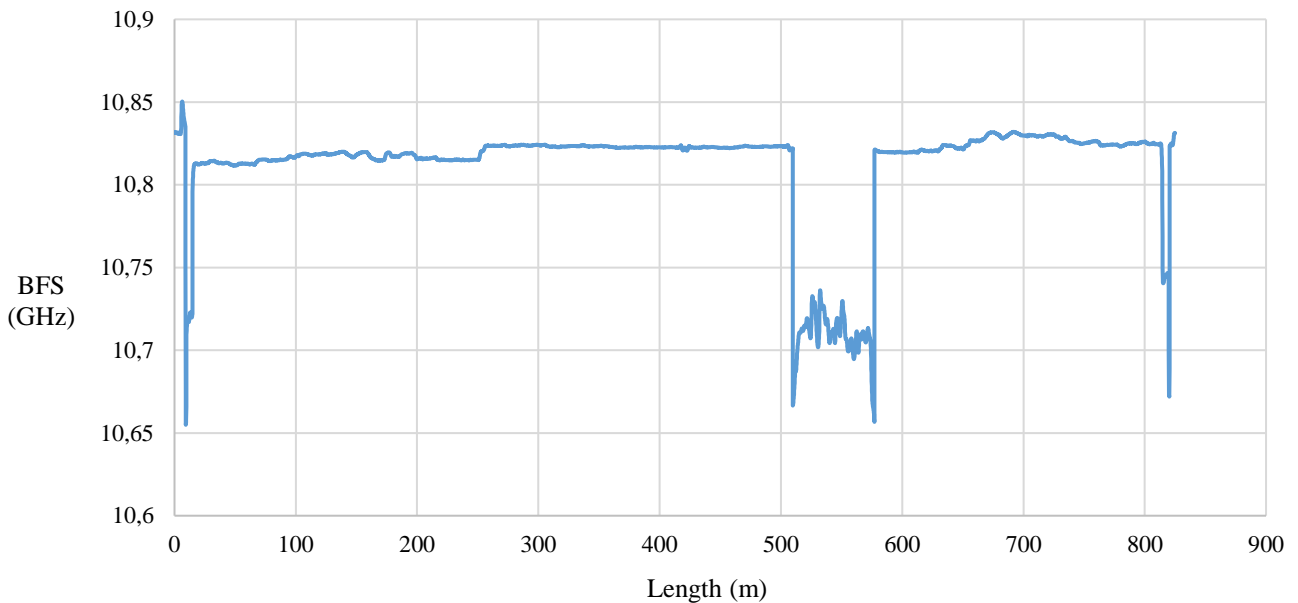


Figure 4-16. An average BFS profile created by averaging 12 profiles logged over a 22 hour time span at 2 hour intervals.

An average BFS profile looks similar to any other BFS profile that was logged at an instant in time. However, it is instead a visual summary of BFS profiles taken over a set period of time conglomerated into a single curve. The greater the time span over which BFS profiles are logged, the more stable the resulting average BFS profile will be as was demonstrated in Figure 4-11. For example, one week's worth of profiles, logged every 2 hours, will create a more stable profile than one day's worth of profiles, logged every 2 hours. The process of logging many profiles to create a stable average BFS profile is establishing a baseline.

A set of average BFS profiles is shown in Figure 4-17.

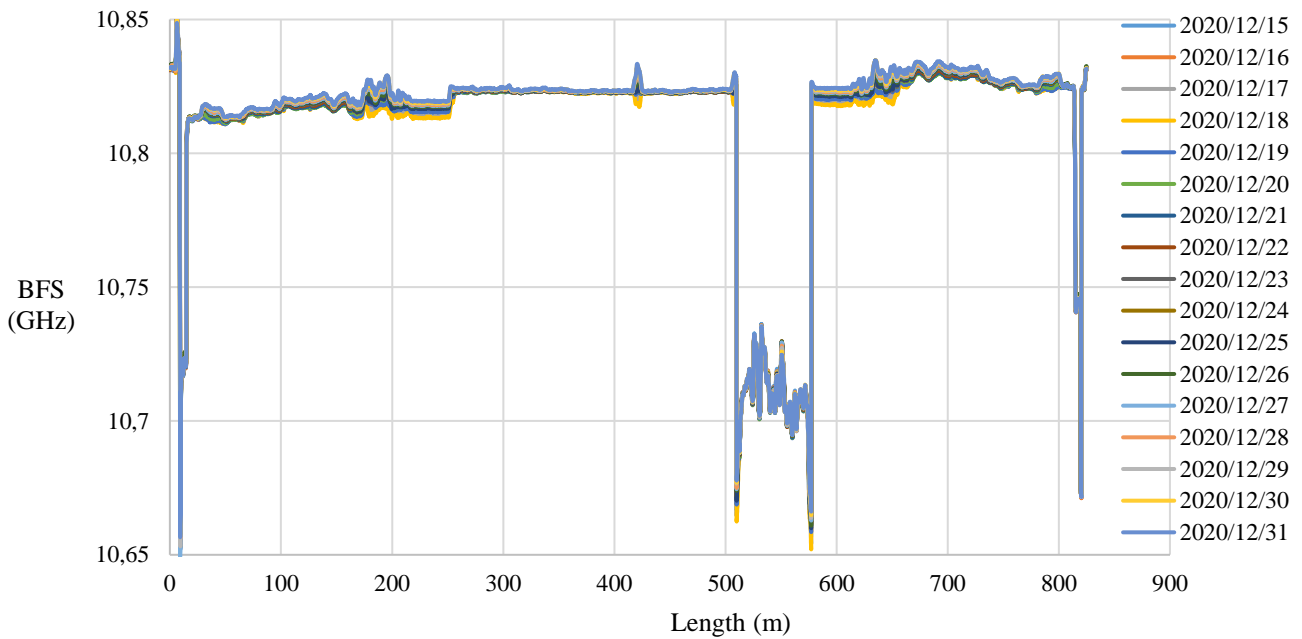


Figure 4-17. A set of average BFS profiles plotted for the 72F-6C-to-Strain Cable.

The set of profiles shown in Figure 4-17 is difficult to distinguish between. This is where a relative BFS profile becomes important. In like manner to what was done in Figure 4-9, an average BFS profile can be chosen as a baseline and can be subtracted from any other profile to generate a relative BFS plot. Choosing the average BFS profile labelled 2020/12/15 from Figure 4-17 as the baseline, and subtracting it from the remainder of the set of average BFS profiles yields Figure 4-18.

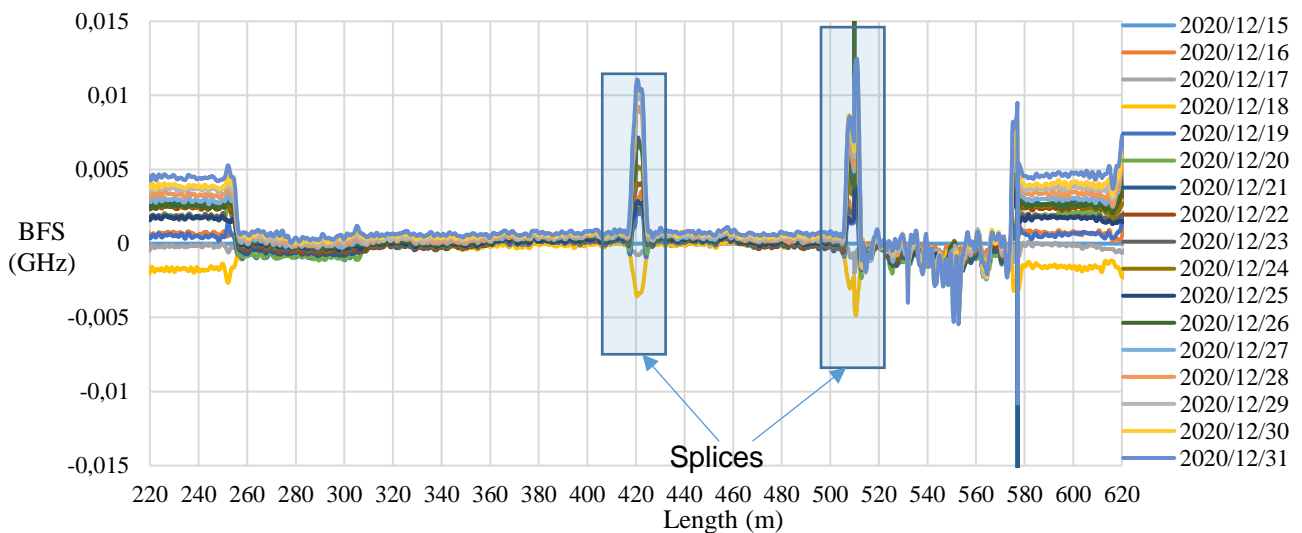


Figure 4-18. Set of average BFS profiles from Figure 4-17 plotted relative to the 2020/12/15 average BFS profile.

As in Figure 4-9, it is easy to see in Figure 4-18 which sections of the cable undergo large temperature variations. Due to the fact that these profiles are daily averages, they give an indication of the average temperature over the course of a day compared to that of a different

day. For example, if an average profile lies above another profile, then the higher profile indicates it experienced a higher average temperature over its day than the lower profile.

Establishing a firm baseline is of utmost importance because it is against the baseline that subsequent readings must be compared in order to detect a disturbance such as a leaking pipe. It is also important to know what the expected BFS output boundaries are for a specific optic fibre as a value that lies outside of this range can also be a flag to indicate a disturbance to the fibre optic cable. Figure 4-19 and Figure 4-20 demonstrate this argument by showing the average BFS plot, and plots of the minimum and maximum BFS values obtained from the 14<sup>th</sup> to the 31<sup>st</sup> of December 2020 for the 72F-6C-to-Strain Cable.

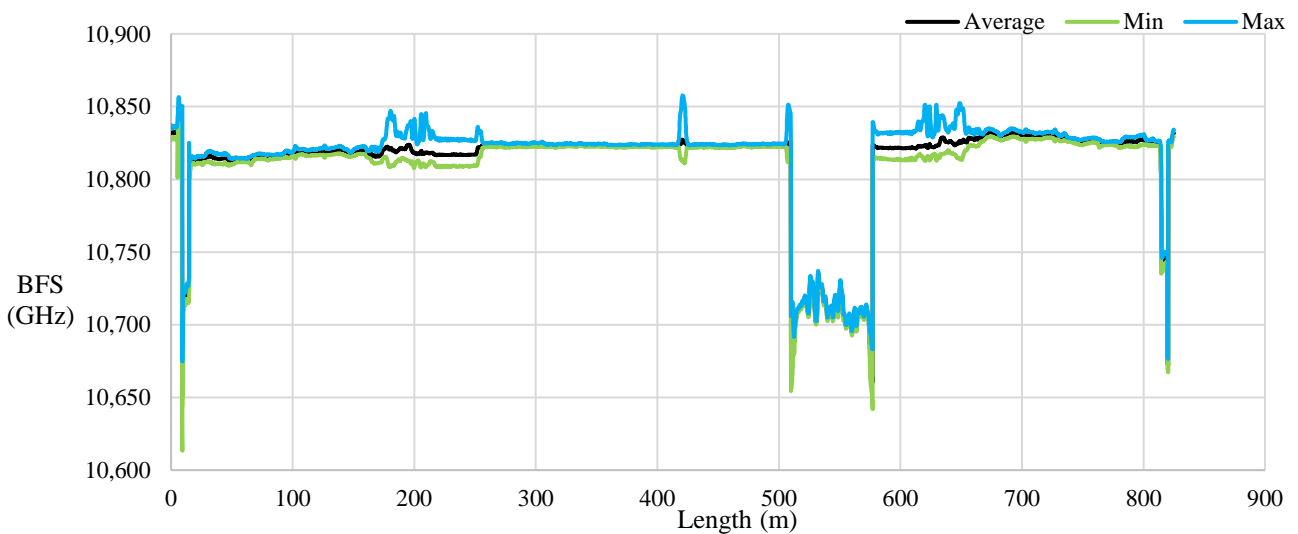


Figure 4-19. Average, minimum and maximum BFS value logged from 14 to 31 December 2020 for the 72F-6C-to-Strain Cable

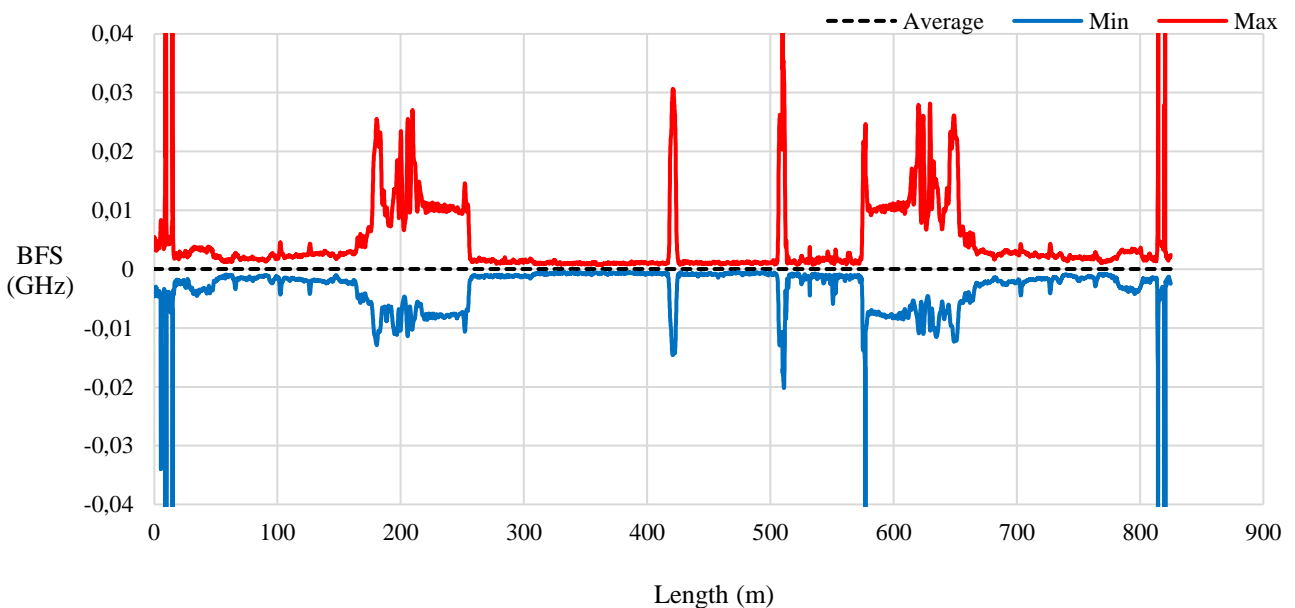


Figure 4-20. Minimum and maximum BFS values logged, as per Figure 4-20, relative to the average BFS profile.

#### 4.4.4 COMPARISON OF THE VARIOUS CABLES

The discussions of Sections 4.4.1 to 4.4.3 have only dealt with the 72F-6C-LC-to-Strain Cable to explain the basin concepts appertaining to the analysis of the data. In this section the results and performance of the various cables shall be discussed.

##### 4.4.4.1 72F-6C-LC-TO-STRAIN CABLE

Consider Figure 4-21, which is repeat of Figure 4-18 without a legend of annotations. The relative BFS profiles of the 72F-6C section of the cable from 260m to 500m plot very smoothly, excluding the splices at 420m and 510m. This is due to the ability of the optic fibre to slide about within the sheath so that it does not experience and register significant changes in BFS due to strains occurring in the soil. The shapes of each BFS profile consecutively logged at a specified time interval are therefore very similar to one another. This is advantageous when establishing a baseline for a cable as the consecutive BFS profiles that are logged are consistent over time and therefore erratic readings will not negatively impact on the average calculated for each length ordinate.

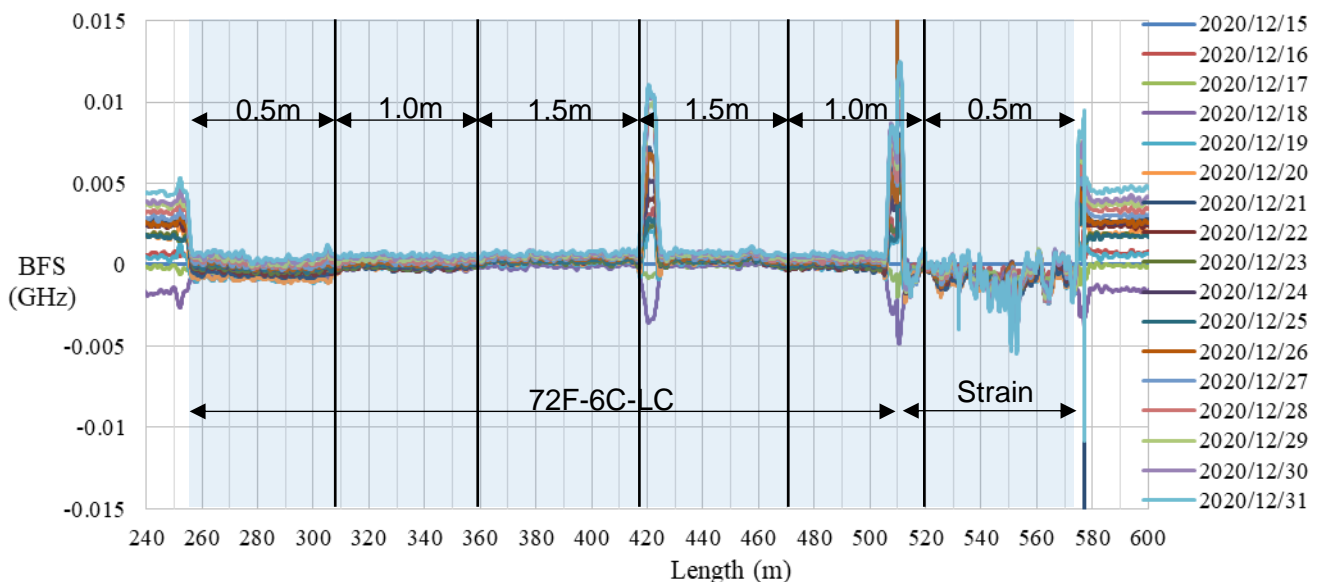


Figure 4-21. Set of relative BFS profiles of the 72F-6C-LC-to-Strain Cable.

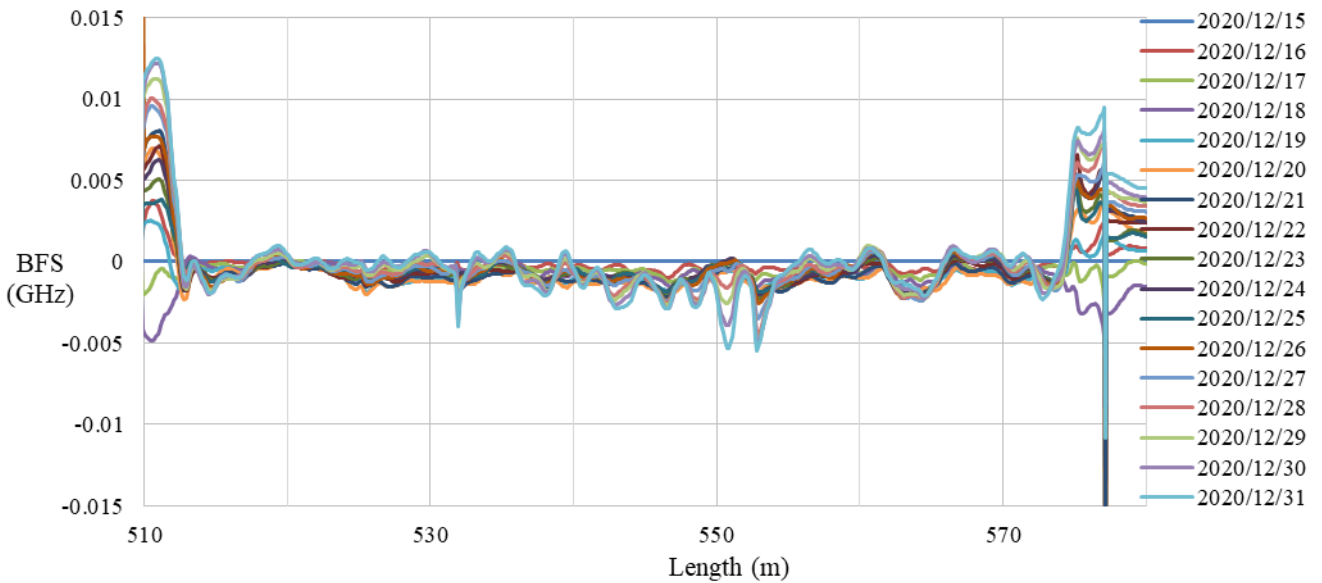


Figure 4-22. Set of relative BFS profiles of the 72F-6C-LC-to-Strain Cable focusing on the Strain Cable section.

Considering the strain segment of the relative BFS profile in Figure 4-21 and Figure 4-22, from 520m to just before 580m, it can be seen that this segment of the profile does not plot as smoothly as the 72F-6C-LC segment. This is due to the contact formulation between the sheath of the cable and the optic fibre it houses. Because the cable is a direct contact design, it means that there is stress transferred onto the optic fibre from the sheath via frictional forces. Therefore, any strains that develop in the soil will have a more pronounced effect on the BFS of the Strain Cable than for the 72F-6C-LC cable. This statement is also backed up by the curves of minimum and maximum registered BFS for the 72F-6C-to-Strain Cable shown in Figure 4-23.

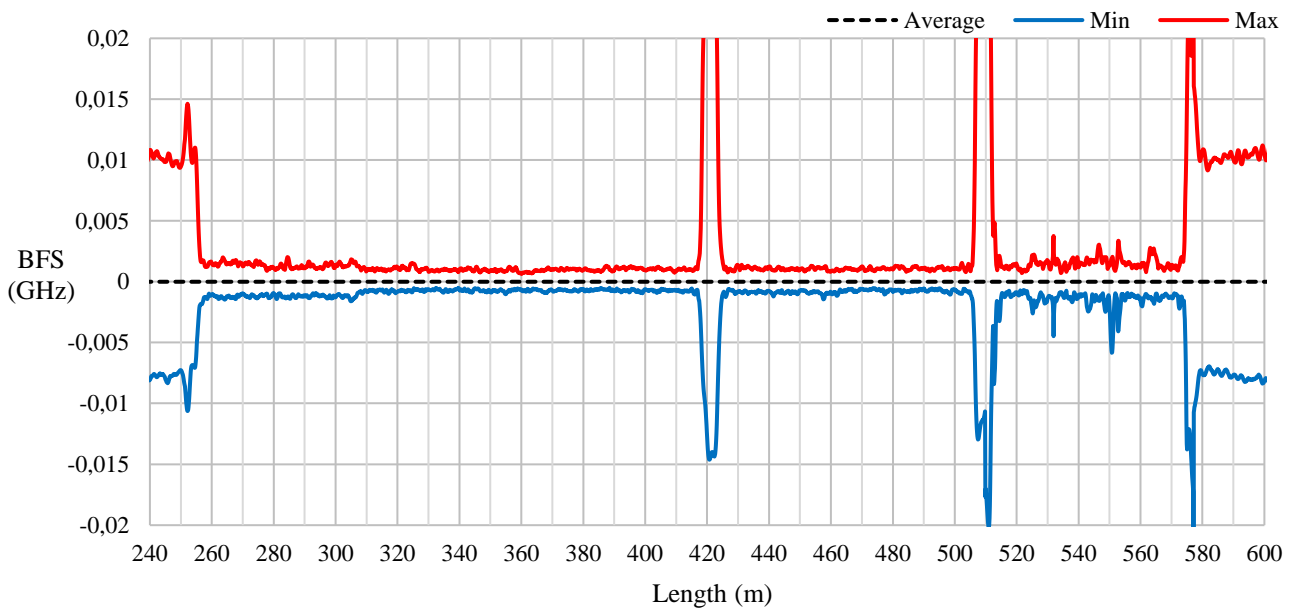


Figure 4-23. Maximum and minimum boundaries of the BFS output logged for the 72F-6C-to-Strain Cable relative to the average BFS profile.

The minimum to maximum envelope relative to the average BFS of the cable, Figure 4-23, is narrower for the 72F-6C-LC cable segment, and wider for the Strain Cable segment. This is because the change in BFS of the 72F-6C-LC cable is primarily caused by temperature variation within the soil, whereas in the strain segment, both temperature and strain play a role in the change in BFS that the optic fibre experiences.

4.4.4.2 6F-TB CABLE

Figure 4-24 presents a set of daily average BFS profiles for the 6F-TB cable. Referring back to Figure 4-4 the 6F-TB cable did not run the full length of the cable. 150m of the 6F-TB cable was used, running one way along the length of the trench and was spliced into a spare fibre of the 72F-6C-LC cable. In Figure 4-24 the 72F-6C-LC cable enters the trench just before 260m and at 420m the splice between the 72F-6C-LC cable and the 6F-TB cable is evident from the sudden jump in the profile. The 6F-TB cable runs from 420m to just before the 570m mark where it is spliced back into the 72F-6C-LC cable to complete the loop.

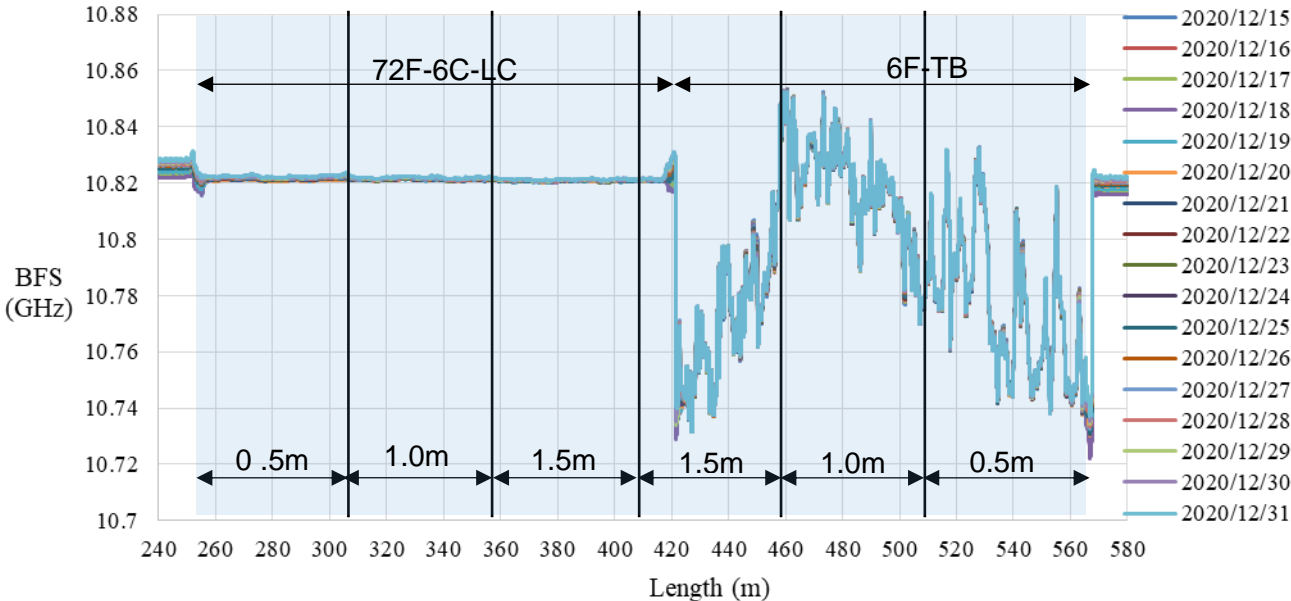


Figure 4-24. Set of daily average BFS profiles for the 72F-6C-to-6F-TB cable from 15/12/2020 to 31/12/2020.

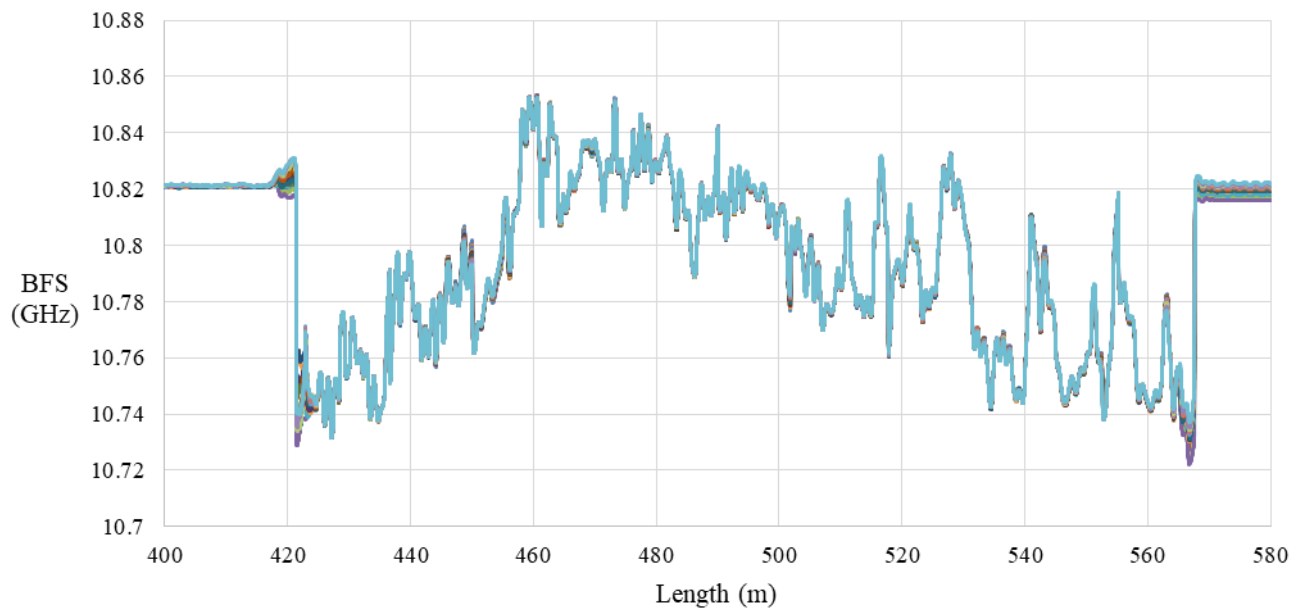


Figure 4-25. Set of daily average BFS profiles for the 72F-6C-to-6F-TB cable focused on the 6F-TB section.

Converting the data in Figure 4-24 into a plot of relative BFS profiles, relative to the 15/12/2020 profile, the set of relative BFS profiles shown in Figure 4-26 is created. Looking at Figure 4-26 and comparing the 72F-6C-LC cable against the 6F-TB cable, the 72F-6C-LC cable profiles are significantly more consistent than the profiles of the 6F-TB cable. The 6F-TB cable is a tight buffered cable, which means that the optic fibres housed by the surrounding sheath experience a significant amount of strain transfer, via friction, from the sheath onto the optic fibre. Like the Strain Cable, the baseline readings of a tight buffered cable will be affected both by temperature variation, and strains that develop in the surrounding soil. This gives rise to the variable daily average BFS profiles, relative to the 15/12/2020 average profile.

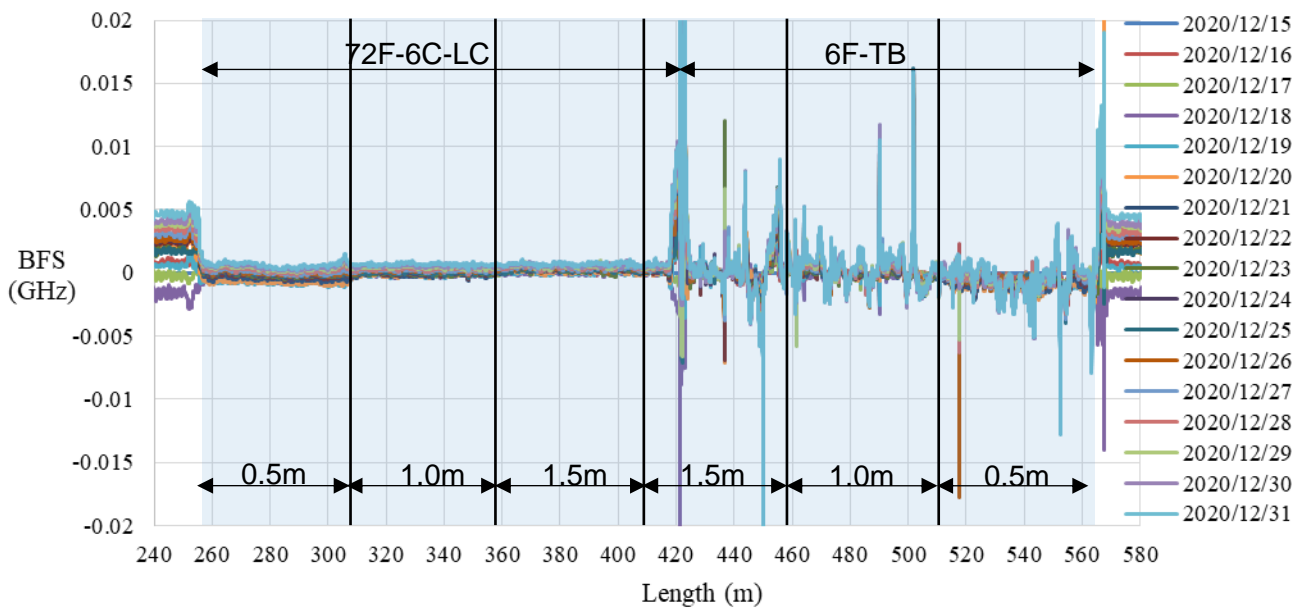


Figure 4-26. Set of daily average BFS profiles relative to the 15/12/20 profile for the 72F-6C-to-6F-TB cable from 15/12/2020 to 31/12/2020.

Plotting the minimum-maximum envelope, relative to the average BFS profile, of the 72F-6C-to-6F-TB cable Figure 4-27 is obtained.

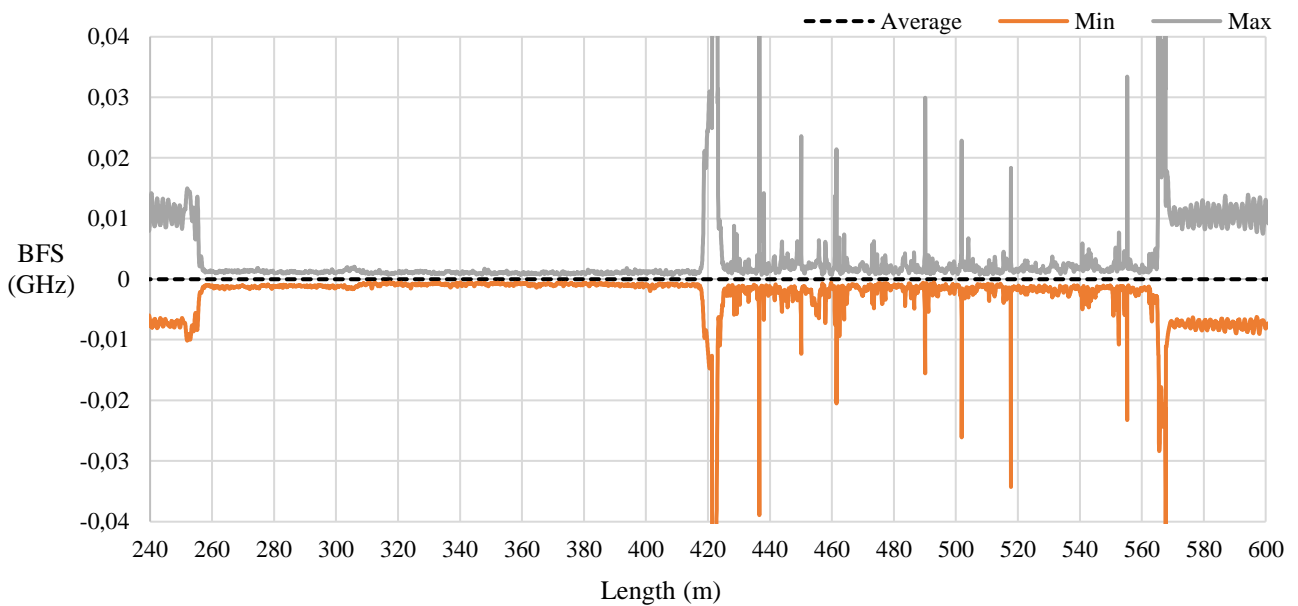


Figure 4-27. Minimum-maximum envelope of the 72F-6C-to-6F-TB cable.

The minimum-maximum envelope for the 6F-TB cable segment has a wider range than that of the 72F-6C-LC cable as expected. However, there are spikes on the envelope that do not fit within the expected boundaries of the envelope (not to be confused with the wider envelope where the splices are located). These outlying data points are the extreme values, but if they occur often enough they could possibly offset the average BFS value that is calculated over time at the length ordinate where they occur.

#### 4.4.4.3 4F-DC-LC CABLE

The set of daily average BFS profiles for the 4F-DC cable is shown in Figure 4-28.

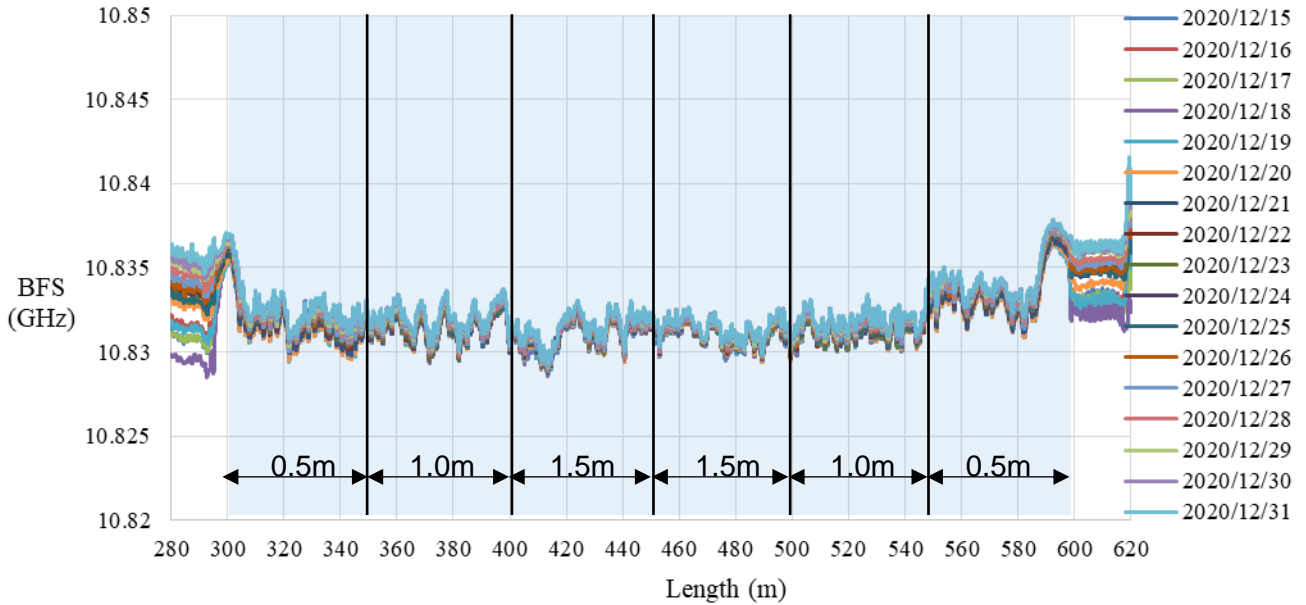


Figure 4-28. Set of daily average BFS profiles for the 4F-DC cable from 15/12/2020 to 31/12/2020.

The BFS of the profiles do not vary over the length of the cable as much as the 6F-TB. The 4F-DC-LC cable behaviour is more like that of the 72F-6C-LC cable, due to the gel surrounding the fibres reducing the effect of frictional force transfer from the sheath onto the optical fibres. Plotting the average BFS profiles from Figure 4-28 relative to the 15/12/2020 profile yields Figure 4-29.

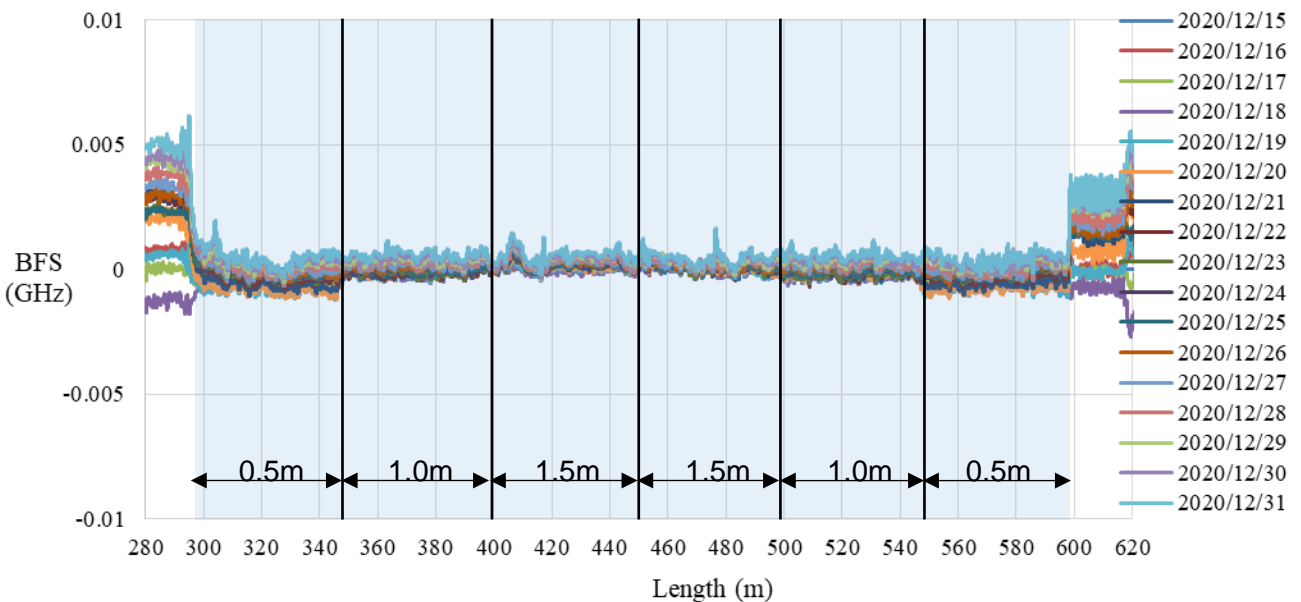


Figure 4-29. Set of daily average BFS profiles relative to the 15/12/2020 profile for the 4F-DC-LC cable from 15/12/2020 to 31/12/2020.

As is illustrated in Figure 4-29 the BFS profiles do not differ from one another as significantly as the 6F-TB and the Strain Cables do. The profiles of the cable therefore give near constant BFS profiles as time progresses. This is further reinforced when considering the minimum-maximum envelope of the 4F-DC cable shown in Figure 4-30.

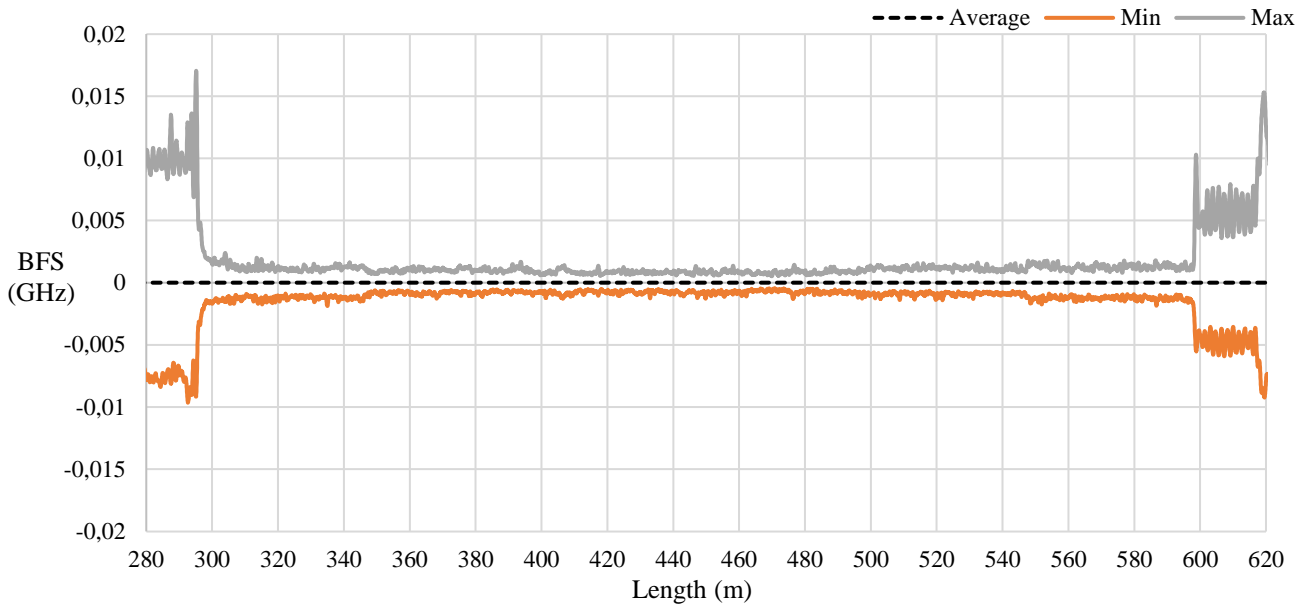


Figure 4-30. Minimum-maximum envelope of the 4F-DC cable.

The minimum-maximum envelope of the 4F-DC cable is flat and smooth like that of 72F-6C-LC cable, showing a consistent baseline.

#### 4.4.4.4 2F-TB CABLE

In Figure 4-31 the set of daily average BFS profiles for the 2F-TB cable is plotted.

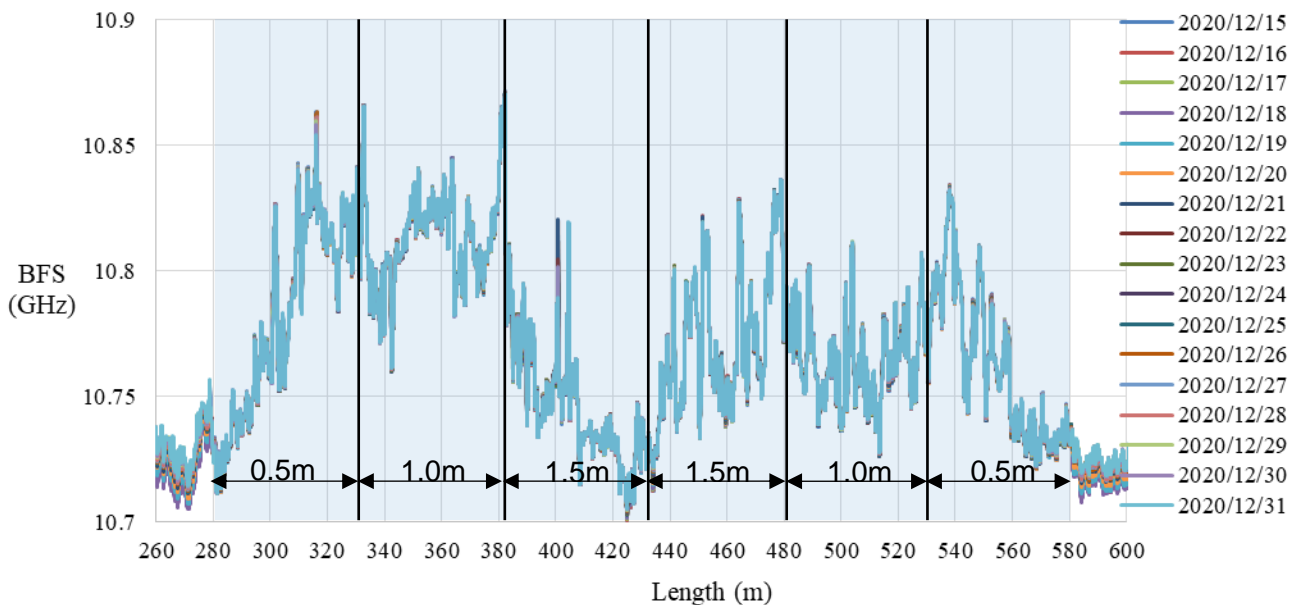


Figure 4-31. Set of daily average BFS profiles for the 2F-TB cable from 15/12/2020 to 31/12/2020.

Like the 6F-TB, the 2F-TB also has a wide variance over which BFS outputs can be expected over the length of the cable. In addition to the wide variance of expected outputs, the profiles have regions with steep gradients between data points. These occurrences of steep gradients not lining up perfectly between consecutive readings could possibly give rise to the spikes seen in the relative BFS profiles shown in Figure 4-32.

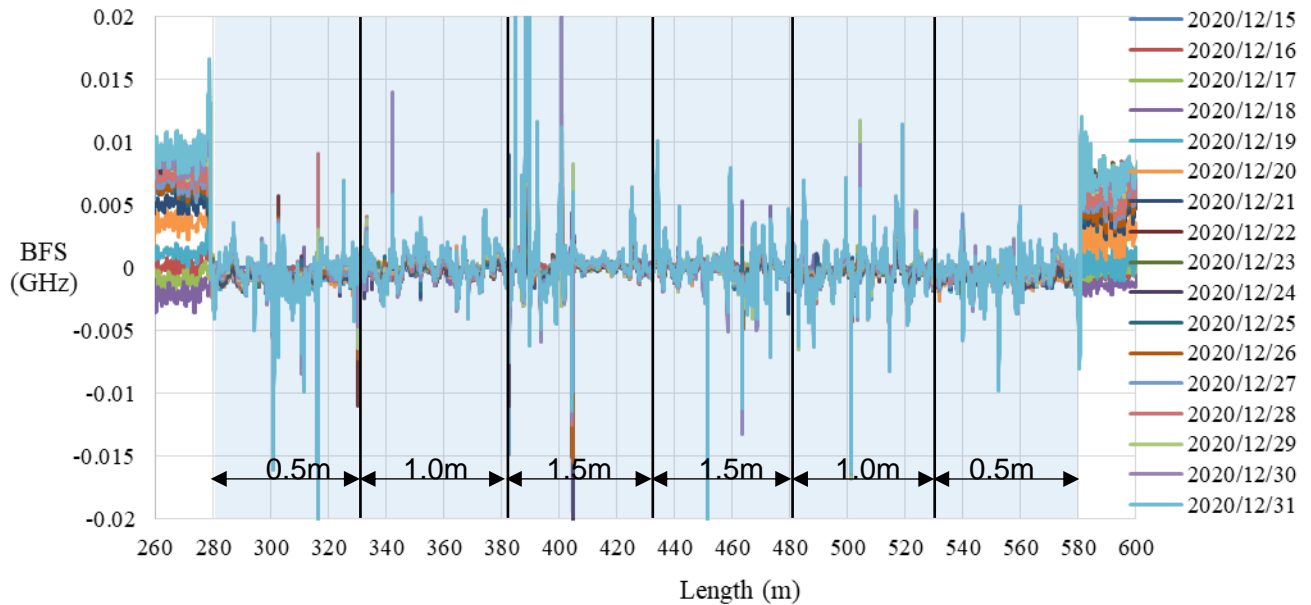


Figure 4-32. Set of daily average BFS profiles relative to the 15/12/20 profile for the 2F-TB cable from 15/12/2020 to 31/12/2020.

The tight buffered cables: 6F-TB and 2F-TB both output BFS profiles which are not consecutively consistent. The problem associated with this inconsistency is that a well-established baseline will require much more data to develop and such a baseline may not be able to be developed from the BFS readings logged for these cables. As can be seen in Figure 4-33 there are again data spikes which lie outside of the expected boundaries of where the maximum and minimum BFS values are expected to occur.

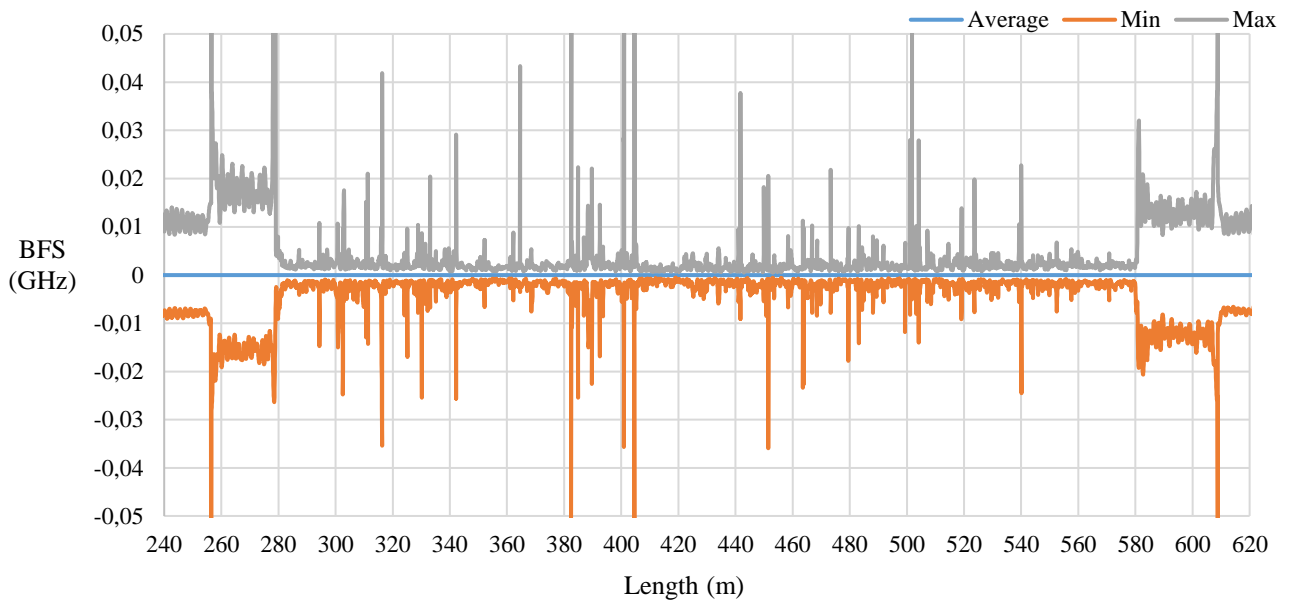


Figure 4-33. Minimum-maximum envelope of the 2F-TB cable.

## 4.5 LEAK TEST RESULTS

To detect a change in the system using the FO cables, Brillouin Frequency Shift (BFS) output profiles were compared. Changes in BFS output indicate that an event, such as a leak, had taken place. In this chapter the computational methods used to process the data acquired from the leak tests, so that leaks can be detected, are discussed.

### 4.5.1 Data Processing Methodology

One set of results from the first leak test on 24 March is used to explain how the raw data can be processed to show whether a leak has occurred. For explanation purposes the 6F-TB to 72F-6C-LC cable are used to explain the results and data processing. Thereafter, each cable's results are plotted for comparison.

The leak test conducted on the 24 March was preceded by acquiring a 24-hour average BFS baseline over the course of the 23<sup>rd</sup> of March. Readings were taken every 2 hours, resulting in 12 readings to compute the 24-hour average BFS baseline. After the water had been introduced into the trench, a 24-hour average baseline was acquired for 24 March. The result of subtracting the 23 March baseline from the 24 March baseline is a relative BFS profile depicting the change that occurred due to the ingress of water into the surrounding soil. The relative BFS profile is shown in Figure 4-34.

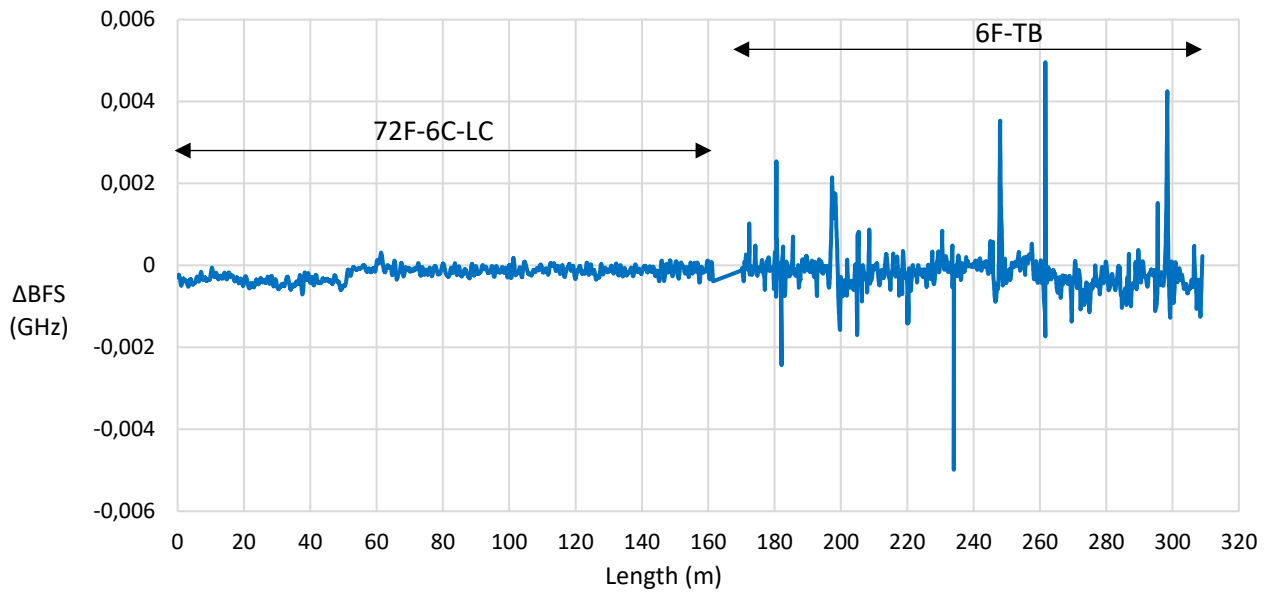


Figure 4-34. Relative BFS plot generated by subtracting the 23 March baseline from the 24 March baseline.

#### 4.5.1.1 Centred Moving Average

As can be seen in Figure 4-34 the output of the relative profile is noisy (there are unwanted, random sharp peaks that occur in the relative plot). The random noise that occurs in the relative profiles can hinder the system's ability to detect leaks, as a sharp peak may be mistaken for a leak by a leak detection algorithm. To rid the profile of this noise, the output can be processed by applying a centred moving average (CMA) using 25 data points. By using a CMA, the random noise of the output can be reduced significantly, generating a well-defined plot of the relative BFS profile. Figure 4-35 shows a comparison between the raw relative output and the "cleaned" 25-point CMA relative profile output.

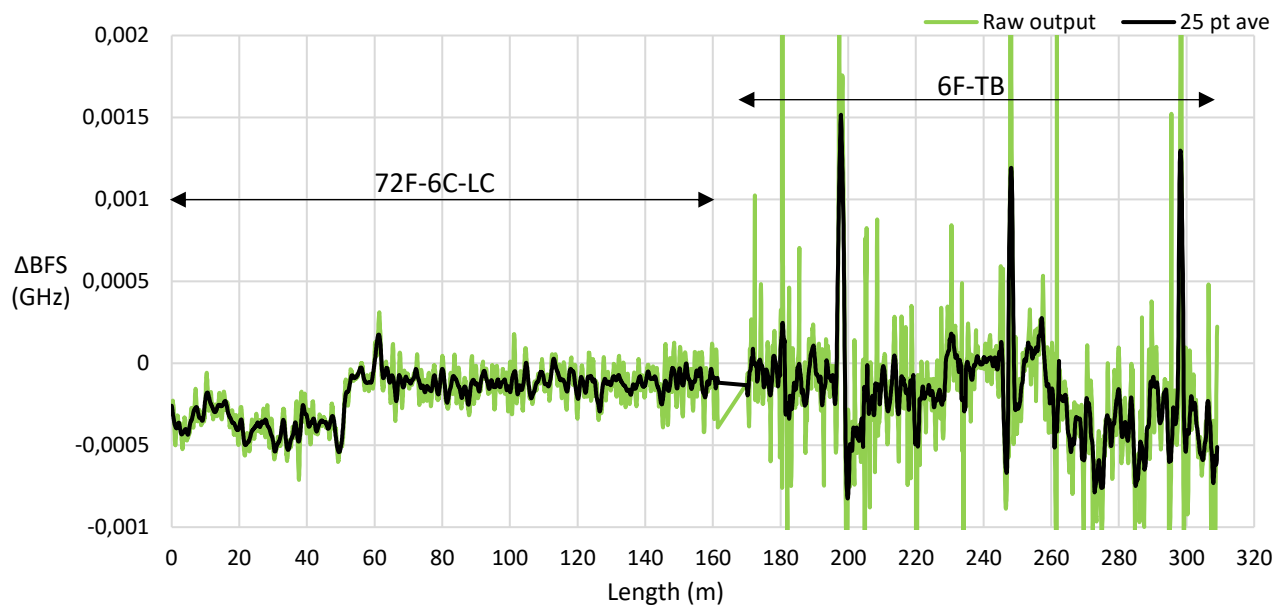


Figure 4-35. A plot of the raw relative profile output as well as the 25-point moving centred average created from the raw data output.

As can be seen in Figure 4-35 the random spikes that occur in the raw relative profile output have been smoothed by applying the CMA. There is a major benefit in applying the CMA as it renders the peaks where the leaks occurred clearly detectable from the rest of the profile. The disadvantage of using the CMA, however, is that the peaks that denote a leak are smaller in magnitude compared to their raw output. It is therefore crucial that enough points be used in the centred CMA so that the output is sufficiently cleaned with minimal reduction in the leak-peak heights.

#### 4.5.1.2 Zeroing Relative Profile

Although the profile in Figure 4-35 has undergone some noise reduction, the profile is not necessarily centred about the horizontal (length) axis. Having the profile centred about the length axis is useful as the regions of the profile that would be further away from the length axis, and deviating away from the trend of the data, would represent possible leak points. To centre the data about the length axis another CMA can be generated from the raw data, but using significantly more points. In this case 601 points are used to generate a CMA that can be used to centre, or zero, the data. 601 data points corresponds to roughly 30m of FO cable length, as the spatial resolution of the interrogator output is around 5cm. By using 601 points the raw output profile is flattened, i.e. the curvature of the data is greatly smoothed out. The result is a smooth line that passes through the data with the same general shape as the original data. The raw relative output, the 25-point CMA and the 601-point CMA are represented in Figure 4-36.

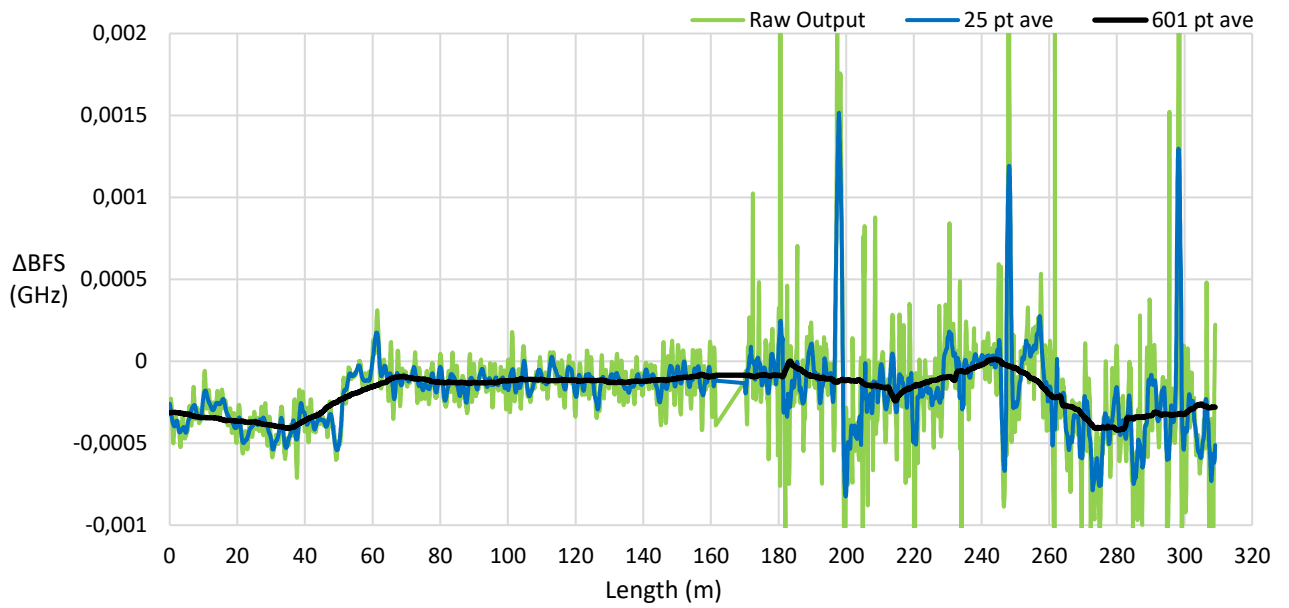


Figure 4-36. A set of curves representing the raw relative BFS output profile, a 25-point CMA and a 601 point CMA.

It is evident from Figure 4-36 that the 601-point CMA follows the same general shape as the raw output and the 25-point CMA. Thus, if the 601-point CMA is subtracted from the raw output or the 25-point CMA the latter profiles will be centred, or zeroed, with respect to the length axis. A comparison of the 25-point CMA relative profile before and after being zeroed about the length axis is shown in Figure 4-37.

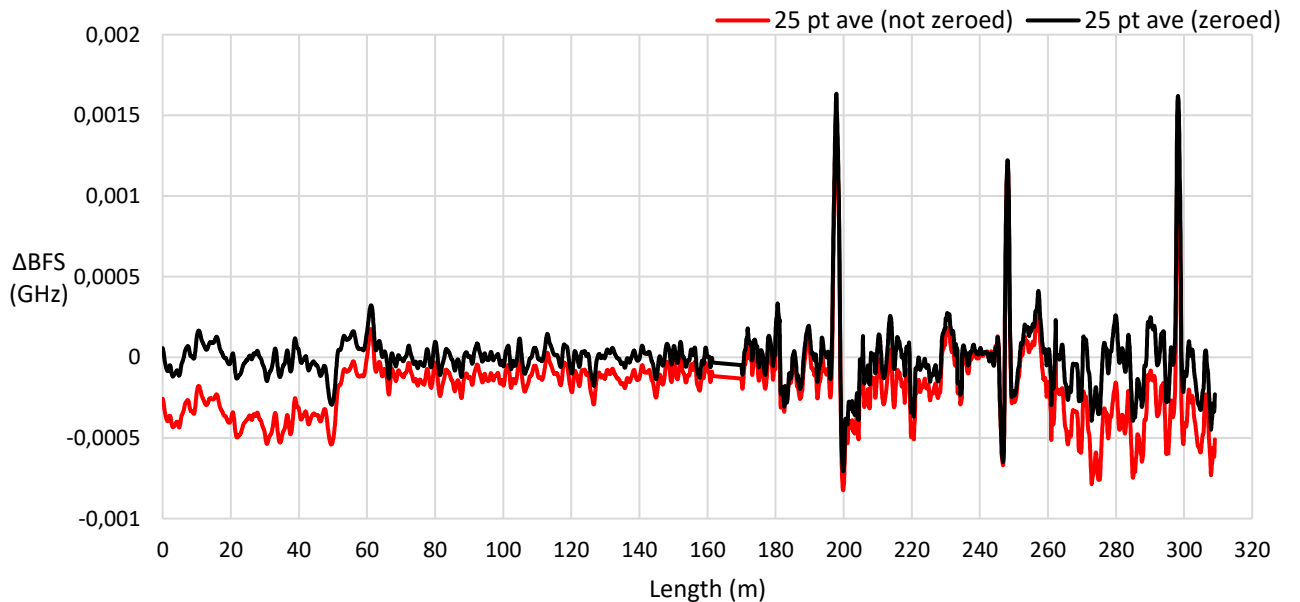


Figure 4-37. 25-point CMA relative profile before being zeroed and after being zeroed.

The zeroed raw and 25pt CMA profiles are both depicted in Figure 4-38.

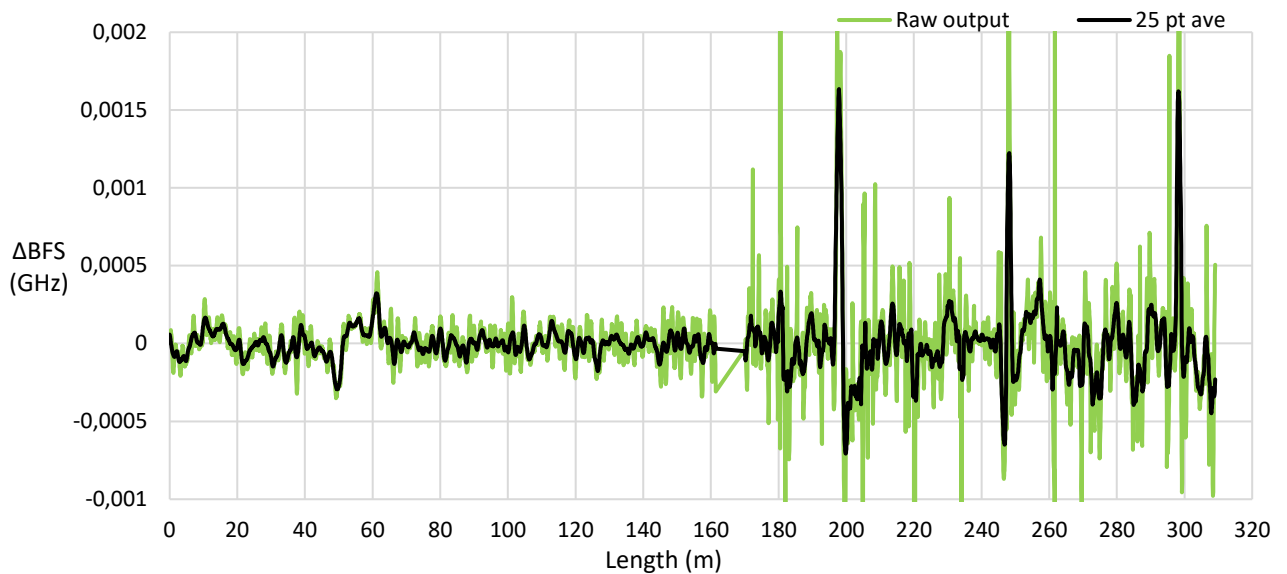


Figure 4-38. Zeroed raw output and 25pt CMA profiles generated by subtracting the 601 point CMA.

#### 4.5.1.3 Squared Relative Profile

The regions where leaks occurred along the 6F-TB FO cable length clearly stand out from the rest of the profile at length ordinates 200m, 250m and 300m. The leak points on the 72F-6C-LC cable, however, are not as evident as the 6F-TB cable. This is because the 6F-TB cable is more sensitive to strain effects imposed by a soil moisture content change than the 72F-6C-LC cable. The leak points can, however, be made even more prominent. If the values comprising the 25-point CMA profile shown in Figure 4-38 are squared then the portions of the profile that show greater change in BFS, i.e. data points further from the length axis, will be made even greater. In addition, the values lying below the length axis will be made positive values due to the nature of the squaring function. The squared 25-point CMA relative profile is shown in Figure 4-39.

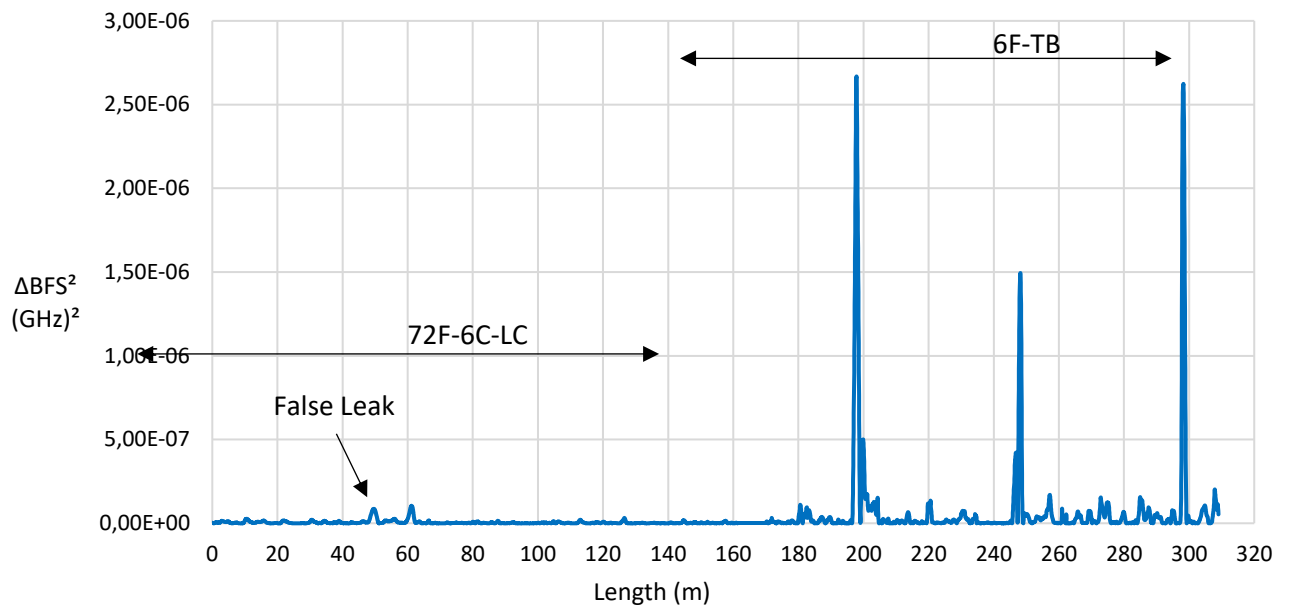


Figure 4-39. Squared 25-point CMA relative profile.

The peaks occurring at 200m, 250m and 300m have been made very distinct from the rest of the profile in Figure 4-39 by squaring the zeroed 25-point CMA relative profile. There is no doubt that these peaks in the 6F-TB segment of Figure 4-39 correspond to the leaks imposed in the trench, as the peaks line up perfectly with the locations of the water-introduction standpipes.

The 72F-6C-LC, on the other hand, was only able to detect one leak in this instance at 60m. The 72F-6C-LC cable should show peaks at 10m, 60m and 110m. Furthermore, a false leak was detected by the 72F-6C-LC cable at 50m.

#### 4.5.1.4 Comparison Against Expected Minimum And Maximum BFS Response

In reality however, it will not be known where, or if a leak has even occurred. An algorithm, or multiple algorithms, shall need to be applied to the data output of FO cable monitoring a pipeline and a decision must be made, based on the output, whether a leak has occurred or not. One algorithm is proposed as follows: if a leak occurs, the expected BFS might change such that the BFS response occurs outside the expected minimum or maximum BFS response. Therefore, if a BFS response occurs outside of the expected BFS response range it could be inferred that a leak has occurred at the length ordinate where such an event has taken place in the data. This methodology is visualised in Figure 4-40.

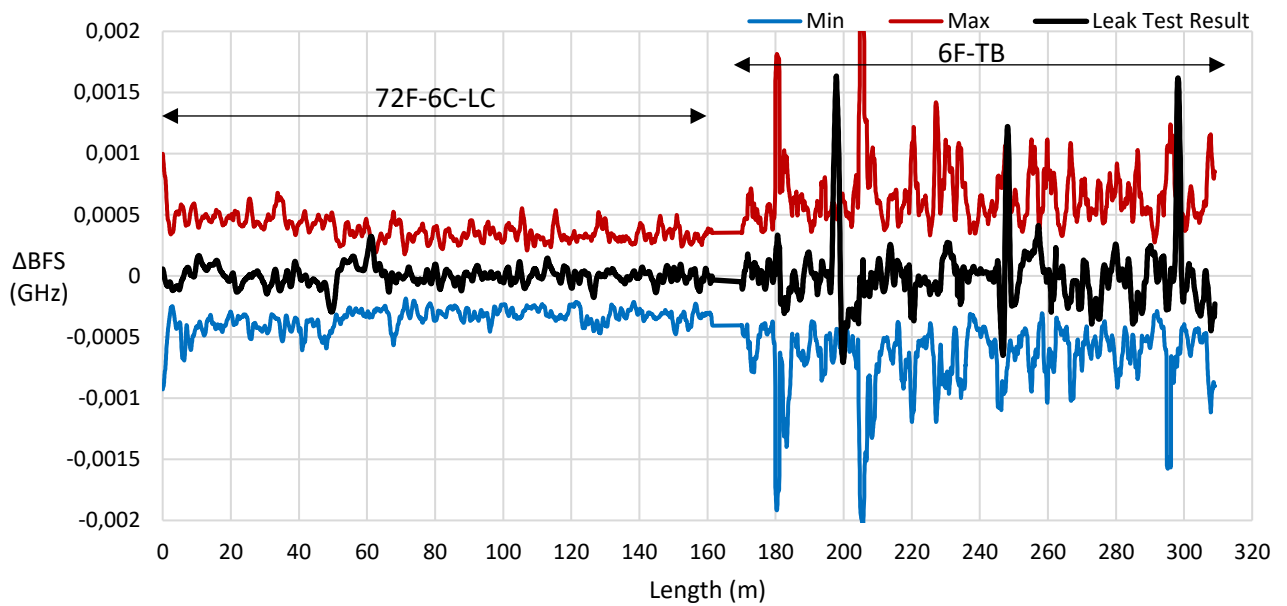


Figure 4-40. Leak test result shown against the minimum and maximum expected bounds of the 72F-6C-LC to 6F-TB cable.

The regions where leaks were induced into the trench are seen to exceed the maximum expected BFS boundary in the 6F-TB cable, but it is not certain in the segment of the 72F-6C-LC cable. To ascertain as to whether a boundary has been exceeded, a simple test can be performed: if the leak test result profile exceeds either boundary, maximum or minimum, then the absolute difference between the result and the respective boundary can be returned. This test is illustrated in Figure 4-41.

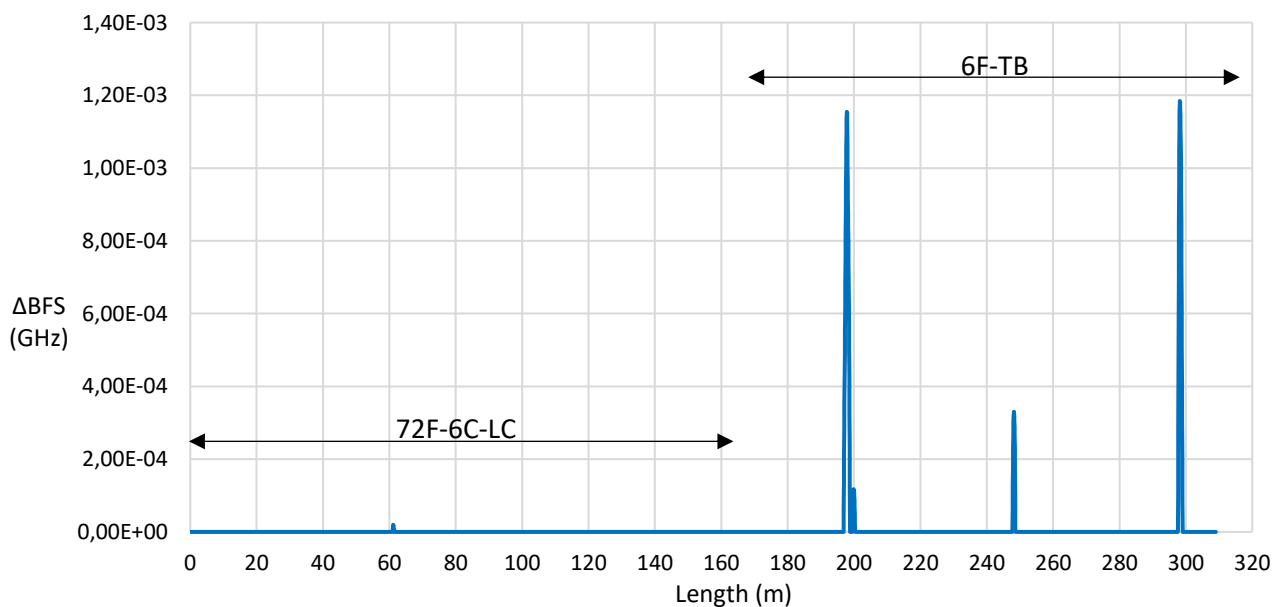


Figure 4-41. Regions of the zeroed 25-point CMA relative profile that exceeded the minimum-maximum expected BFS boundary.

As can be seen in Figure 4-40 and Figure 4-41, this detection method appears to work when applied to the 6F-TB cable output. It has also been successful when applied to the output

supplied by the 72F-6C-LC cable, as seen by the small spike at the 60m length ordinate in Figure 4-41. However, the change in BFS of the 6F-TB cable beyond the boundary was far greater than the 72F-6C-LC cable. This is because the method of comparing a result to the maximum and minimum boundaries is dependent on the mechanical properties of the cable. The maximum and minimum expected BFS boundary for a FO cable is dependent on the temperature fluctuation that the cable experiences. Cables that respond well to strain responses can exceed their maximum and minimum boundaries more easily when influence by a changing soil moisture content imposing strain on the cable. Cables that are sensitive primarily to temperature changes are less sensitive to imposed strain. Because the 6F-TB cable is more sensitive to soil strains than the 72F-6C-LC cable, the 6F-TB cable BFS response is more greatly affected by a leak and it is able to exceed the maximum-minimum boundary at all three leak points as demonstrated in Figure 4-41. The 72F-6C-LC cable only exceeded the maximum boundary at the 60m length ordinate, but to a much lesser extent in comparison to the 6F-TB cable.

This comparison of the two cables types, loose-core (LC) versus tight-buffered (TB), shows that the performance of a FO cable is dependent on its structure. Although TB cables produce more noisy raw data, their performance as leak detection sensors seems significantly better than that of LC cables once the data has been processed.

#### 4.5.1.5 Repeatability of Detection

It has been shown that the FO cables are indeed capable of detecting leaks that could occur along a length of pipeline. However, it would be beneficial if the system could detect a leak at the same length ordinate even if a leak has previously occurred at that length ordinate. To test this the results of the first leak test (24 March) and the second leak test (1 April) can be plotted relative to the baseline recorded on the 23<sup>rd</sup> of March. The results of both leak tests relative to the 23<sup>rd</sup> of March are plotted in Figure 4-42.

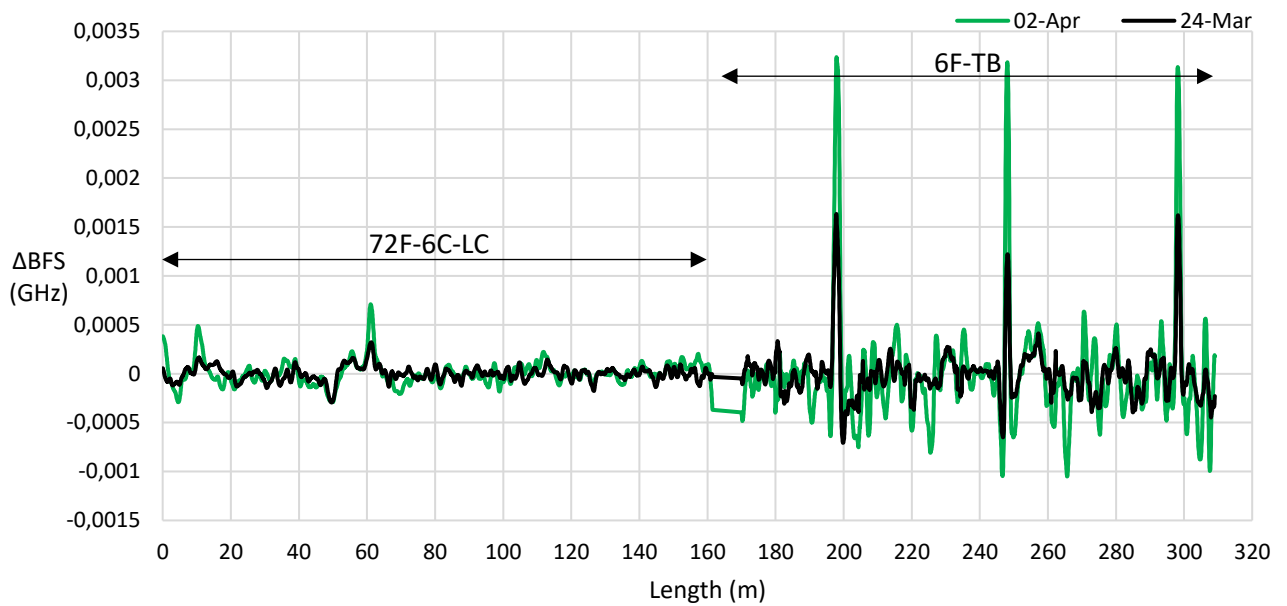


Figure 4-42. Results of the first (24 March) and second (1 April) leak test plotted relative to the 23<sup>rd</sup> of March baseline. The curve labelled 02-Apr is indicative that it is generated from a baseline logged on the 2<sup>nd</sup> of April after the second leak had taken place on the 1<sup>st</sup> of April.

From Figure 4-42 the proposition that a leak can be detected at the same length-ordinate more than once has proven successful in both the 72F-6C-LC and the 6F-TB cables. In the 6F-TB segment it appears as though the results of the second leak test yield peaks that are roughly double the height of the first leak test. This is attributed to the fact that the result of the second leak test, relative to the 23<sup>rd</sup> of March is showing the combined effect of the two leak tests. The strain response from the second leak test has been added to the strain response of the first leak test. The 72F-6C-LC cable was also able to register a response at two of the three leak points along the cable length. It can therefore be concluded that repeatability of detection is viable even after a section of soil has been wetted by a previous leak.

#### 4.5.2 BFS Response In The Time Domain

In order for a FO cable to detect a leak along a working pipeline a change in BFS output must be registered. It is therefore necessary to understand how the BFS response behaves in the time domain to assess how a change in BFS develops and whether there is any signal decay after a leak has occurred.

The result of the leak test conducted on the 1<sup>st</sup> of April, introducing 50 litres without a monitored flow rate, recorded by the 6F-TB cable is shown in Figure 4-43. The 6F-TB was able to again detect all three water leaks, whereas the 72F-6C-LC cable was only able to clearly detect two of the three leaks at standpipes 1 and 4, with the leak at standpipe 7 not clearly indicated.

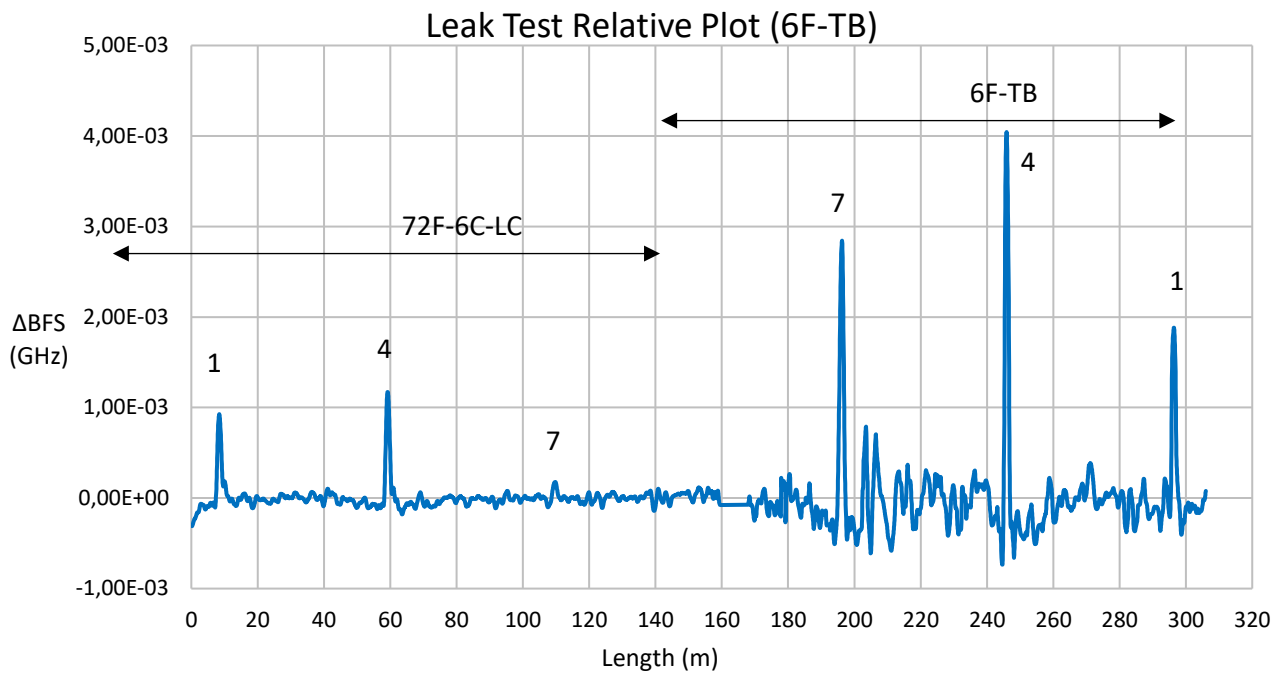


Figure 4-43. Results of the leak test conducted on the 31<sup>st</sup> of March output by the 6F-TB cable.

The result displayed in Figure 4-43, however, is a static plot of the change in BFS output displaying the locations where the leaks were detected. If the attention is shifted from the length domain to the time domain it can be seen how the BFS changes as a short leak (50 L) occurs. A plot of the change in BFS at the three leak points for the 6F-TB cable and the 72F-6C-LC cable is shown in Figure 4-44.

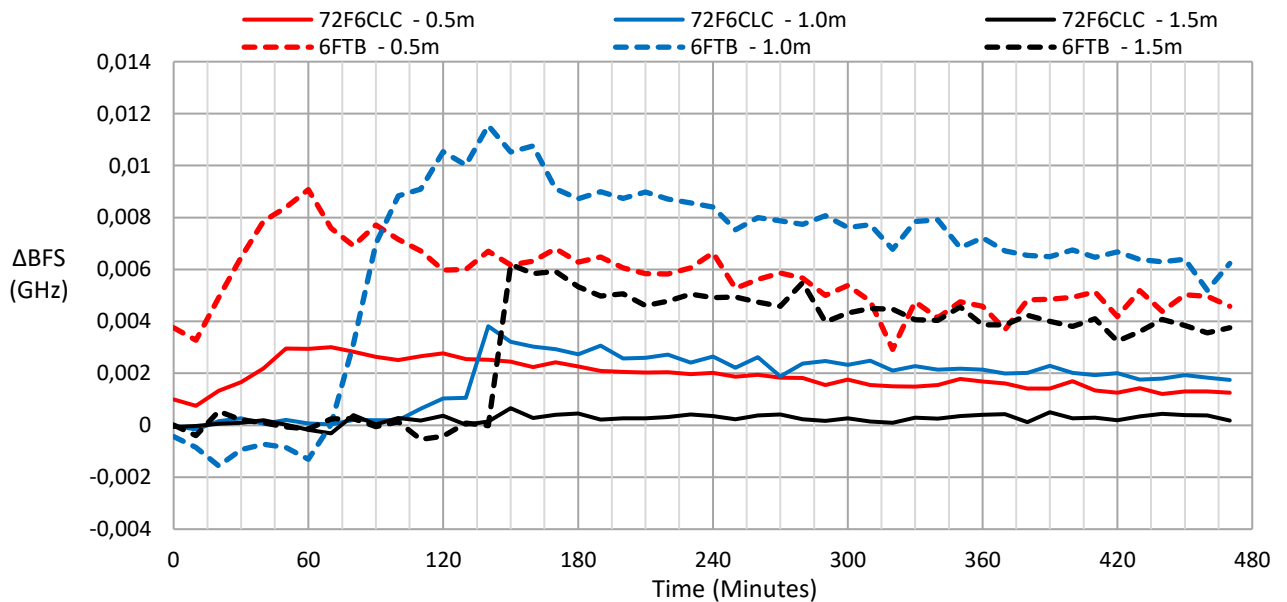


Figure 4-44. Time domain plot of the change in BFS at the three leak points for the two cables (72F-6C-LC and 6F-TB) as the leak test was conducted.

Figure 4-44 shows a change in the BFS at the three leak points for the two different cables as water is introduced. While water is being introduced into the trench, the BFS undergoes a

positive change, but after the introduction of water has ended the signal begins to decay. This is attributed to the fact that the water introduced into the trench is generating both a temperature effect as well as a strain effect in the soil. The temperature effect is only present while the water is being introduced into the soil and once the flow of water has ceased, the temperature effect dissipates until a temperature equilibrium has been reached in the soil. Once the temperature has equilibrated, only the strain effect in the soil surrounding the FO cables remains. Table 4.1 shows the cable type, length ordinate and standpipe number for the leaks detected in Figure 4-43 and Figure 4-44.

Table 4.1. Summary of the length-ordinates, trench segment depths, cable types and standpipe number at the 3 leak points.

Cable Type	Trench Segment Depth	Length Ordinate (m)	Standpipe
72F6CLC	-0.5m	8.52	1
72F6CLC	-1.0m	59.25	4
72F6CLC	-1.5m	109.71	7
6FTB	-1.5m	196.24	7
6FTB	-1.0m	245.87	4
6FTB	-0.5m	296.39	1

Due to the nature of the experiment, i.e. introducing a small volume of water, the temperature effect attributed to the introduction of water dissipated after the inflow of water had ceased. However, on a working pipeline this would not be the case. A working pipeline would continue to leak until it is repaired. Therefore, the temperature effect demonstrated in Figure 4-44 would be present without dissipation taking place. This would, theoretically, make the detection of leaks far more likely on a working pipeline as both the effect of strain and temperature would be present for detection by the FO cables.

### 4.5.3 Comparison of the Different Fibre Optic Cables

To compare the results of the various cables, the results of the second leak test conducted on the 1<sup>st</sup> of April was used to assess the performance of each cable.

#### 4.5.3.1 Strain to 72F-6C-LC

The Strain to 72F-6C-LC cable results are depicted in Figure 4-45.

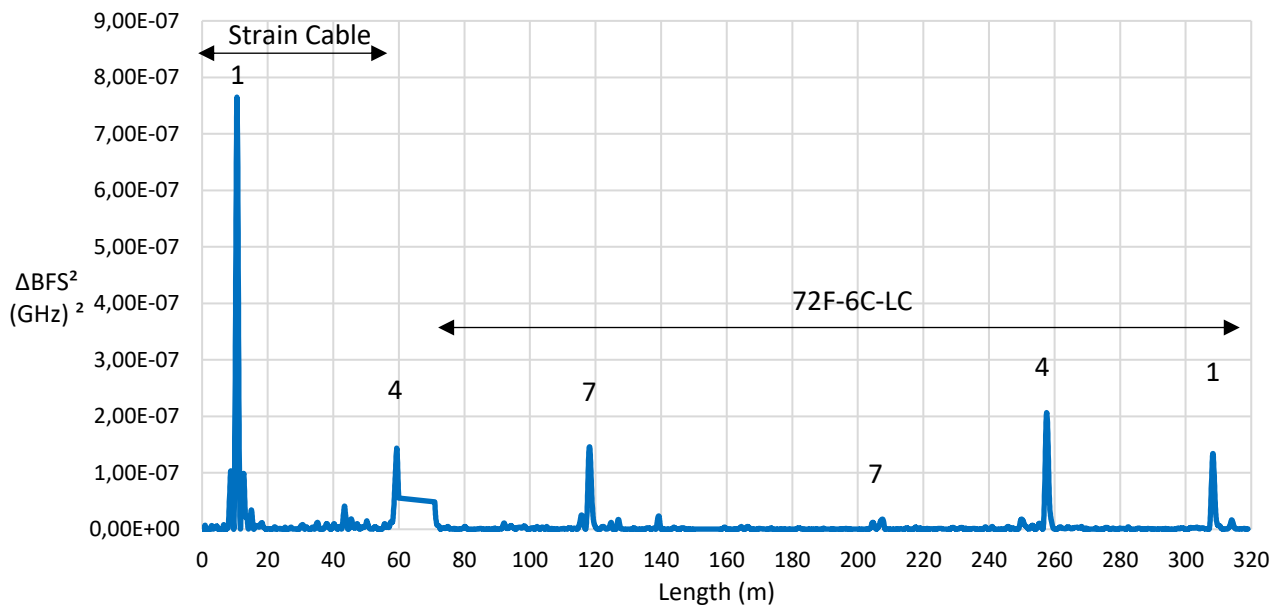


Figure 4-45. Results of the second leak test measured using the Strain to 72F-6C-LC FO cable.

The Strain FO cable worked well as a strain detection sensor because it gave a stronger response when compared against the 72F-6C-LC cable. Due to the nature of the experimental setup the Strain Cable is only able to detect leaks that occur in the first 50m segment. The peak occurring at 60m is a partial detection of a leak by the Strain Cable, but it is hindered by the splice that also occurs in that region.

The Strain Cable, however, when compared to the 6F-TB cable did not register as great a response as the 6F-TB cable. This phenomenon is interesting because the Strain Cable, as its name implies, is a cable designed to measure strain. The lesser response registered by the Strain Cable is due to the stiffness of the sheath housing the Strain Cable's optic fibre. The 6F-TB cable has a more flexible protective sheath allowing its optic fibres to undergo greater strain due to soil displacement.

The 72F-6C-LC cable registered a lesser response than that of both the Strain Cable and the 6F-TB cable. The 72F-6C-LC cable gave an interesting response to the leaks induced in the trench in this instance. In the latter half of the profile the 72F-6C-LC cable detected the leaks at standpipes 1 and 4 with great certainty, but not at standpipe 7. However, in the former half of the profile it is clear that the 72F-6C-LC cable did detect the leak at standpipe 7. Referring to the experimental setup shown in Figure 4-4, it can be seen that the 72F-6C-LC FO cable runs on opposite sides of the trench, looping around at the end of the trench. Therefore, the direction of the optic signal heads away from the interrogator on the input side, and returns to the interrogator after the loop, giving rise to double detection. The response registered at standpipe 7 with the 72F-6C-LC cable is attributed to the one half of the cable picking up the effect of water ingress on the one side of the trench, but not on the opposite side at the same

standpipe location. It is therefore necessary that the FO cable be strategically placed along a pipeline to obtain maximum exposure to water due to a leaking pipe.

#### 4.5.3.2 4F-DC-LC

The results of the second leak test output by the 4F-DC-LC cable are displayed in Figure 4-46.

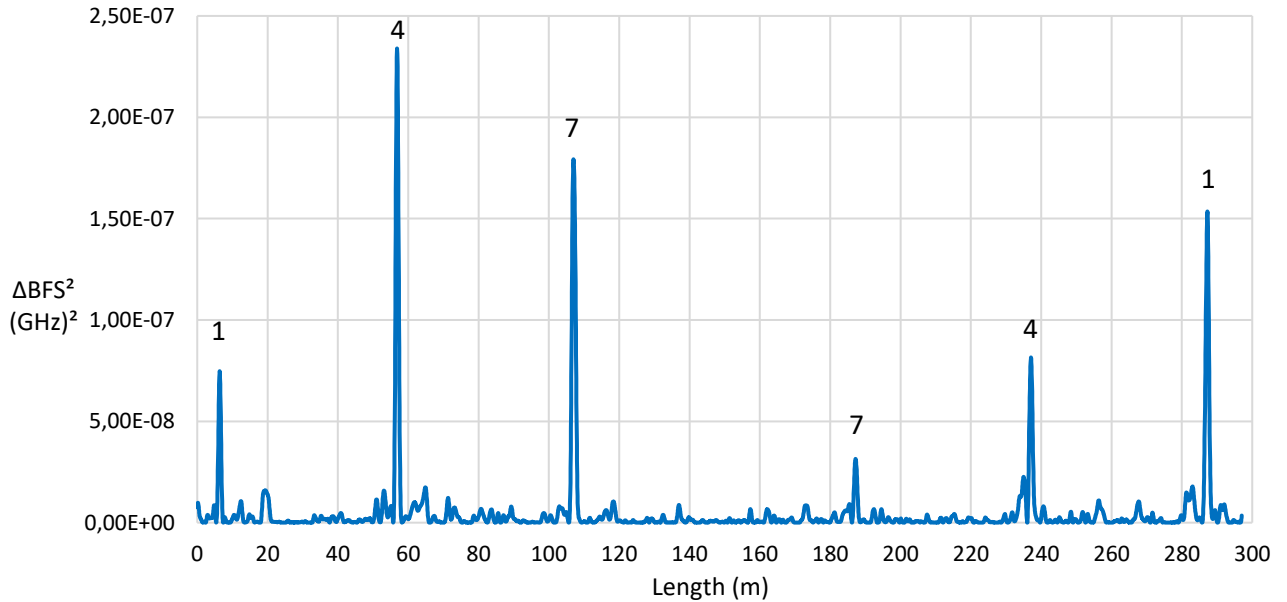


Figure 4-46. Results of the second leak test measured using the 4F-DC-LC FO cable.

The 4F-DC-LC cable, due to it being a loose core cable, gave very a similar performance to the 72F-6C-LC cable. The expected result would be that the 4F-DC-LC cable would give greater change in BFS responses due to it being smaller and less stiff, and therefore more affected by soil movement than the 72F-6C-LC cable. However, due to the gel matrix surrounding the fibre in the 4F-DC-LC cable, the optic fibres are shielded from strain effects due to soil displacement around the FO cables. The two loose core cables therefore produced similar responses due to both being affect almost entirely by the temperature effect of the water introduction into the trench.

### 4.5.3.3 2F-TB

The results of the second leak test output by the 2F-TB cable are displayed in Figure 4-47.

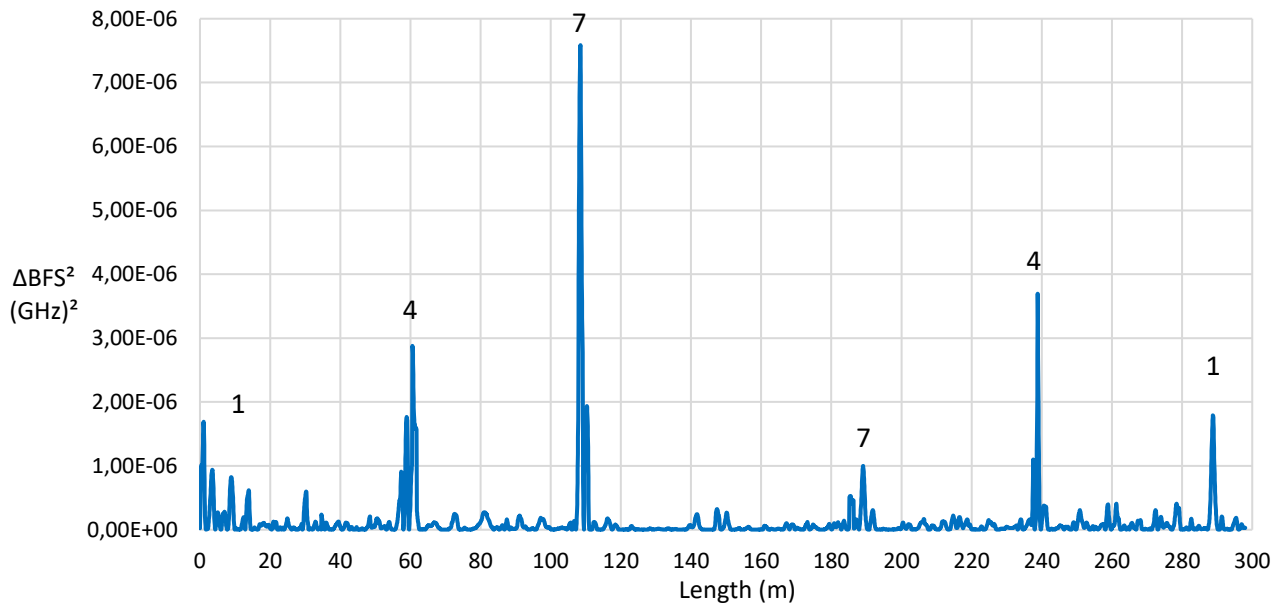


Figure 4-47. Results of the second leak test measured using the 2F-TB FO cable.

The 2F-TB cable and the 6F-TB cable both produced the largest responses of any of the cable types. The TB cables consistently produced squared change in BFS responses which were an order of magnitude greater than the LC cables and the Strain Cable. A problem with the TB cables is that the random noise generated by the TB cables is significantly greater than the noise generated by the LC and Strain Cables. As can be seen in Figure 4-47 at standpipe 1 on the left side of the profile, the leak was not able to be detected because of a noisy output. The leak was, however detected at standpipe 1 on the right side of the profile. The TB cable performed the best as leak detection sensors. However, it is necessary that improved signal processing techniques be developed to mitigate noise and amplify the change in BFS response triggered by a leak.

#### 4.5.3.4 6F-TB to 72F-6C-LC

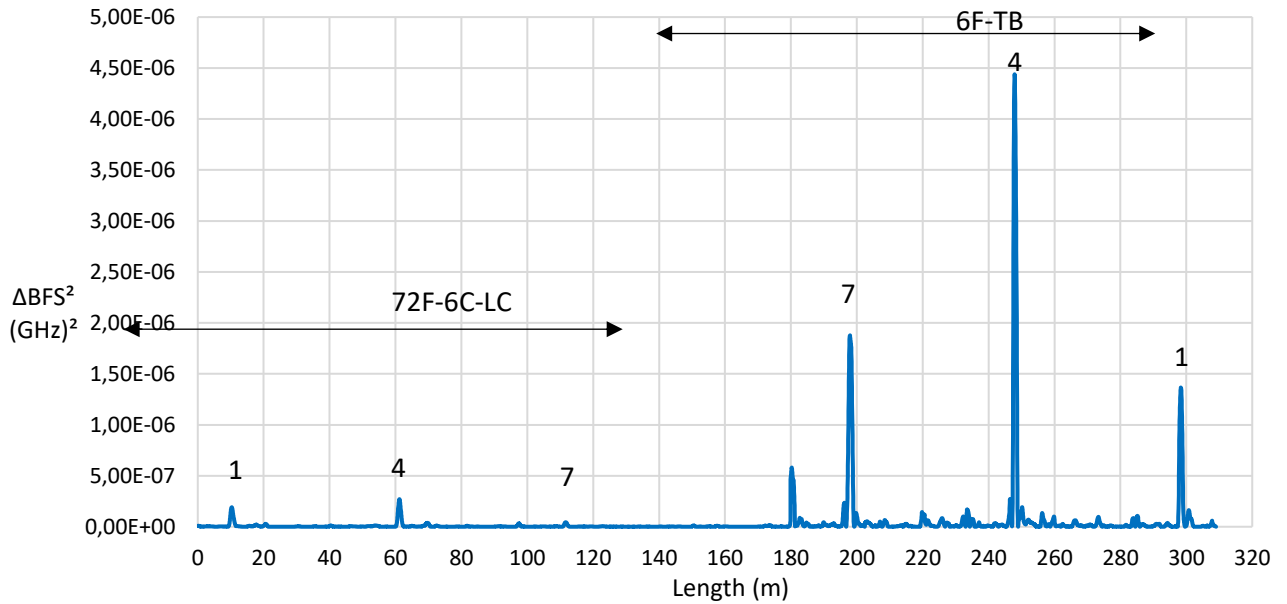


Figure 4-48. Results of the second leak test measured using the 6F-TB to 72F-6C-LC FO cable.

It is interesting to note in Figure 4-48 that the 6F-TB cable does not experience as much noise surrounding its peaks, due to the leaks, as the 2F-TB cable. This may be attributed to the fact that the 6F-TB cable has 6 optic fibres as opposed to the 2 optic fibres in the 2F-TB cable, resulting in less optic fibre movement in the sheath of the 6F-TB cable.

Figure 4-48 also gives a good perspective of the superior performance of the 6F-TB cable compared to the 72F-6C-LC cable.

Table 4.2 summarises the maximum squared change in BFS response registered by each cable type, clearly demonstrating the superiority of the TB cables' performance as leak detection sensors.

Table 4.2. Comparison of the maximum  $\Delta\text{BFS}^2$  responses registered by the different tested cable types.

Cable Type	Maximum $(\Delta\text{BFS})^2$ due to leak
Strain	7.65E-07
4F-DC-LC	2.34E-07
2F-TB	7.59E-06
6F-TB	4.44E-06
72F-6C-LC	2.70E-07

## **5 FIELD INVESTIGATION ON ACTIVE PIPELINE – RIETONDALE, PRETORIA**

### **5.1 INTRODUCTION**

In addition to the trench setup created on the University of Pretoria's Hillcrest Campus to assess the suitability of various types of fibre optic cables as potential leak detection sensors, a section of a municipal potable water pipeline in Rietondale, Pretoria, was instrumented with a fibre optic cable. The purpose was to test the performance of the proposed leak detection system on an active pipeline.

The City of Tshwane was in the process of replacing the potable water network in Rietondale, Pretoria at the time of the study and gave permission for the installation of a fibre optic cable with the newly installed pipe. The project involved the installation of new 200mm lines to replace the old system.

### **5.2 SITE LOCATION**

The proposed leak detection system requires a continuous length of fibre optic cable to be installed along the length of the pipeline being monitored and to minimise the number of splices in the fibre optic cable as this can deteriorate the quality of the measurements. To achieve this, it is ideal to start with the fibre optic cable installation at a given location and then to advance with the installation progressively to where the leak detection system would end. However, the installation of the new pipes often occurred in a staggered fashion so that long continuous open lengths of pipe trenches were not generally available. With the assistance of the pipeline contractor the most suitable site for the installation of a relatively long uninterrupted length of fibre optic cable was Kameel Street and a length of approximately 180m of Tom Jenkins Drive as illustrated in Figure 5-1.

Property owners in the area were approached to volunteer to host the fibre optic strain interrogator and 172 Tom Jenkins Drive was identified as the most suitable host. The interrogator location is illustrated in Figure 5-1. A Wi-Fi router placed with the interrogator allowed the system to be monitored remotely.



Figure 5-1. Fibre optic cable installation in Rietondale, Pretoria (Google Earth)

### 5.3 FIBRE OPTIC CABLE INSTALLATION

This study made use of a fibrisTerre2505 Brillouin Frequency Shift interrogator as readout unit. The instrument requires the fibre optic cable to form a loop. Both ends of the loop need to be connected to the interrogator. The use of a dual-core cable meant that a loop can easily be created by simply splicing the two fibres together at the end of the fibre optic cable. There was therefore no need for two parallel lengths of cable in the pipe trench.

From the field study carried out on the Hillcrest campus of the University of Pretoria, the dual fibre tight-buffered fibre optic cable (2F-TB) was identified as the most suitable leak detection sensor. The most suitable sensors for leak detection are highly flexible tight-buffered fibre optic cables. Being tight-buffered means that the fibre optic cable is sensitive to both strain and temperature effects. A high flexibility means that the cable is easily deformed as the ground in which it is buried strains in response to a leak.

The fibre optic cable being installed adjacent to the pipeline is illustrated in Figure 5-2. It was attempted to place the cable as close as possible to the pipe, partially underneath the pipe, to award it a degree of protection during backfilling of the trench. The installation took place from 16-27 August 2021.

The installation of the fibre optic cable proved challenging as it sometimes interfered with the activities of the contractor who was working to a tight schedule. Installation of the cable unavoidably required some assistance from the contractor, something for which he was not compensated. It was unfortunate that the cable was severed at a location in Kameel Street shown in Figure 5-1. The trench was backfilled before the fibre optic cable could be spliced. A significant amount of time and effort was spent to attempt to excavate and locate the severed ends but they could unfortunately not be located. As a result, the fibre optic cable had to be spliced to create a loop at the northern end of Tom Jenkins Drive. This resulted in a length of only about 180m of pipeline being monitored by the fibre optic cable which was a disappointment.



Figure 5-2. Fibre optic cable being laid next to the uPVC water pipe.

#### 5.4 LEAK TEST

Due to the fact that the pipeline monitored was new, it was unlikely that it would leak shortly after commissioning. As in the case of the trials on the Hillcrest Campus of the University of Pretoria, a number of downpipes were therefore installed along the length of the instrumented pipeline to allow water to be introduced near the trench invert to impose artificial leaks. The down pipes comprised 25mm class 3 HDPE irrigation pipe. One downpipe shown prior to backfilling of the pipe trench is shown in Figure 5-3.

A leak test was carried out from 24 September to 1 October 2021, a period of 7 days, during which 40 litre per hour (approximately 1m<sup>3</sup> per day) was introduced using a downpipe just

outside the property where the interrogator was housed. Prior to and after the leak, the fibre optic BFS was monitored at two-hourly intervals from mid-day on 25 August until just after 05h00 on 1 December 2021 providing just over three months' worth of data.



Figure 5-3. HDEP downpipe used to impose artificial leak shown prior to backfilling of the pipe trench.

## 5.5 LEAK TEST RESULTS

Following the installation of the 2F-TB fibre optic cable along the potable water pipeline installed in Tom Jenkins Drive and Kameel Street in August 2021, the fibre optic strain interrogator was installed at 172 Tom Jenkins Drive and set to measure the Brillouin Frequency Shift (BFS) in the fibre optic cable at two-hourly intervals. The BFS recorded in a fibre optic cable is strain and temperature sensitive and these parameters are affected by water leaks into ground. It was decided to record baseline behaviour (i.e. the BFS response of the fibre optic cable) over period of one month before imposing an artificial leak. This would allow the baseline behaviour against which the leak-induced response, to be understood before the leak was imposed.

Following a study of the baseline behaviour, a leak was imposed by introducing 40 litres per hour using flexible hose starting on 24 Sept 2021 and ending on 1 October 2021. Following the termination of the leak tests, baseline behaviour was studied by recording the BFS profile in the fibre optic cable until 1 December 2021.

### 5.5.1 BASELINE MONITORING

Figure 5-4 presents the BFS profiles recorded along the entire length of optical fibre monitored over a 24-hour period at four-hourly intervals immediately after commencement of monitoring on 25 August 2021. The fibre optic cable ran above ground over a distance of approximately 60m to the pipe trench where it entered the ground. Substantial variation in BFS is evident in the 60m above-ground section at the start and end of the optical fibre. This is because of daily temperature variation affecting the above-ground sections. As soon as the optical fibre entered the ground, very little variation in BFS was observed due to the thermal insulation provided by the ground. Figure 5-5 provides a zoomed-in image of the first 150m of the optical fibre, clearly showing the variation along the first 60m, with very little variation occurring along the buried section. Figure 5-6 presents the last 140m of optical fibre clearing showing the end of the buried part of the optical fibre at 420m. The total length of buried fibre was therefore 360m forming a loop along the 180m length of pipeline monitored.

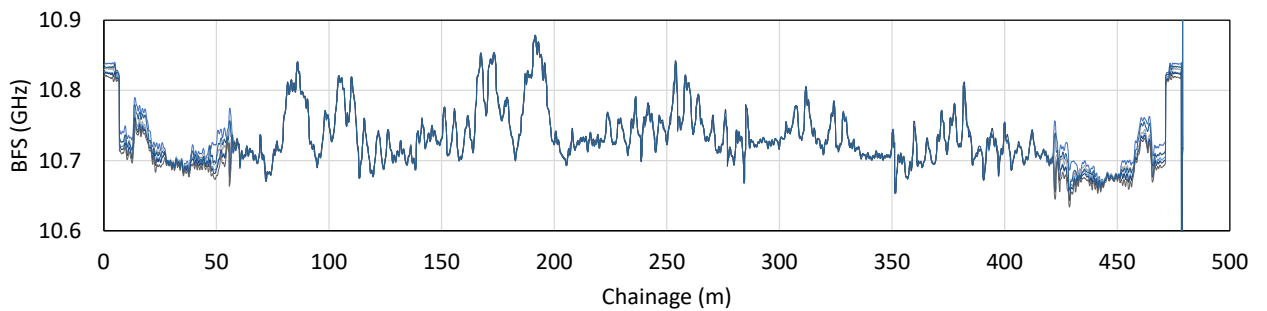


Figure 5-4. BFS profiles recorded over a 24-hr cycle at 4-hourly intervals along entire monitored fibre optic cable length.

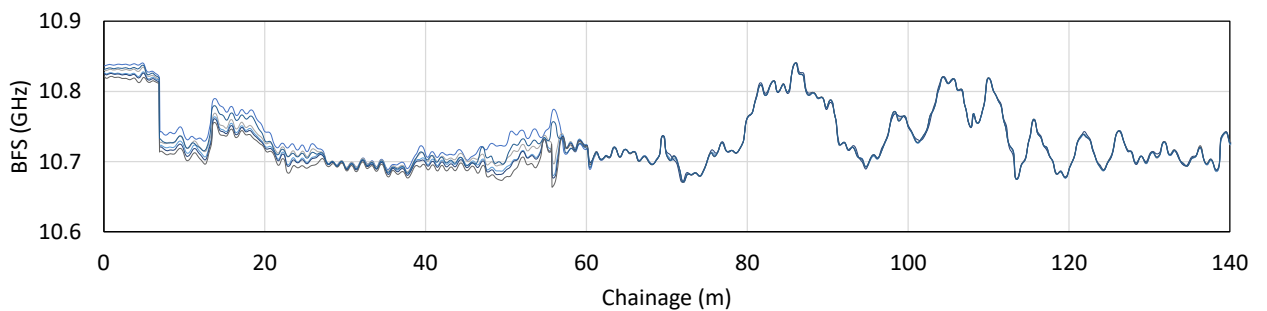


Figure 5-5. EBFS profiles recorded over a 24-hr cycle at 4-hourly intervals along the first 140m of fibre optic cable length.

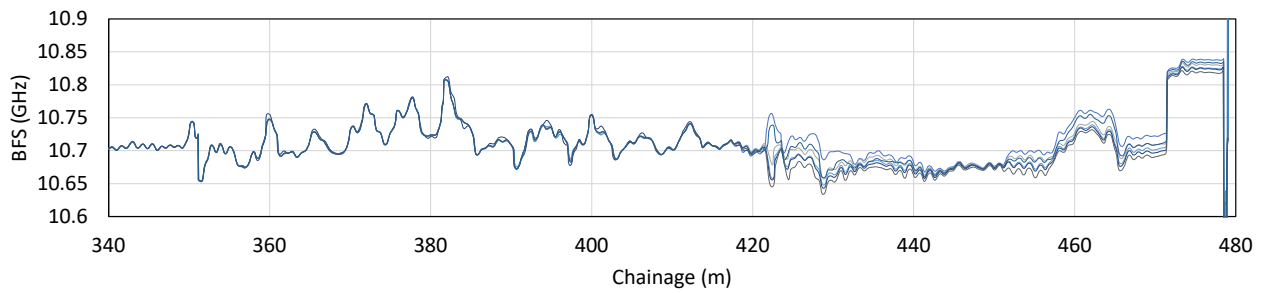


Figure 5-6. BFS profiles recorded over a 24-hr cycle at 4-hourly intervals along the last 140m of fibre optic cable length.

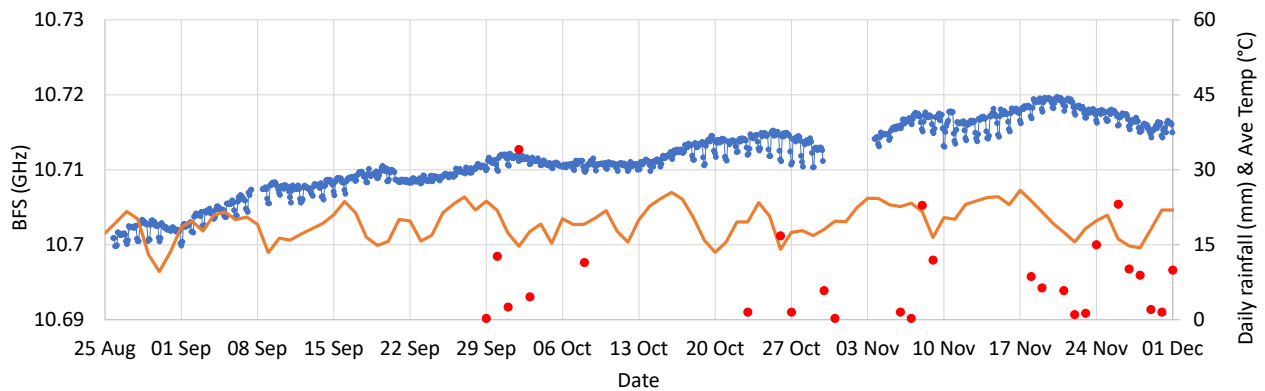


Figure 5-7. Variation in BFS in the absence of a pipe leak (Ch 182.68).

Figure 5-7 presents the variation BFS over time at Chainage 182.68 for the duration of the study period at a location where no leak was imposed. The figure also indicates daily rainfall events. The small spikes correspond with daily temperature cycles. The gently rising BFS trend is the result of the gradually increasing ground temperature from the end of August to beginning December 2021. The figure also illustrates the average daily temperature and daily rainfall. It appears that rainfall events slowed down the rise in ground temperature somewhat, but never resulted in sharp spikes in the BFS response. As observed during the study on the Hillcrest campus of the University of Pretoria, BFS trench in the absence of leak vary gently over time, reflecting the slowly changing ground temperature.

## 5.5.2 LEAK RESPONSE

An artificial water leak of 40 litres per hour, was imposed from 24 Sept-1 Oct 2021. A schematic layout of the cable, indicating chainages at key points, is presented in Figure 5-8. Due to the fibre optic cable forming a loop, the leak point coincided with two chainages, i.e. Ch 67 and Ch 205 along the fibre optic cable. The BFS record recorded at the leak location (Ch 205) over the entire monitoring period is presented in Figure 5-9. It can be seen that the leak resulted in a sharp deviation from the preceding BFS trend. The BFS kept changing over the leak duration, whereafter it stabilised. Prominent slope changes are evident at the start and end of the leak allowing the leak to be detected. The BFS trend is in clear contrast with the trend in the absence of a leak presented in Figure 5-7.

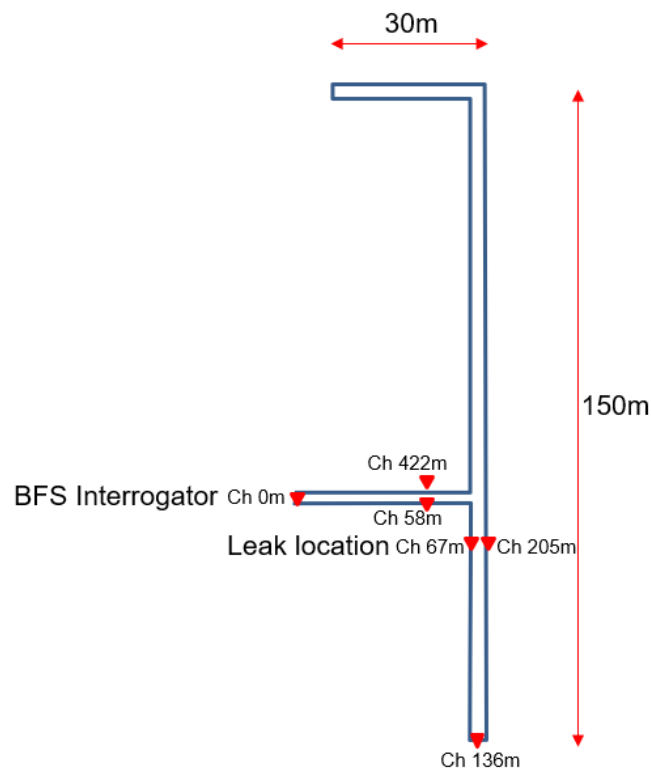


Figure 5-8. Schematic layout of fibre optic cable monitored.

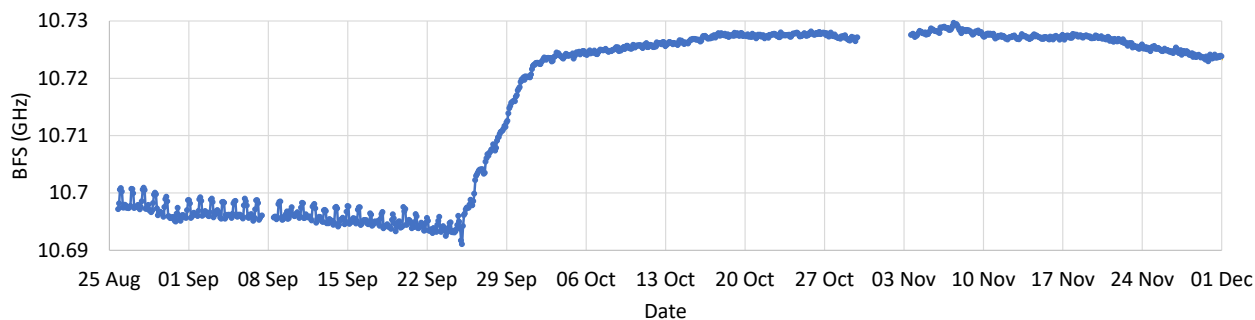


Figure 5-9. Variation in BFS at the leak location (Ch 205).

Figure 5-10 presents plots of BFS along the entire length of fibre optic cable monitored at four dates, split into three graphs to allow the entire BFS sequence to be studied. Significant changes are evident along the length of fibre outside the trench as these were subject to temperature change (0 to 60m and beyond 420m). The cable sections delineated in red coincide with the leak location. Due to the cable forming a loop, the leak was registered at two locations. Upon closer inspection it can also be seen that the two BFS profiles around the leak location are mirror images of each other, reflecting the fact that the two locations coincide with a single location along the cable. Little change in BFS occurred along the buried length of the fibre optic cable away from the leak location.

Figure 5-11 presents a zoomed-in BFS profiles in the area of the leak over the duration of the leak. It can be seen that the effect extended over a relatively long length of pipe trench around the leak location (CH 205). Insignificant changes in BFS were visible outside the area influenced by the leak over this time.

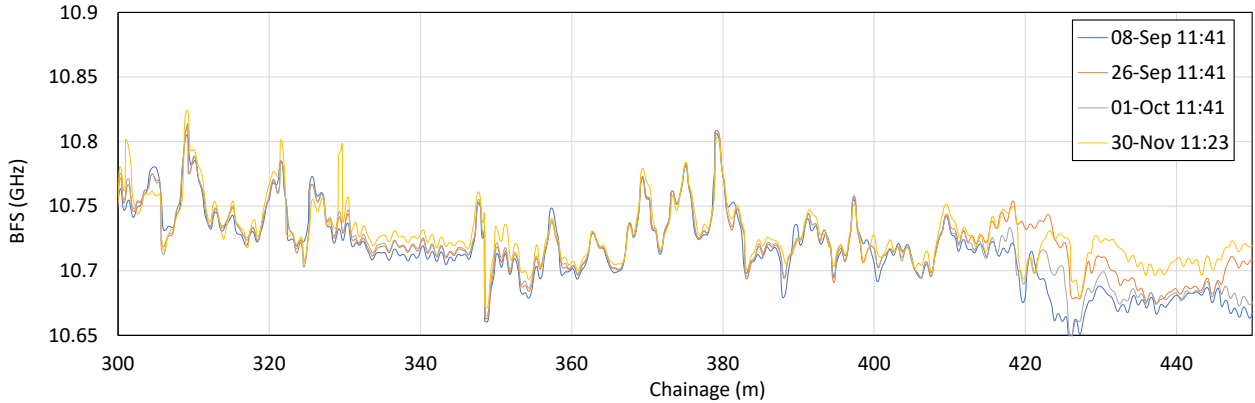
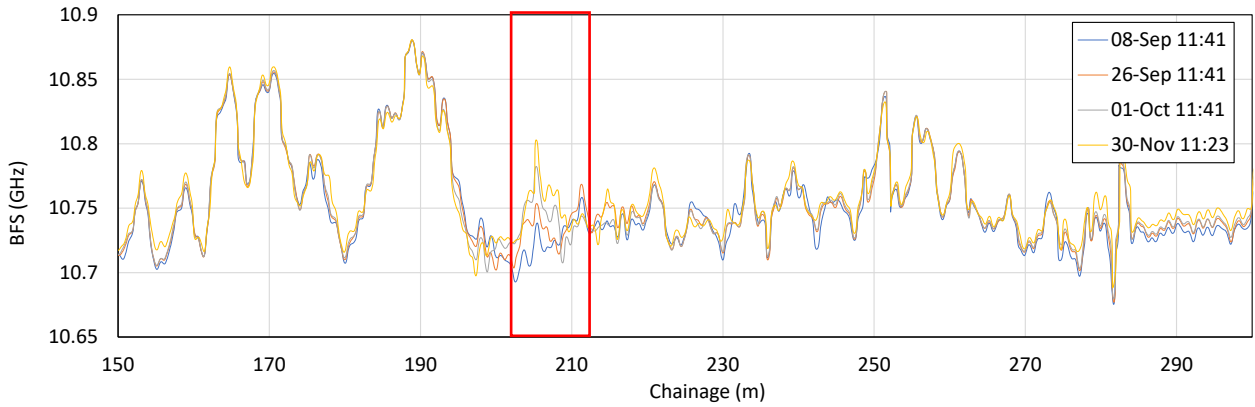
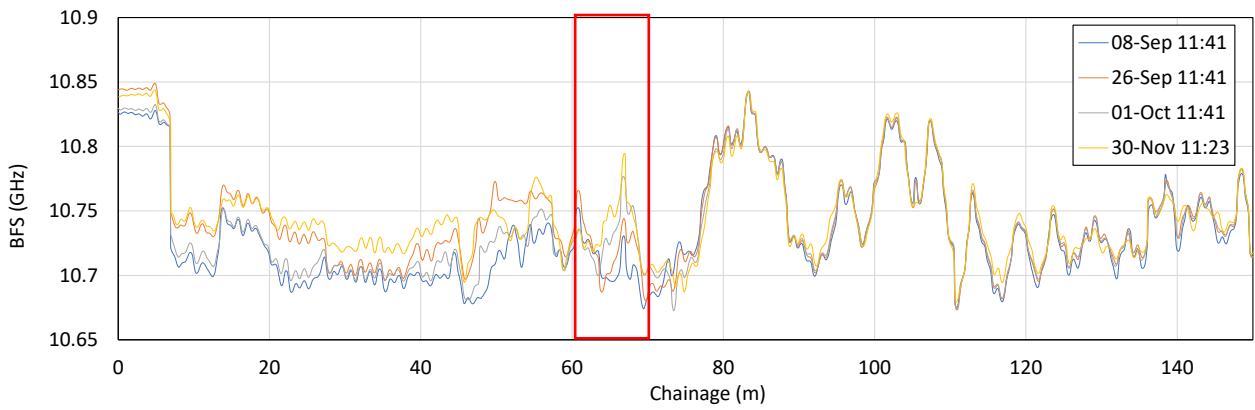


Figure 5-10. BFS profiles along the fibre optic cable before during and after the leak.

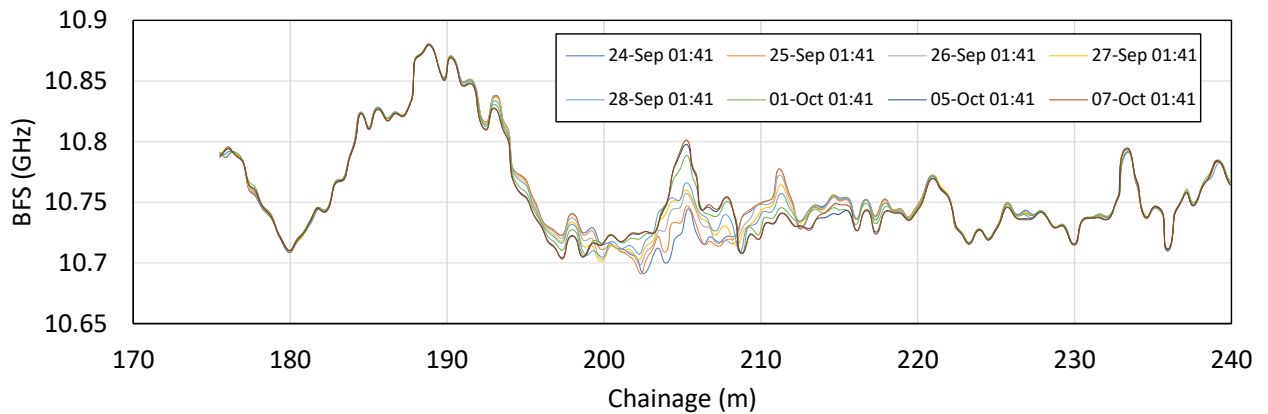


Figure 5-11. Raw BFS profiles shortly before, during and shortly after the leak.

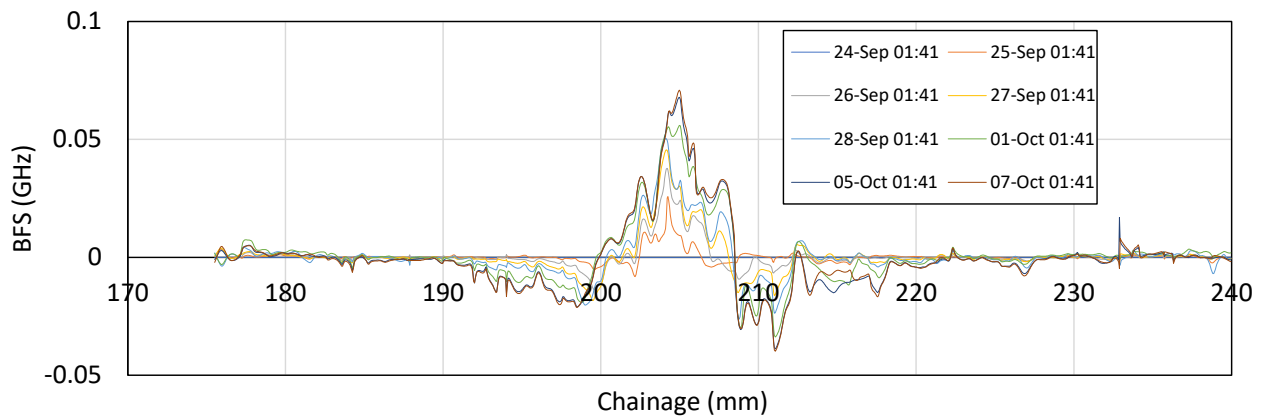


Figure 5-12. Zeroed BFS profiles shortly before, during and shortly after the leak

Figure 5-12 presents BFS plots zeroed prior to the start of the leak. Studying the area of influence indicates how the leak effect spread during the course of the leak. During the leak a total volume of approximately  $1\text{m}^3$  of water was introduced over a 24hr period. The water introduced would first have saturated the soil around the leak location, after which it would have spread to the north and south of the leak location along the pipe trench. It is interesting to note that the leak-induced influence appears to match the bending moment profile that would be associated with sagging in the vicinity of the leak itself, with hogging occurring adjacent to the sagging zone. The introduction of water would have softened the soil around the leak location and also increased its self-weight, resulting in the sagging at the leak location, accompanied by hogging in the adjacent zones. As the optical fibre was placed very close to the pipe, somewhat underneath it, it seemed to reflect the bending response of the pipe due to the leak.

## 5.6 RECOMMENDED LEAK DETECTION PROCEDURE

Based on the BFS response observed during a leak test, the following procedure is recommended for leak detection.

- Compare the latest BFS scan to a scan one month earlier. Scans should be taken at the same time of the day to compensate for normal daily temperature cycles.
- Identify prominent spikes in the BFS record. Ignore spikes extending only one or two length ordinates as these are likely to be associated with noise.
- Generate time series for remaining spikes.
- Leaks are probable when time series show continuous change with time.
- Consult rainfall record if numerous leaks seem to appear.

## **6 LEAK DETECTION BY MEANS OF VIBRATION DETECTION**

Leak detection by means of vibration detection could not be investigated due to the necessary equipment not being available in South Africa. Negotiations were initiated with equipment manufacturers in Russia (T8 Sensor) and Germany (AP Sensing) to invite them to take part in the research projects. However, the companies were not interested in a joint research project, but rather in selling their equipment. The companies were especially hesitant to travel to SA during the Covid pandemic. In addition, a literature search and communication with the equipment suppliers have indicated that leakage detection by means of vibration detection is complex because leak-related vibration will have to be isolated from the background noise, which is problematic in an urban environment. It requires considerable expertise and specialised algorithms, which means that reliance will need to be placed on the expertise of the equipment manufacturer, which is not ideal for a stand-alone leak detection system as pursued by this project.

## 7 CONCLUSIONS AND RECOMMENDATIONS

### 7.1 CONCLUSIONS FROM LABORATORY STUDY

The results of the experiment work demonstrated that BFS in fibre optic cables can be used to detect leaks by detecting the strain that a soil experiences when its moisture content is changed due to a leaking pipe. By performing the data processing methodology outlined in Chapter 4, the observed raw BFS profile outputs from an interrogator can be used to generate plots that can indicate if and where a leak is taking place. In the case where a more sensitive fibre optic cable is used, both the location and the severity of the leak can be quantified.

The results of the experiments have indicated that a leak detection system would give the best performance in finer grained soils. This is due to the fact that finer grained soils undergo larger strains when their moisture contents are changed due to increased matric suctions, or increased swelling upon wetting. This is because the magnitude of the change in BFS of an optic fibre is dependent on the strain that the fibre experiences. Hence, soils that strain more when their moisture contents are changed will output larger detectable changes in BFS. However, the results from the telecom cable suggested that cables that are less stiff can be used as leak detection sensors in coarse grain soils. Coarse-grained soils will undergo less strain with a change in moisture content. Therefore, cables that are less stiff will be able to strain to a greater extent in a coarse-grained soil.

Touching on the performance of the different cables, the telecom cable is adept at giving readings with large changes in BFS if disturbances take place. It is not, however, suited to giving an indication of the magnitude of the disturbance. In each soil the telecom cable gave similar changes in BFS that were not indicative of the amount of strain the soil experienced. However, for practical application the telecom cable appears to be well suited as a leak detection sensor. All that is required from a simple leak detection system is the detection of a disturbance, i.e. a leaking pipe. The magnitude of the disturbance is less relevant.

The Strain Cable was clearly the best cable in terms of overall performance. It is able to detect changes in moisture content in each soil tested and give a meaningful indication of the strain magnitude. From the test results, the Strain Cable, if used in a leak detection system, would be able to detect a pipe leak and indicate how severe the leak is.

The results of testing the Temperature Cable confirmed that this cable is designed to be a temperature sensor. Although it was able to detect strains in the fine sand and the clay, the magnitude of the change in BFS was much smaller than the Strain Cable, which is designed to detect mechanical strain.

Pre-tensioning of a fibre optic cable intended to act as a leak detection sensor is not recommended. Perhaps in this experiment the 2kg weight used to tension the cable was

excessive. Further research will have to be conducted to confirm this. However, the results of the experiment indicate that smaller changes in BFS are registered by cables that are tensioned as opposed to non-tensioned cables. Considering the fact that in a leak detection system a maximum change in BFS is desirable for reasons of sensitivity, tensioning a cable appears to hamper the function of a leak detection system.

## **7.2 CONCLUSIONS FROM FIELD INSTALLATION ON HILLCREST CAMPUS**

Pre-leak baseline monitoring data from the field showed that the performance of tight buffered and loose core fibre optic cables differ significantly, with the former giving apparently noisy BFS profiles due their sensitivity to both strain and temperature changes. LC cables, on the other hand, provided smooth BFS profiles along their length due to their insensitivity to mechanical strain. Based on the results of the laboratory study referred to above, it was expected that the tight buffered cables will be more sensitive to indicate leaks due to their ability to react to strain in addition to temperature.

Two leak tests involving the discharge of respectively 40 and 50 litres of water were conducted on the fibre optic cable trench experimental setup on the University of Pretoria's Hillcrest Campus. The results of the leaks tests show that each type of fibre optic cable tested was able to detect the ingress of water into the surrounding soil, either by registering a temporary temperature response, or a combination of a temperature and a soil strain response. The different cable types did not all perform equally well as leak detection sensors. It has been conclusively shown that tight buffered cables provide the best performance as leak detection sensors and that loose core cables and even cables designed to measure strain give inferior performance to fibre optic cables. Comparing different fibre optic cables showed that the less stiff fibre optic cables gave the best performance as leak detection sensors.

Following the abovementioned leak tests, a longer term leak test amounting to 40 litres per hour over the course of one week was imposed. This leak test was easily detected on all fibre optic cable, with the flexible tight buffered cables provided the most sensitive response.

## **7.3 CONCLUSIONS FROM FIELD INSTALLATION ON ACTIVE PIPELINE**

A 180m length of a newly constructed potable municipal water pipeline in Rietondale, Pretoria was instrumented with a flexible, dual-core, tight-buffered fibre optic cable which was monitored for Brillouin Frequency Shift (BFS) every two hours.

The monitoring started on 24 August 2021 and ended on 1 December 2021. The cable was located partly underneath and parallel to the 200mm diameter uPVC pipe.

The BFS baseline profile was monitored for a month after which an artificial water leak amounting to 40 litres per hour (approximately 1m<sup>3</sup> per day) was imposed from 24 September to 1 October 2021.

The leak caused the BFS response to deviate sharply from the pre-leak baseline. Upon termination of the leak, a second deviation in the BFS trend was observed.

The BFS in optical fibres are influenced by both strain and temperature effects. A water leak in unsaturated ground results in both. Firstly, water leaking from a potable water pipeline is typically colder than the surroundings and, secondly, wetting up of the partially saturated soil surrounding a fibre optic cable changes the stress state in the soil, causing strains which are transferred into the fibre optic cable, allowing it to be detected.

The results of the leak tests showed that a water leak can be detected by comparing the latest BFS profile with a baseline recorded some time earlier. It appears that a baseline one prior to the latest reading is a suitable baseline. If the baseline is defined too far into the past, gradual seasonal changes in BFS tend to obscure leak. Deviations from the baseline should be investigated further by generating time histories at the locations in question. A long-term trend deviating from the pre-leak baseline is likely to be indicative of a leak.

Leak detection using BFS should consider the rainfall record of the area of interest because heavy rainfall may influence BFS trends over large areas because of the spatial extent over which rainfall events occur.

## **7.4 RECOMMENDATIONS**

Experience with the installation of the fibre optic cable on a working pipeline showed that it is essential that the buy-in of the pipeline contractor be obtained to deliver an undamaged and continuous fibre optic cable. Even robust fibre optic cables are easily damaged during the construction process. The installation of the cable must be a billed item in terms of the list of deliverables required from the contractor and the contractor must not be expected to do this work as a favour.

It is essential that continuity of the optical fibre be verified prior to backfilling of the pipe trench.

Because the fibre optic cable must be installed in close proximity to the pipe in the same pipe trench, their installation should take place together. As splicing of the optical fibre is not ideal, the best results in terms of a leak detection system performance will be obtained if construction proceeds progressively from the start to the end of the pipeline. Staggered construction causes difficulty with insuring a continuous high-quality fibre optic cable as splicing is required when the optical fibre is cut.

The best opportunity for installation of a fibre optic leak detection system as investigated in this study is to install it during the installation of a new pipe network. Fibre optic cables can be routed to a central location where they can be monitored using a single fibre optic readout unit and multiplexing technology. The system can be monitored remotely via the internet. Software can be developed to automatically scan BFS profiles for leaks, providing warning messages whenever a leak is detected which will enable early remedial measures to be taken to repair the pipe to minimise water loss.

## 8 REFERENCES

- Curran, M. Shirik, B. 2018. Basics of Fibre Optics. *Communication*
- Galindez-Jamioy, C.A. López-Higuera, J.M. 2012. Brillouin Distributed Fibre Sensors: An Overview and Applications. *Journal of Sensors*. Volume 2012, No 1, August, 17 pages.
- González-Gómez, F. García-Rubio, M.A. Guardiola, J. 2011. Why Is Non-revenue Water So High in So Many Cities? *Water Resources Management*, Volume 27, No 2, June, pp 345-360.
- Grattan, K.T.V. Sun, T. 1999. Fibre Optic Sensor Technology: An Overview. *Sensors and Actuators*, Volume 82, November, pp 41-60.
- Khademi, F. Budiman, J. 2016. Expansive Soil Causes and Treatments. *i-manager's Journal on Civil Engineering*, Volume 6, No 3, June, pp 1-14.
- Knappet, J.A. Craig, R.F. 2012. *Craig's Soil Mechanics*. 8th ed, Spon Press, 2 Square Park, Milton Park, Abingdon, Oxon.
- Le Roux, SF. 2019. The Effect of Surface Tension on the Development of Suction in Drying Soils. *Final Year Civil Engineering Research Project*.
- Li, J. Cameron, D.A. Ren, G. 2013. Case study and back analysis of a residential building damaged by expansive soils. *Computers and Geotechnics*, Volume 56, No 1, December, pp 89-99.
- Li, P. Vanipalli, S.K. Li, T. 2016. Review of collapse triggering mechanism of collapsible soils due to wetting. *Journal of Rock Mechanics and Geotechnical Engineering*, Volume 8, No 1, January, pp 256-274.
- Mckenzie, R. Siqalaba, Z.N. Wegelin, W.A. 2012. *The State Of Non-Revenue Water in South Africa. Communication*.
- Mokhtari, M. Dehghani, M. 2012. Swell-Shrink Behaviour of Expansive Soils, Damage and Control. *Edge*, Volume 17, No 1, pp 1-10.
- Motil, A. Bergman, A. Tur, M. 2015. State of the art of Brillouin fibre-optic distributed sensing. *Optics & Laser Technology*, Volume 78, No 1, October, pp 81-103.
- Nel, E. 2019. The Slope Stability of a Seawall Layer Considering the Effect of Clay at Various Depths. *Final Year Civil Engineering Research Project*.
- Ng, C.W.W. Menzies, B. 2007. *Advanced Unsaturated Soil Mechanics and Engineering*. 1st ed, Taylor & Francis, 2 Square Park, Milton Park, Abingdon, Oxon.
- Pedersen, J. Baadsgaard (Ed.) & Klee, P. (Ed.in C.), 2013. Meeting an increasing demand for water by reducing urban water loss – Reducing Non-Revenue Water in water distribution. The

Rethink Water network and Danish Water Forum White Papers, Copenhagen. Available at [www.rethinkwater.dk](http://www.rethinkwater.dk)

Vanapalli, S.K. Fredlund, D.G. Pufahl, D.E. Clifton A.W. 2016. Model for the prediction of shear strength with respect to soil suction. *Canadian Geotechnical Journal*, Volume 33, No 1, January, pp 379-392.

Van Zyl, J.E. Alsaydalani, M.O.A. Clayton, C.R.I. Bird, T. Dennis, A. 2013. Soil fluidisation outside leaks in water distribution pipes – preliminary observations. *Water Management*, Volume 166, No 1, November, pp 546-555.

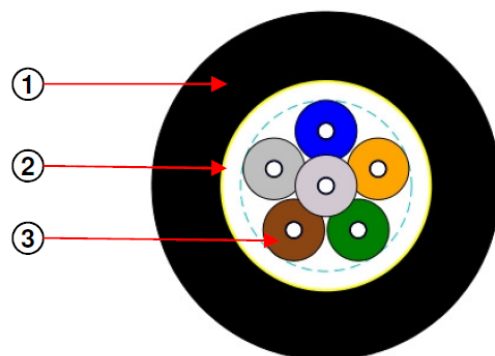
Van Zyl, J.E. Clayton, C.R.I. 2007. The effect of pressure on leakage in water distribution systems. *Water Management*, Volume 000, No 1, January, pp 1-6.

# **APPENDIX A 6F-TB and 2F-TB CABLE SPEC SHEET**

# DATA SHEET

## Field Deployable Cable (Tight Buffered Cable For Re-usable, Temporary or Mobile Links)

CABLE DESCRIPTION	
1	Hytrel Sheath
2	Aramid Yarn Overall Strength Member
3	Colour Coded " Easy Strip" Tight Buffer Optical Fibres



FIBRE COUNT	ELEMENTS PER LAYER (na)												FIBRES	
	1	2	3	4	5	6	7	8	9	10	11	12		
6														6 Fibres

**Optical Fibres** are coloured in accordance with TIA/EIA-598  
**Colour sequence:** Blue, Orange, Green, Brown, Grey and White.

PRODUCT FEATURES
* The CBI-Electric Telecom cables "field deployable " cable is a compact, tight buffered cable specially designed for military applications, to provide fast communication links.
* As a temporary measure, the reusable cable can be used like a jumper, skirting the damaged section to a fixed optical installation in double quick time with the use of mechanical splices. This allows a maintenance team time to repair or replace damaged cable at leisure, and to link in this repaired cable with permanent fusion splices, outside of peak times.
* The cable is however suitable for a vast variety of applications where quick deployment and recovery is necessary, and has also been found to be ideal for mobile links.
* The cable will tolerate vertical installations and can support its own weight for considerable drops, making it ideal for risers, mine shafts, boreholes, etc.
* Ideally suited for point to point links, eliminating the need for fibre patch cords in many instances.
* The cable is small, lightweight, flexible, and will tolerate small bend radii, yet is surprisingly resistant to kinking, making it ideal for easy deployment and recovery.
* The special sheathing compound has been specially chosen for its excellent abrasion and cut resistance, in order to withstand damage when deployed over hostile terrain.
* The sheath is well dosed with Carbon Black to give the cable excellent UV resistance.
* The fibres are protected by a tough easy strip, tight buffered nylon jacket.
* The fibres are individually coloured for easy of identification.

# DATA SHEET



DATA SHEET: CBI Telecom-OFC-FIELD DEPLOYABLE-01

PHYSICAL PROPERTIES		
Parameter	Fibre Count	Test Method
	6	
Cable diameter (nominal)	5.1 mm	
Cable weight (nominal)	24 kg/km	
Maximum tensile load- Short Term(N)*	800 N	
Maximum tensile load- Long Term(N)**	300	IEC 60794-1-21
Minimum bend radius	100 mm	IEC 60794-1-21
Crush Resistance (via 100mm plates)	800 N	IEC 60794-1-21
Impact resistance (25mm anvil / 10 blows)	2 Nm Blows	IEC 60794-1-21
Temperature Performance	-20°C to +70°C	IEC 60794-1-22
Maximum unsupported vertical drop (m)	1000m	
Note: *Short term load is the load at which the fibre strain is less than one third of the fibre proof strain. ** Long term load load is the load at which no fibre strain occurs.		

# DATA SHEET



## DATA SHEET: CBI Telecom-OFC-FIELD DEPLOYABLE-01

OPTICAL PROPERTIES (Single-Mode Optical Fibres) (Alternative fibre types/properties are available on request)	
Specification	ITU-T G.652.D/G.657.A1
Attenuation	$\leq 0.35$ dB/km @ 1310 nm $\leq 0.22$ dB/km @ 1550 nm $\leq 0.24$ dB/km @ 1625 nm
Chromatic Dispersion [ps/(nm.km)]	1285-1330 nm $\leq 3$ 1550 nm $\leq 18$ 1625 nm $\leq 22$
Polarisation Mode Dispersion (PMD <sub>D</sub> )	$\leq 0.1$ ps/ $\sqrt{\text{km}}$
Mode Field Diameter	$9.2 \pm 0.4$ $\mu\text{m}$ @ 1310 nm $10.4 \pm 0.5$ $\mu\text{m}$ @ 1550 nm
Cladding Diameter	$125 \pm 0.7$ $\mu\text{m}$
Coating Diameter	$242 \pm 5$ $\mu\text{m}$
Core-Clad Concentricity	$\leq 0.5$ $\mu\text{m}$
Cladding Non-circularity	$\leq 0.7$ %
Cable Cut-off Wavelength	$\leq 1260$ nm
Macro-bend loss	$\leq 0.5 / 1.5$ dB @ <b>10mm Radius</b> , 1 turn @ 1550/1625 nm $\leq 0.05 / 0.3$ dB @ <b>15 mm Radius</b> , 10 turns @ 1550/1625 nm

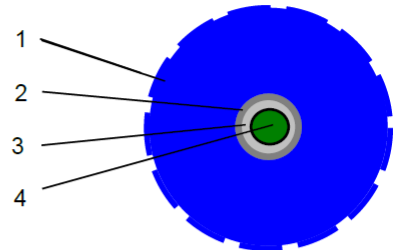
# APPENDIX B STRAIN CABLE SPEC SHEET

# BRUsens strain V9

3\_50\_2\_005

Flexible, mini armored fiber optic strain sensing cable with central metal tube, structured PA outer sheath, one optical fiber, strain range up to 1% (10000 µstrain)

LLK-BSST V9 3.2 mm



**Construction:**

- 1) PA outer sheath, with structured surface with interlocking system
- 2) Metal tube SS316L for protection and hermetic seal
- 3) Multi layer buffer and strain transfer layer with interlocking system
- 4) Special strain sensing optical single mode fiber

**Description:**

- Central metal tube with 1 optical fiber
- Good tensile strength
- Longitudinally and laterally watertight
- Good rodent protection
- High strain sensitivity
- Compact design, good flexibility, small bending radius
- Abrasion resistant structured sheath, for better strain transfer
- Halogen-free cable sheath

**Applications:**

- Distributed strain sensing
- Sensing technologies: Brillouin, FBG
- Precision measurement and alarm systems
- Soil movement, ground monitoring
- Pipeline monitoring
- Structural monitoring
- Direct burial in soil, concrete
- Harsh environment, subsea, outdoors

**Standard optical fiber:**

- Single-mode fiber: ITU-T G.657
- Other fiber types and fiber quality available upon request

**Temperature range:**

- Operating temperature: - 30° C ... +70° C
- Storage temperature: - 40° C ... +70° C
- Installation temperature: - 10° C ... +50° C
- Short term temperature (60 min) +150°C (during installation)

**Cable sheath color:**

- Blue, similar RAL 5005
- Other colors upon request

**Standards:**

- Cable tests complying with IEC 60794-1-2

**Remarks:**

- Fiber colored
- Final test reports OTDR and BOTDA measurement
- Other cable designs and temperature ranges available
- Standard cable marking with meter marks, special labeling of outer sheath upon request
- Preassembled cable sets available, special field termination kit available
- Accessories such as anchors, loops, fan-outs, splice enclosures, connectors, etc. available
- Deployment training upon request
- For improved UV resistance, black cable sheath available upon request

**Technical data:**

Type	Max. no. of fibres units	Cable ø mm	Weight kg/km	Max. tensile strength installation N	Typical Load at 1% elongation N
1F	1	3.2	10.5	260	470

Type	Min. bending radius		Max. crush resistance N/cm
	with tensile mm	without tensile mm	
1F	64 (20xD)	48 (15xD)	250

**Optical fiber data (cabled) at 20°C**

Fiber Type	Attenuation, dB/km 1550 nm	Typical Brillouin parameters BOTDR or BOTDA at 1550 nm		
		Temperature sensitivity df <sub>B</sub> / dT	Strain sensitivity df <sub>B</sub> /dε	Centr. Brillouin Freq.
SMF	≤ 0.5	1.1 MHz/°C	450 MHz/%	10.6 GHz

© Copyright 2016 by Brugg Cable AG – THE INFORMATION CONTAINED IN THIS DOCUMENT IS THE SOLE PROPERTY OF BRUGG KABEL AG. ANY REPRODUCTION IN PART OR AS A WHOLE WITHOUT THE PERMISSION OF BRUGG KABEL AG IS PROHIBITED.

Subject to changes without notice

2016/06/07 Rev. 02 TH



**SENSING TECHNOLOGIES**

Brugg Kabel AG • Klosterzelgstrasse 28 • 5201 Brugg • Switzerland  
Phone +41 56 460 3333 • info.sensing@brugg.com • www.bruggcables.com/sensing

## **APPENDIX C 72F-6C-LC CABLE SPEC SHEET**

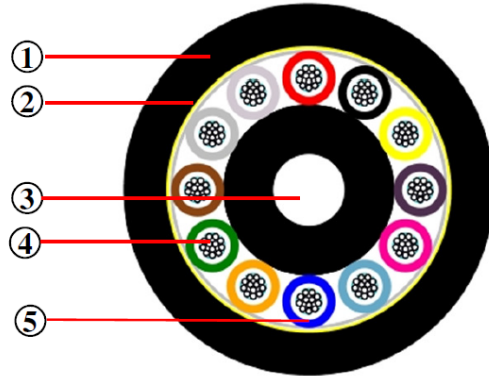
# DATA SHEET OPTICAL FIBRE CABLE



DATA SHEET : ADSS-Industrial

## Aerial Self Support ( Industrial Strength)

CABLE DESCRIPTION	
1	UV resistant Polyethylene outer sheath (Black)
2	Aramid yarn peripheral strength member (Optimized load transfer between aramid & sheath)
3	Glass reinforced plastic centre strength member (GRP) (Over-sheathed in some cases)
4	Optical fibres
5	PBT loose tube (Thixotropic gel filled)



The drawing depicts a 144 fibre cable

FIBRE COUNT	ELEMENTS PER LAYER												
	1	2	3	4	5	6	7	8	9	10	11	12	
4	BE	FL	FL	FL	4 Fibres per Ø 2.2mm tube								
12	BE	FL	FL	FL	12 Fibres per Ø 2.2mm tube								
24	BE	OE	FL	FL	12 Fibres per Ø 2.2mm tube								
48	BE	OE	GN	BN	12 Fibres per Ø 2.2mm tube								
72	BE	OE	GN	BN	GY	WE	12 Fibres per Ø 2.2mm tube						
96	BE	OE	GN	BN	GY	WE	RD	BK	12 Fibres per Ø 2.2mm tube				
144	BE	OE	GN	BN	GY	WE	RD	BK	YW	VT	PK	TE	12 Fibre per Ø2.2mm tube

The loose tubes contain 12 fibres per tube.  
 The fibre colours follows the TIA/EIA-598 colour coding scheme: Blue, Orange, Green, Brown, Grey, White, Red, Black, Yellow, Violet, Pink and Turquoise.  
 The loose tubes colours follows TIA/EIA-598 colour coding scheme: Blue, Orange, Green, Brown, Grey and White, Red, Black, Yellow, Violet, Pink and Turquoise.  
 Fillers are Black in colour

PRODUCT FEATURES	
* The CBI Telecom "short span" series are compact loose tube aerial self-supporting cables specifically designed for installation on pole routes with spans up to 70m.	
* The cable's main feature is its low installation cost, and the speed with which this can be effected due to its lightweight and self-supporting characteristics.	
* A non-metallic construction ensures lightning immunity.	
* The series is furnished with high modulus, creep resistant, aramid strength members which enable the cable to withstand sustained Every Day Stress (EDS), as well as high loading during environmental extremes. The aramid is applied contra-helicly in layers to eliminate torsional stress.	
* The cable's smooth circular profile inhibits galloping, and the gel in the tubes provides additional protection against vibration, ensuring excellent optical reliability for all service conditions.	
* The sheathing material is well dosed with Carbon Black to give the cable excellent UV resistance.	
Extensive cable/clamp compatibility tests were carried out to ensure optimum load transfer properties over a wide temperature range. It is recommended that only installation hardware verified according to the ATC CLAMP-APPROVAL SPECIFICATION be used (Please contact the CBI Telecom Technical Department in this regard).	
* Printing (Indelible printing) CBI TELECOM "NO OF FIBRES" (G657A INDUSTRIAL STRENGTH BEND TOLERANT) FIBRE OPTIC CABLE + LENGTH MARK + UNIQUE NUMBER	

# DATA SHEET OPTICAL FIBRE CABLE



DATA SHEET : ADSS-Industrial

TYPICAL PROPERTIES					
Parameter	Property / Pass criteria				Test Method
	Fibre Count				
	4 - 48 Fibre Cables	72 Fibre Cables	96 Fibre Cable	144 Fibre Cable	
Number of elements	4	6	8	12	
Cable diameter (nominal)	9.4mm	10.5mm	12mm	15.3mm	
Cable weight (nominal)	65 kg/km	87 kg/km	117 kg/km	184 kg.km	
Maximum load using the formula (0.6*9.81*2*Weight)	765N	1024N	1150 N	2166 N	IEC 60794-1-E1
Maximum installation load (aerial self-support, based on 70m span, 0.8m sag)	618 N	850 N	1562 N	1810 N	
Maximum working load (anticipating no ice, but winds up to 125 km/h)	1200 N	1530 N	1840 N	2500 N	
Crush resistance (via 100 mm plates)	1200 N	1500 N	2000 N	2000 N	IEC 60794-1-E3
Long term creep test (10 days)	< 0.1% cable length increase				ATC Internal
Cable / Termination clamp compatibility (up to 70 °C)	100% load transfer				ATC Internal
Minimum bend radius	12 x Cable Diameter				IEC 60794-1-11
Impact resistance (25mm anvil / 10 blows)	2 Nm Blows				IEC 60794-1-E4
Temperature performance	-10 to +70° C				IEC 60794-1-F1
Drip test (300 mm sample of loose tube @ 80 °C)	No leakage				IEC 60794-1-14

# DATA SHEET OPTICAL FIBRE CABLE



DATA SHEET : ADSS-Industrial

## OPTICAL PROPERTIES (Alternative fibre types/properties are available on request)

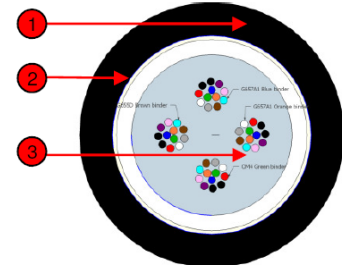
Fibre Type	SSMF
Specification	ITU-T G.657A
Attenuation	0.35 dB/km @ 1310 nm 0.20 dB/km @ 1550 nm 0.23 dB/km @ 1625 nm
Mode Field Diameter	9.2 ± 0.4 µm @ 1310 nm 10.4 ± 0.5 µm @ 1550 nm
Polarisation Mode Dispersion (PMD <sub>0</sub> )	≤ 0.06 ps/√km
Dynamic and static fatigue (Unaged and aged)	N <sub>d</sub> ≥ 20
Cladding Diameter	125 ± 0.7 µm
Core Concentricity Error	≤ 0.6 µm
Cladding Non-circularity	≤ 0.7 %
Chromatic Dispersion (ps/[nm.km]) 1285-1330nm 1550nm 1625nm	≤ 3  ≤18 ≤22
Cable Cut-off Wavelength	≤ 1260 nm
Macro-bend loss *	≤ 0.75 / 1.5 dB @ <b>10mm Radius</b> , 1 turn @ 1550/1625 nm ≤ 0.25 / 1.0 dB @ <b>15 mm Radius</b> , 10 turns @ 1550/1625 nm
Proof strain	0.7 GPa

## **APPENDIX D 4F-DC-LC CABLE SPEC SHEET**

# DATA SHEET MICRO FIBRE OPTIC CABLE

## MICRO BLOWN FIBRE OPTIC CABLE (Drop Cable- Multi Fibre )

CABLE DESCRIPTION	
1	Black UV Stabilized Hytrel Sheath
2	Glass Composite Oval strength members
3	Polycarbonate mono tube (Thixotropic gel filled) with 48 Colour coded optical Fibres, bundled/binded in 4 units of 12 Fibers each.



Drawing depicts a 48Fibre construction

FIBRE COUNT	ELEMENTS PER LAYER												Fibres per tube	
	1	2	3	4	5	6	7	8	9	10	11	12		
Blue Binder	G657A1	G657A1	G657A1	G657A1	G657A1	G657A1	G657A1	G657A1	G657A1	G657A1	G657A1	G657A1	G657A1	12 Fibres per bundle
Orange Binder	G657A1	G657A1	G657A1	G657A1	G657A1	G657A1	G657A1	G657A1	G657A1	G657A1	G657A1	G657A1	G657A1	12 Fibres per bundle
Green Binder	OM4	OM4	OM4	OM4	OM4	OM4	OM4	OM4	OM4	OM4	OM4	OM4	OM4	12 Fibres per bundle
Brown Binder	G655D	G655D	G655D	G655D	G655D	G655D	G655D	G655D	G655D	G655D	G655D	G655D	G655D	12 Fibres per bundle

Each bundle contain up to 12 individually coloured fibres. The fibre colours follows the TIA/EIA-598 colour coding scheme: Blue, Orange, Green, Brown, Grey, White, Red, Black, Yellow, Violet, Pink and Turquoise.  
 Blue binder: G657A1  
 Orange binder: G657A1  
 Green binder: OM4  
 Brown binder: G655D

PRODUCT FEATURES
<ul style="list-style-type: none"> <li>The cable design is such that cables may be installed by means of hauling or pushing techniques into (6 ID mm micro ducts).</li> <li>The thixotropic jell filled tube allows for excellent sustained reliability over a wide temperature range, and is engineered to ensure the optical fibres remain stress free over the designated temperature range.</li> <li>Resistance to moisture ingress is achieved though dry water blocking GCO materials. The design facilitates in the hand ability of the fibre optic duct cable during installation, termination and splicing.</li> <li>The Black TPE (Hytrel ) is UV stabilised for outdoor applications including aerial installations.</li> <li>The fibre optic cable is a totally non-metallic construction and immune to any RF interference.</li> <li>The cable is designed for flexibility in dynamic conditions.</li> <li>Printing: CBI TELECOM SKA SA (12F A1-BE)+(12F A1-OE) +(12F 55D-BN)+(12F OM4-BN)+DROP CABLE+“DATE”+ “LENGTH MARK” + UNIQUE NUMBER</li> </ul>

## DATA SHEET MICRO FIBRE OPTIC CABLE

<b>PHYSICAL PROPERTIES</b>		
Parameter	Fibre Count	Test Method
	48	
Number of elements	1	
Cable diameter (nominal)	less than 5.8 mm	
Cable weight (nominal)	37 kg/km	
Installation load ( fibre strain reversible)	400 N	
Minimum bend radius (long term/short term )	12 x Cable diameter	IEC 60794-1-11
Crush Resistance (via 100mm plates)	500 N	IEC 60794-1-E3
Impact resistance	1 Joule	IEC 60794-1-E4
Torsion (20N load, 1meter sample)	10 Cycles 180° apart	IEC 60794-1-2-E7
Flexing through 90 degrees	60 000 cycles	IEC 60794-1-2-E8
Repeated Bending (20N load)	35 Cycles R=20xD	IEC 60794-1-2-E6
Cable kink test	Pass: Bending radius of 25mm	IEC 60794-1-2-E10
Temperature Performance	-10°C to +70°C	IEC 60794-1-F1
Water penetration (3m cable, 1m head of water)	No leakage	IEC 60794-1-5B
Drip test (300 mm sample of loose tube @ 80°C)	No leakage	IEC 60794-1-14
Ageing Test: See Flexing and Temperature Performance	2000 Cycles 85° C for 14 days 2000 Cycles	CBI internal

## DATA SHEET MICRO FIBRE OPTIC CABLE

<b>OPTICAL PROPERTIES</b> <small>(Alternative fibre types/properties are available on request)</small>		
<b>FIBRE TYPE</b>	<b>Multi Mode 50/125 µm OM4</b>	
Specification	ITU-T G. 651	
Fibre core size	50 µm	
Cladding diameter	125 ± 0.7 µm	
Primary coating diameter	245 µm	
Operating wavelength	850 nm	1300 nm
Max. Attenuation	2.5 dB/km	0.7 dB/km
Overfilled modal Bandwidth	3500 MHz.km	500 MHz.km

<b>OPTICAL PROPERTIES</b>		
<b>Fibre Type</b>	<b>NZDSF</b>	<b>SSMF</b>
Specification	ITU-T G.655D	ITU-T G.657A1
Effective Area	72 µm <sup>2</sup>	N/A
Attenuation	0.25 dB/km @ 1550 nm 0.28 dB/km @ 1625 nm	0.36 dB/km @ 1310 nm 0.24 dB/km @ 1550nm 0.25 dB/km @ 1625 nm
Mode Field Diameter	9.6 ± 0.4 µm @ 1550 nm	9.2 ± 0.4 µm @ 1310 nm 10.4 ± 0.5 µm @ 1550 nm
Polarisation Mode Dispersion (PMD <sub>0</sub> )	≤ 0.05 ps/√km	≤ 0.06 ps/√km
Cladding Diameter	125 ± 0.7 µm	125 ± 0.7 µm
Core Concentricity Error	≤ 0.5 µm	≤ 0.5 µm
Cladding Non-circularity	≤ 0.7 %	≤ 0.8 %
Cable Cut-off Wavelength	≤ 1450 nm	≤ 1260 nm
Macro-bend loss	≤ 0.50 dB @ 16mm Radius, 1 turn @ 1550 nm ≤ 0.05 dB @ 30 mm Radius, 100 turns @ 1550 nm	≤ 0.5 dB @ 10 mm Radius, 1 turn @ 1550 nm ≤ 1.5 dB @ 10 mm Radius, 1 turn @ 1625 nm ≤ 0.05 dB @ 15 mm Radius, 10 turns @ 1550 nm ≤ 0.3 dB @ 15 mm Radius, 10 turns @ 1625 nm
Proof strain	0.7 Gpa	0.7 GPa

## **APPENDIX E BFS INTERROGATOR SPEC SHEET**

## Performance, features and technical data

Fiber type	Standard single-mode		
Optical connectors	E-2000 / APC		
Sensor configuration	loop		
Distance range (fiber loop)	50 km <sup>(1)</sup>		
Spatial resolution	up to 1 km fiber	0.2 m <sup>(2)</sup>	
	up to 25 km fiber	0.5 m	
	up to 50 km fiber	1.0 m	
Spatial accuracy	0.05 m		
Dynamic range <sup>(3)</sup>	> 20 dB		
Measurable parameters	Brillouin frequency shift, temperature, strain		
Accuracy and Range		Accuracy	Range
	strain	< 2 $\mu\epsilon$	-3% to +3% <sup>(4)</sup>
	temperature	< 0.1°C	-273 to +1000°C <sup>(4)</sup>
	Brillouin freq. shift	< 100 kHz	10 – 13 GHz
Acquisition time <sup>(5)</sup>	0.2 km fiber	20 seconds	
	2 km fiber	1 minute	
	10 km fiber	8 minutes	
	25 km fiber	25 minutes	
Communication interface	Ethernet		
Data export formats	binary, ASCII		
Measurement modes	Single measurements on demand; continuous monitoring Automatic detection of fiber length and attenuation		
Remote operation	Remote measurements, system diagnostics		
Operating temperature	5 - 40°C		
Dimensions	L x W x H	495 x 482 x 145 mm (19" rack case)	
Weight	10.5 kg		
Power consumption	60 W		
Laser class	1M		

(1) Standard distance range is 25 km. Distance range enhancement to 50 km available upon request.

(2) Software resolution enhancement selectable in user interface

(3) High optical losses along the sensing fiber may degrade the strain / temperature accuracy.

(4) Limited by optical fiber

(5) Estimated for typical measurements. Measurement time will vary with resolution, accuracy and strain / temperature range.

